nature portfolio

Peer Review File

An electrochemically driven hybrid interphase supported multi-scene compatible zinc metal anodes

Corresponding Author: Professor Peixin Zhang

This file contains all reviewer reports in order by version, followed by all author rebuttals in order by version.

Version 0:

Reviewer comments:

Reviewer #1

(Remarks to the Author)
The authors reported an electrochemically driven artificial solid-state electrolyte interface by using a 2-Hydroxyethyl methacrylate phosphate artificial coating on Zn surface. Driven by this in-situ formed hybrid SEI, it shows a stable cycling performance over 1500 hours at 10 mA cm-2. The in-situ formation of Zn3(PO4)2 on Zn surface is already reported by many papers (https://onlinelibrary.wiley.com/doi/full/10.1002/smll.202310497; https://doi.org/10.1002/adfm.202004885; https://doi.org/10.1002/adfm.202208230; https://doi.org/10.1038/s41467-023-41276-9). Although, the author evidence it in different systems (temperatures, bending angles, external pressure, Zn||MnO2/I2/O2), however, the evidence of SEI transformation mechanism and corresponding analysis is insufficient, lacking logic and rigor.
For example, the author claims that from Fig. 1e, the thickness of SEI is approximately 7 μm. However, from the side view SEM of Fig 1e, there is no obvious SEI boundary. So how is the thickness of 7 microns obtained ? In addition, this cross section image is not a complete cross section, but a side view with a tilt, which is not rigorous.
The author described that the adsorption energy of $SO4^{2-}$ at the three sites of Zn3(PO4)2 is much larger than that of Zn2+. While detailed information about these three different sites is missing. And the basis of selection of these sites, as well as the specific structure information is also missing.
In addition, generally, TEM characterization is commonly used to investigate the morphology, structure information of a known species. However, only from TEM lattice, the author determined the species is originated from Zn3(PO4)2, which is not reasonable. It is suggested to add direct evidence such as Grazing Incidence XRD, Raman, and others.
More specific comments are as follows.
1. There are too many wirting issues, such as inconsistent capitalization, spacing, strange abbreviations, non-uniform abbreviations, inconsistent units, inconsistent specific terms, etc. throughout the whole paper. This means that the manuscript was not carefully prepared.
2. The name “2-methyl-2-acrylate-2-hydroxyethyl ester phosphate ester” is really strange. Why do the authors refer to it as “2-Hydroxyethyl methacrylate phosphate” in the experimental section but use “2-methyl-2-acrylate-2-hydroxyethyl ester phosphate ester” in the main text?
3. 2-Hydroxyethyl methacrylate phosphate is generally considered to be water-soluble. How can this coating remain stable in aqueous electrolytes?
4. Many descriptions in the manuscript are superficial and lack depth. For instance, the electrochemical analyses.
5. The thickness of the Zn in Figure 1d clearly does not match the stated 200 μm in the Methods section.
6. In the in-situ DEMS test, the authors claim a condition of 1 mA cm-2 and 1 mAh cm-2, which is completely incorrect. The figures 4a-b clearly indicate that the current density is 1.5 mA cm-2.
7. The DRT analysis is not rigorous. The authors claim there are peaks at ~0.01s and ~1s, but there are actually no peaks at those points.
8. The overpotentials appear inconsistent. In Fig. 4c-d, how can the overpotential reach 1 V? In Fig. 5b, the nucleation overpotential is not representative when compared to the figures in the SI. In Fig. 6b, why is the overpotential for Pure Zn lower than that of SEI Zn?
9. Since the SEI transformation occurs, the conclusions about hydrophobicity derived from the contact angle results are invalid.

Reviewer #2

(Remarks to the Author)
This paper addresses the development of an electrochemically driven artificial solid electrolyte interface (SEI) to enhance the performance of zinc anodes in aqueous zinc-ion batteries. The authors applied a phosphate ester coating called MAHEPE on the zinc surface to create a protective layer, which transforms into a hybrid phase rich in $Zn_3(PO_4)_2$ nanocrystals through periodic cycling. This transformation facilitates a uniform zinc ion flux, suppresses dendrite growth, and mitigates side reactions. The approach maintains stable zinc anode performance under various conditions, including high temperatures, bending, and pressure, and shows potential applicability for Zn-I_2 and Zn-O_2 batteries.
1. The author stated that Fig. 1b is FESEM image, but it appears to be a digital image based on the figure and citation. Could you please check and revise this accordingly?
2. The author refers to Fig. 1c as the contact angle measurement, but it should be Fig. 1g.
3. It would be helpful to add a dotted line at the boundary between Zn metal and SEI layer to improve clarity.
4. In Fig. 2b and 2c, after the 1st and 3rd cycles, there appears to be some dots visible on the surface. Could you explain what they are and how they are formed?
5. The author mentions that TOF-SIMS analysis shows three components are uniformly distributed. However, in Fig. 2(g), only PO43- appears as scans go deeper, and in Fig. 2(i) and Fig. 2(k), certain regions are shown in black, suggesting the distribution may not be uniform. Could you clarify this?
6. One question arises regarding the SEI formation: after inorganic phase is established, the organic coating layer reportedly continues decomposing, which reduces adhesion. Given this low adhesion, is there a risk of the coated layer peeling off from the Zn metal? A tangible experimental evidence that resolves this issue is required.
7. In Supplementary Fig. 12, how did the author calculate corrosion current density? Typically, fitting is required to obtain this value (i.e., Tafel plot); could you clarify the methodology?
8. The author suggests that the high adsorption energy of SO42- in Zn3(PO4)2 indicates accelerated Zn2+ transport, but this appears to be a superficial and overinterpretation. Could the author provide additional evidence or clarify this correlation?
9. In Fig. 5b and S16, the authors determined the nucleation overpotential as the difference between the lowest and the stable points on the curve. However, this calculation appears to reflect the difference in driving force between nucleation and crystal growth, rather than the nucleation overpotential. Please check this.
10. In Fig. 5d, as deposition continues, the layer's thickness increases. Does this imply that zinc is deposited on top of the existing layer? Also, please add scale bars to improve clarity.
11. In Fig. S19, it would be helpful to label the Miller indices for all the peaks and to add 'Intensity (a.u.)' on the y-axis for clarity.
12. The concept of the paper might be challenging to grasp without scheme 1. Would it be better to place Scheme 1 earlier in the manuscript for improved comprehension?
13. For all cycling performance data, could you provide a zoomed-in view of the long term cycling performance (Time (h) vs Voltage (V))? This would help clarify the reaction behavior during cycling, particularly indicating whether the pattern resembles a square wave (suggesting non-uniform or unstable plating/stripping) or a typical curve shape (indicating uniform and stable ion flux and plating/stripping)?
14. Could the author include CV data for the full cell to determine whether any side reactions occur during cycling?
15. To clearly assess the performance of SEI Zn at full cell made with MnO2, it is essential to isolate the SEI Zn electrode as the sole independent variable. However, the author has added MnSO4 as an electrolyte additive, which could influence the results. Could you rerun the cell without MnSO4 additive to better isolate the SEI Zn electrode's performance?

Reviewer #3

(Remarks to the Author)
Manuscript ID: NCOMMS-24-62966
An Electrochemically Driven Hybrid Interphase-Supported Multi-scene Compatible Zinc Metal Anodes
Comments to the Authors

In this manuscript, the authors developed organic-inorganic (Zn3(PO4)2)-based solid electrolyte interphase (SEI) during electrochemical cycling. The SEI fabrication method is very impressive because it is thought to be an application of the concept that electrolyte additives participate in the formation of stable SEI during electrochemical reactions to artificial SEI. It seems that this transition in occurrence allowed for the formation of a more robust and stable SEI. Also, the authors especially closely evaluated the performance of the developed SEI Zn from various aspects (the Scheme 1 in the Supporting Information) for practical aqueous Zn metal batteries and demonstrated excellent performances. However, studies on forming in-situ Zn3(PO4)2-based SEI have already been reported in various previous researches. Therefore, the authors should present a more definite novelty and merits for the electrochemically driven hybrid interphase. In addition, some of the analyses need to be supplemented in the discussion and logicality. After the major comments mentioned below are well addressed, this manuscript should be considered for publication in Nature Communication.

1. There have been many previous reports on Zn3(PO4)2-based SEI (10.1002/smll.202310497, 10.1002/anie.202215600, 10.1002/aenm.202301193, 10.1002/adma.202007416, and 10.1039/D1EE00308A, etc.). This study should be supplemented with a clearer explanation of the differences from previously reported Zn3(PO4)2-based SEI.

2. A clear discussion is needed regarding the mechanism by which the 2-methyl-2-acrylate-2-hydroxyethyl ester phosphate ester (MAHEPE) layer transformed to Zn3(PO4)2 during electrochemical cycling.

3. How were the concentration and coating thickness of the solution containing MAHEPE optimized?

4. Generally, the binding energy for C-C of C 1s is known to be 284.8 eV. In Fig. 1i-j and Supplementary Fig. 1, is there a reason why the binding energy of C-C of C 1s is 284.58? If not, refitting after calibration based on C-C binding energy is required.

5. To further demonstrate the transformation of MAHEPE to Zn3(PO4)2 during electrochemical cycling, it would be helpful to also present the XPS data after cycling.

6. In TOF-SIMS depth profiles (Fig. 2g-k), C-, PO43-, and O- species appear to be observed in the MAHEPE layer before electrochemical cycling as well. Therefore, TOF-SIMS data on species related to Zn ions are required to observe the evolution of Zn3(PO4)2 in MAHEPE.

7. Why is the AYM of Zn dendrites larger than that of pure Zn anodes?

8. As shown in Fig. 3f, as Zn3(PO4)2 is formed in MAHEPE layer, the adhesion of the SEI layer decrease rapidly. Due to the weak adhesion of about 50 nN, it is necessary to evaluate whether there is any peeling or detachment of the SEI layer after cycling.

9. A clear basis is needed for the cause of SEI Zn inducing growth of Zn deposits along the Zn(002) plane. The authors attributed this phenomenon to zincophilic phosphate groups, but the presented DFT results show that the affinity between Zn3(PO4)2 and Zn atoms is not high at all. In addition, the Zn(002) surface deposition phenomenon is not a phenomenon that appears only when Zn affinity is high. Therefore, a clear explanation of this will be able to improve readers' understanding.

10. Please correct the typos in the text.
e.g.) page 2, line 6, Zn3(PO4)2nanocrytals / Zn3(PO4)2 nanocrystals
page 12, line 5, 1 mAcm-2 / 1 mA cm-2
page 12, line 20, 3M ZnSO4 / 3 M ZnSO4

Version 1:

Reviewer comments:

Reviewer #1

(Remarks to the Author)
This paper is well revised resolving all concerns that I raised. However, the key concept about the in-situ formation of hybrid interphase and interfacial chemistry should be more clarified in the session of introduction considering the recently published important papers (Nat. Commun., 2023, 14, 5443; EES, 2024, 17, 7870; ACS Energy Lett., 2024, 9, 209). The originality of this work needs to be further emphasized in the introduction part.

Reviewer #2

(Remarks to the Author)
I can see the substantial improvements made in response to the reviewers' comments. However, some essential revisions are still required for clarity and completeness:

1. Electrochemical decomposition (Point 4): Authors stated that the observed dots result from the electrochemical decomposition of organic components. However, further validation is required to confirm that these dots do not induce any side reactions that could impact long-term battery stability. Please provide experimental evidence supporting this claim.

2. Peeling off during cycling (Point 6): In the side-view image of the zinc metal, some void spaces are observed. However, this image alone does not sufficiently address the concern regarding potential peeling off the SEI layer during cycling. A more detailed analysis would be required to enhance the argument.

3. In-situ morphology analysis (Fig. 5d): The provided figure appears to depict in-situ morphological observations, potentially from digital microscopy. However, it lacks scale bars and clear proof that Zn^{2+} ions are depositing beneath the SEI layer. Please add a scale bar and provide more conclusive evidence.

4. XRD (Fig. S19): The Miller indices and y-axis labels remain unchanged. Authors did not address the previous concerns about this.

5. CV data for the MnO2 full cells (Fig. S51): It is notable that no SEI formation peak appears in the first cycle. Furthermore, while authors mentioned that the observed dots are due to the electrochemical decomposition of organic components, this process does not seem to be manifested in the CV data either. Can authors clarify why these phenomena do not produce distinguishable peaks in the CV curves?

Reviewer #3

(Remarks to the Author)
The author has significantly improved the manuscript in response to the previous suggestions and addressed the concerns I raised during the initial review. The author employed an in-situ Zn3(PO4)2-based organic-inorganic hybrid interphase. This strategy makes a significant contribution to the field of Aqueous Rechargeable Zinc-Metal Batteries.

The author provides a clear exposition of the study's background, objectives, methods, and results. The structure and logic of the article have been thoughtfully organized, enabling readers to gain a clear understanding of the research's significance and contributions.

I believe the manuscript has reached the level suitable for publication.

Version 2:

Reviewer comments:

Reviewer #2

(Remarks to the Author)
The authors have properly addressed all the concerns from the reviewer, thus the current manuscript can be publishable.

Point-by-point response to the reviewers' comments

Dear Reviewers:

We sincerely appreciate your precious time and very valuable comments on improving the quality of this manuscript. In this revision, we have studied the comments carefully and have made full correction which we hope to meet with approval. Provided below is our detailed response to every question.

Reviewer #1 (Remarks to the Author):

The authors reported an electrochemically driven artificial solid-state electrolyte interface by using a 2-Hydroxyethyl methacrylate phosphate artificial coating on Zn surface. Driven by this in-situ formed hybrid SEI, it shows a stable cycling performance over 1500 hours at 10 mA cm^{-2}. The in-situ formation of $Zn_3(PO_4)_2$ on Zn surface is already reported by many papers (https://onlinelibrary.wiley.com/doi/full/10.1002/smll.202310497;https://doi.org/10.1002/adfm.202004885;https://doi.org/10.1002/adfm.202208230;https://doi.org/10.1038/s41467-023-41276-9). Although, the author evidence it in different systems (temperatures, bending angles, external pressure, Zn||MnO_2/I_2/O_2), however, the evidence of SEI transformation mechanism and corresponding analysis is insufficient, lacking logic and rigor.

Our Response: We appreciate the expert advice provided by the reviewer. We will undertake meticulous revisions in response to these comments and concerns. While the use of $Zn_3(PO_4)_2$ for the modification of Zn anodes has been extensively reported in the literature, we have thoroughly reviewed the relevant references provided by the reviewers, as well as other studies focused on the design of $Zn_3(PO_4)_2$-based SEIs. However, we have identified certain limitations in these approaches when compared to the current work. For instance, in previous research, investigators have employed NaH_2PO_4 solution to etch the Zn anode surface (10.1002/smll.202310497), or fabricated $Zn_3(PO_4)_2$ or phosphate-based protective layers using techniques such as

blade coating (10.1002/adfm.202004885) and hydrothermal methods (10.1002/adfm.202208230). These methods are primarily ex situ approaches. In contrast, in situ SEI layers can dynamically adjust their structure and composition during the battery's charge-discharge cycles, effectively accommodating changes on the electrode surface, thus offering superior compatibility. Furthermore, many studies have explored electrolyte modification strategies to form $Zn_3(PO_4)_2$-based SEIs. However, these approaches often involve the incorporation of substantial amounts of phosphorus-containing organic solvents (10.1038/s41467-023-41276-9; 10.1002/anie.202215600; 10.1002/aenm.202301193), which impede the reaction kinetics of the battery and run counter to the design principles of aqueous Zn-ion batteries. Although some works have suggested the use of small quantities of inorganic additives to promote the in-situ formation of $Zn_3(PO_4)_2$ SEIs (10.1002/adma.202007416; 10.1039/D1EE00308A), the purely inorganic $Zn_3(PO_4)_2$ SEIs often lack sufficient flexibility and strong adhesion to the anode, making the SEI susceptible to cracking or detachment, thereby compromising the battery's performance. In this work, we have developed an organic-inorganic hybrid $Zn_3(PO_4)_2$-based SEI using an electrochemical in situ method, which exhibits superior interfacial adhesion and rapid reaction kinetics, offering significant advantages over previously reported approaches. To elucidate the formation mechanism of the in situ generated hybrid SEI, we conducted phase analyses such as XRD and TOF-SIMS. These analyses demonstrate that the formation of $Zn_3(PO_4)_2$ is electrochemically driven, a finding that will be further elaborated in the subsequent section.

Related modification has been made in the revised manuscript.

(Main article, Page 4)

In detail, single organic component will be in-situ transformed into highly dispersed $Zn_3(PO_4)_2$ nanocrystalline-enriched hybrid phases after initial electrochemical cycles. This electrochemically mediated in situ synthesis approach facilitates the development of a highly compatible and flexible $Zn_3(PO_4)_2$-based hybrid SEI on the Zn anode surface,

obviating the need for extensive incorporation of organic solvents. Ex-situ atomic force microscopy (AFM) research also indicates the significantly enhanced modulus but reduced adhesion of the interphase, owing to the decomposition of high-adhesion organic component and formation of high-modulus inorganic nanocrystalline.

For example, the author claims that from Fig. 1e, the thickness of SEI is approximately 7 μm. However, from the side view SEM of Fig 1e, there is no obvious SEI boundary. So how is the thickness of 7 microns obtained? In addition, this cross section image is not a complete cross section, but a side view with a tilt, which is not rigorous.

Our Response: Thanks for the question from the reviewer. We acknowledge the challenges associated with directly observing SEI boundaries in SEM images. Measuring thickness and defining SEI boundaries primarily involve analyzing contrast differences in images, understanding known material properties, and utilizing scales in SEM images for calibration. You have pointed out that the cross-section image in the figure is not a full cross-section but a slanted side view. This slanted view was chosen to better illustrate the structural features of the SEI. However, the slanted view may have introduced a certain degree of error in the thickness measurements, and we apologize for any misunderstanding this may have caused. In this revision, to eliminate misunderstandings, the section of the SEI material has been retested without tilt. Additionally, the text content has been updated to reflect the current side view measurement results: the tested thickness is 5.8 μm, and a dotted line has been added at the boundary for clearer identification.

Related modification has been made in the revised manuscript.

(Main article, Page 6)

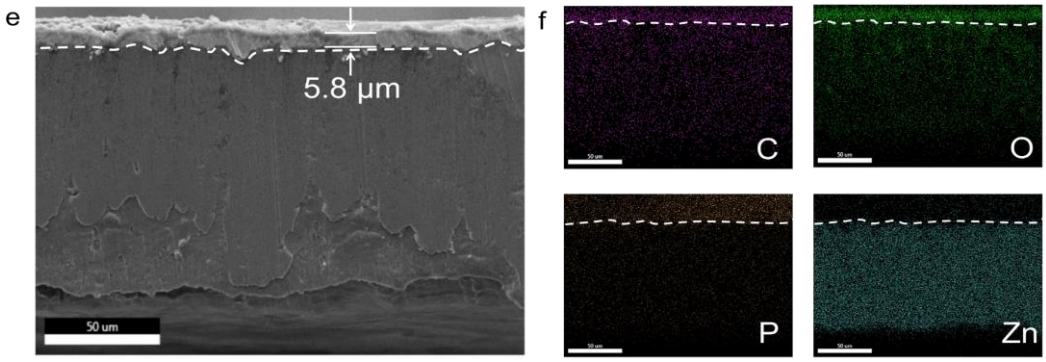

Fig. 1 | (**e**) Side-view FESEM image of SEI Zn and (**f**) corresponding EDS mapping.

(Main article, Page 7)

The SEI Zn surface morphology is shown in Fig. 1e, and the side view shows that the coating thickness is approximately 5.8 μm.

The author described that the adsorption energy of SO_4^{2-} at the three sites of $Zn_3(PO_4)_2$ is much larger than that of Zn^{2+}. While detailed information about these three different sites is missing. And the basis of selection of these sites, as well as the specific structure information is also missing.

Our Response: Thanks for the question from the reviewer. After careful consideration of your feedback, we have identified three adsorption sites for SO_4^{2-} within the crystal structure of $Zn_3(PO_4)_2$ and provided corresponding adsorption models. The selection of these sites was based on our previous theoretical calculations and experimental verification results. Through density functional theory (DFT) calculations, we discovered that the three sites are mainly determined based on the high chemical affinity between Zn atom and O atom in SO_4^{2-}. In addition to these additions and improvements, we have further revised the relevant expressions in the paper to enhance their accuracy and readability.

Related modifications have been made in the revised manuscript and supplementary information.

(Main article, Page 16)

As shown in Fig. 4e and Supplementary Figs. 33-34, The adsorption energy and the corresponding adsorption model are shown, the three adsorption sites of SO_4^{2-} in the crystal structure of $Zn_3(PO_4)_2$ are mainly determined based on the high chemical affinity between Zn atom and O atom in SO_4^{2-}. The result shows that the adsorption energy of SO_4^{2-} at the three sites of $Zn_3(PO_4)_2$ is much larger than that of Zn^{2+}, …

(Supplementary Information, Pages 37 and 38)

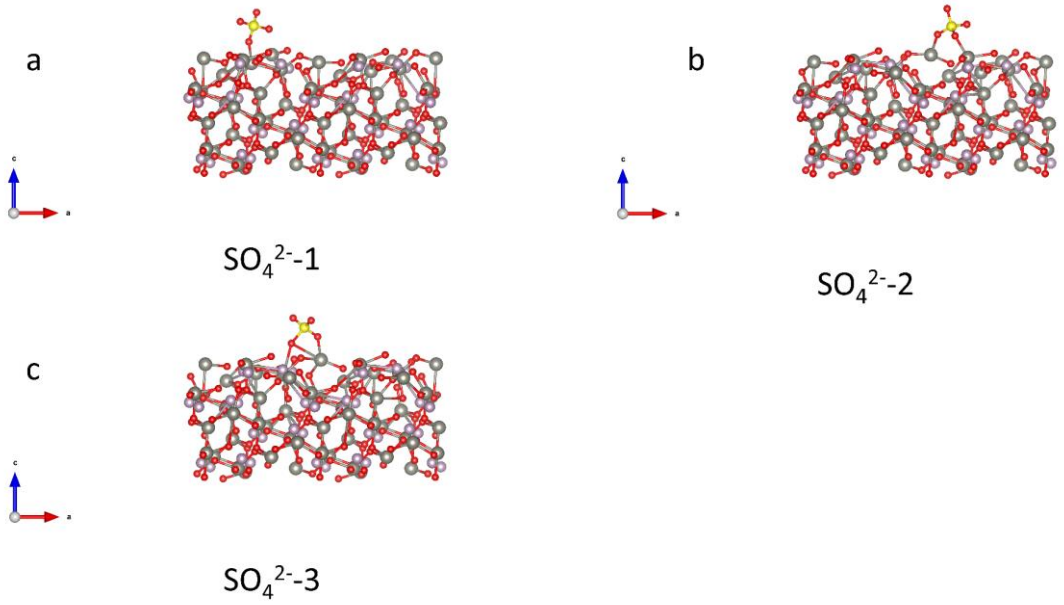

Supplementary Fig. 33 | Side view of different optimized structure models for SO_4^{2-} adsorption on $Zn_3(PO_4)_2$ surface: (a) SO_4^{2-}-1, (b) SO_4^{2-}-2 and (c) SO_4^{2-}-3.

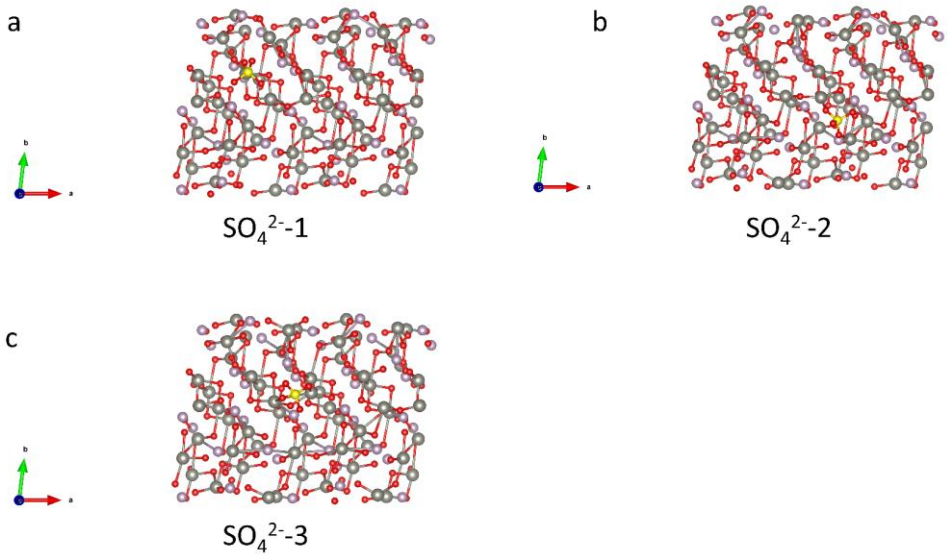

Supplementary Fig. 34 | Top view of different optimized structure models for SO_4^{2-} adsorption on $Zn_3(PO_4)_2$ surface: (a) SO_4^{2-}-1, (b) SO_4^{2-}-2 and (c) SO_4^{2-}-3.

In addition, generally, TEM characterization is commonly used to investigate the morphology, structure information of a known species. However, only from TEM lattice, the author determined the species is originated from $Zn_3(PO_4)_2$, which is not reasonable. It is suggested to add direct evidence such as Grazing Incidence XRD, Raman, and others.

Our Response: Thanks for the question from the reviewer. We incorporate the results of XRD, FTIR spectroscopy, XPS and TOF-SIMS analyses in the revised version of the paper. These techniques will provide complementary data that will help confirm the identity of the substance as $Zn_3(PO_4)_2$.

Related modifications have been made in the revised manuscript and supplementary information.

(Main article, Pages 9-10)

To further explore the phase evolution of the solid electrolyte interface (SEI) on the Zn surface after cycling, the XRD, XPS and FTIR characterization were performed (Supplementary Figs. 7-9). The findings reveal that the immersion of SEI Zn in a 3 M

$ZnSO_4$ did not induce the formation of any novel phases on its surface. Conversely, characteristic diffraction peaks of the $Zn_3(PO_4)_2$ phase were detected at 31.96°, 33.11°, and 34.68° on the surface of SEI Zn after cycling. These peaks correspond to the ($\overline{3}$ 02), ($\overline{1}$ 06) and (106) crystal planes (PDF#97-006-8362). This phenomenon suggests that, under the electrochemical driving force, Zn^{2+} migrate through the SEI and engage in a reaction with PO_4^{3-}, thereby catalyzing the formation of insoluble $Zn_3(PO_4)_2$. Note that, the peaks were skewed to the left due to the smaller grain size and larger lattice constant. In the XPS spectrum, for the P 2p region, peaks at 133.58 eV and 134.43 eV associated with P-O bonds were clearly visible. In the infrared spectrum, the wavenumbers at 1161.15 cm^{-1} confirm the existence of P=O bond, which were representative peaks of $Zn_3(PO_4)_2$. Based on the above experimental results indicate that the surface of the SEI Zn anode spontaneously evolves into an organic-inorganic hybrid layer after cycling.

The evolutionary process of interphase can be further confirmed by time-of-flight secondary ion mass spectrometry (TOF-SIMS). Fig. 2g depict the 3D elemental distributions of PO_4^{3-}, C, and O. It is evident that the PO_4^{3-} signal is relatively uniformly distributed across the entire plane, indicating the spontaneous construction of the artificial SEI into inorganic $Zn_3(PO_4)_2$. TOF-SIMS analysis was performed in positive ion mode to carefully analyze the three-dimensional distribution of Zn, Zn-O, Zn-PO_x and Zn-PO bonds before and after the 3 cycles process, as shown in Supplementary Figs. 10-11. The comparative analysis shows that the signal strength of Zn-O bonds is basically unchanged before and after the cycle. The results show that Zn preferentially binds oxygen atoms on organic components at SEI Zn. Notably, at the initial state, the Zn-PO_x and Zn-PO components mainly originate from the intimate contact between the Zn anode and the PO_4^{3-} groups in the SEI. After cycling, the signal strength of both Zn-PO_x and Zn-PO bonds increased after cycling. This enhancement is attributed to electrochemically derived $Zn_3(PO_4)_2$ during cycling, resulting in the conversion of the organic coating to the organic/inorganic hybrid phase.

(Supplementary Information, Pages 10-14)

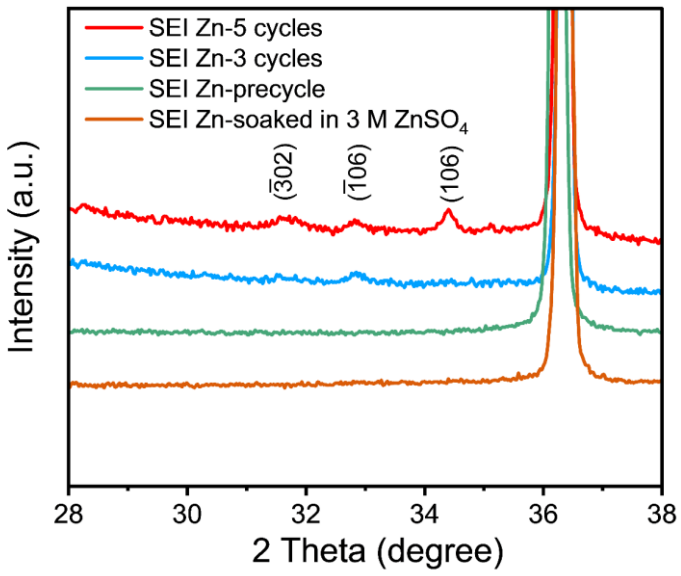

Supplementary Fig. 7 | XRD patterns of the cycled SEI Zn, precycle SEI Zn and soaked SEI Zn surface.

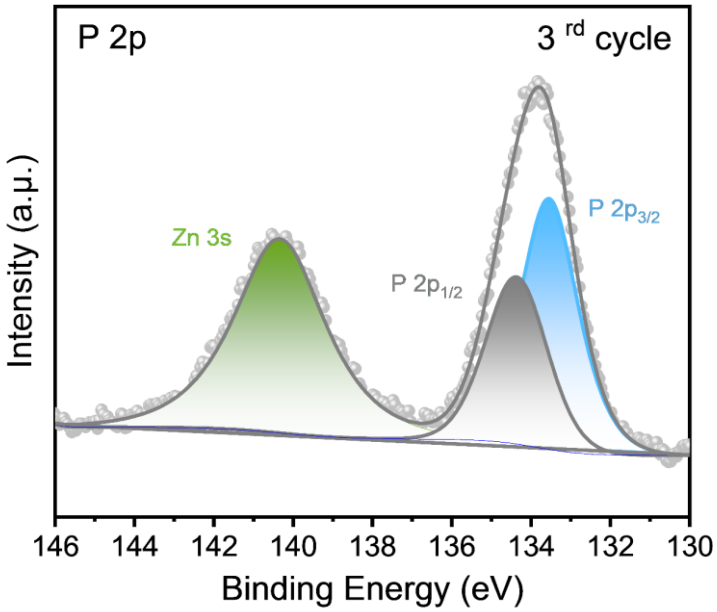

Supplementary Fig. 8 | P 2p XPS spectra of SEI Zn surface after 3 cycles.

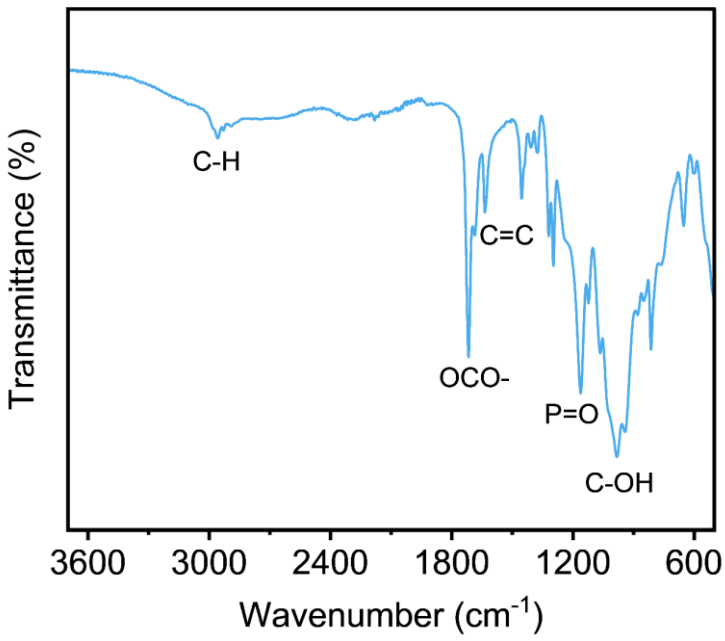

Supplementary Fig. 9 | FTIR spectra of SEI Zn surface after 3 cycles.

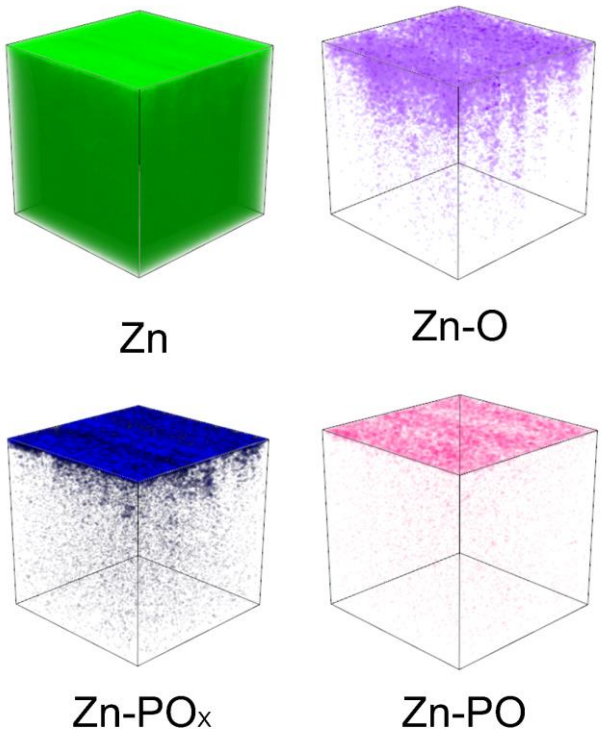

Supplementary Fig. 10 | TOF-SIMS 3D reconstruction of SEI Zn surface before cycling.

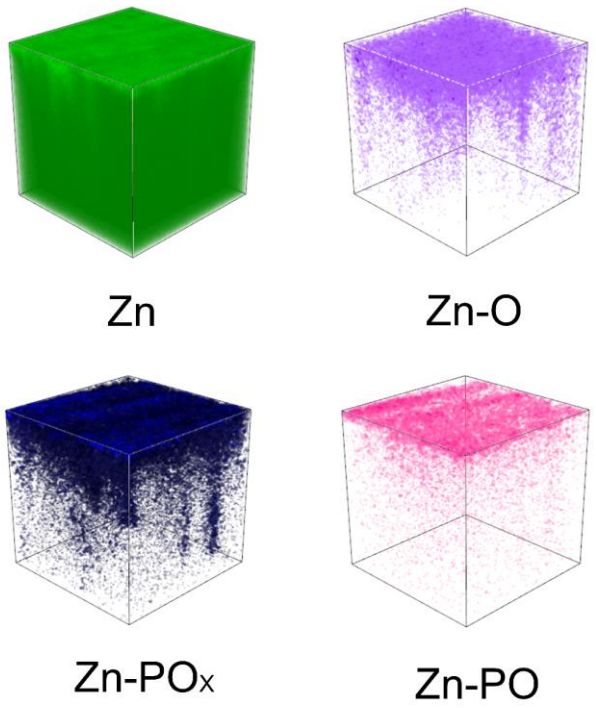

Supplementary Fig. 11 | TOF-SIMS 3D reconstruction of SEI Zn surface after 3 cycles.

More specific comments are as follows.

1. There are too many wirting issues, such as inconsistent capitalization, spacing, strange abbreviations, non-uniform abbreviations, inconsistent units, inconsistent specific terms, etc. throughout the whole paper. This means that the manuscript was not carefully prepared.

Our Response: Thanks for the question from the reviewer. We are deeply aware that these issues reflect negligence in the preparation of the manuscript, for which we are deeply sorry. We have conducted a comprehensive review of the manuscript, paying particular attention to the use of capital letters, Spaces, abbreviations and terminology to ensure that the format and style remain consistent throughout the document. We have combed through the abbreviations and terms that appear in the article to ensure that only one correct form is used throughout the document. For strange abbreviations that may cause confusion, we have substituted or explained them. We have carefully checked all mentioned units to ensure that the use of units is consistent throughout the article and complies with scientific norms. For the specific terms in the article, we have

referred to the authoritative literature and materials in the relevant fields to ensure the accuracy and consistency of their use. We have gone to great lengths to correct these issues and to ensure that when the revised version is submitted, the manuscript will be more carefully and thoroughly prepared.

Related modifications have been made in the revised manuscript.

(Main article, Page 15)

The digital photos of the SEI Zn electrode and pure Zn electrode, soaked in 3 M $ZnSO_4$ for three days at room temperature, are shown in Supplementary Fig. 26. According to the FESEM images, the SEI Zn surface is smooth and flat, and the corresponding EDS image shows that the coating remains firmly attached to the Zn foil surface, …

(Main article, Page 24)

Fig. 6 | Wide temperature range application and large capacity pouch cell performance of SEI Zn. Long-term cycle performance of pure Zn and SEI Zn anodes at the conditions of **(a)** 5 mA cm^{-2}, 1 mAh cm^{-2} and 0°C; **b** 10 mA cm^{-2}, 1 mAh cm^{-2} and 25°C; and (**c**) 5 mA cm^{-2}, 1 mAh cm^{-2} and 60°C.

(Main article, Page 30)

After a long cycle of 190 hours, the discharge and charge potentials of the SEI Zn air battery were 1.08 V and 2.04 V, respectively, while those of the pure Zn air battery were 0.86 V and 2.6 V after ...

2. The name “2-methyl-2-acrylate-2-hydroxyethyl ester phosphate ester” is really strange. Why do the authors refer to it as “2-Hydroxyethyl methacrylate phosphate” in the experimental section but use “2-methyl-2-acrylate-2-hydroxyethyl ester phosphate ester” in the main text?

Our Response: Thanks for the question from the reviewer. We named it based on the chemical formula. Meanwhile, we recognize that inconsistency in naming may cause

confusion for readers. In order to avoid this situation, we have uniformly used the name "2-methyl-2-acrylate-2-hydroxyethyl ester phosphate ester" in the revised paper to ensure the consistency and accuracy of the full text. In addition, we will carefully review other parts of the paper to ensure that all chemical substances are correctly named to avoid similar problems.

Related modification has been made in the revised manuscript.

(Main article, Page 32)

Preparation of SEI Zn anode

Weighing 0.02 g of 2-methyl-2-acrylate-2-hydroxyethyl ester phosphate ester and dissolve it in 1 mL of absolute ethanol. Stir until completely dissolved and then apply it to the polished Zn foil surface (15*5 cm with a 200 μm scraper), and then immediately put it into a vacuum drying oven at 60°C to dry for 2 hours.

3. 2-Hydroxyethyl methacrylate phosphate is generally considered to be water-soluble. How can this coating remain stable in aqueous electrolytes?

Our Response: Thanks for the question from the reviewer. An experiment was conducted to investigate the water solubility of 2-methyl-2-acrylate-2-hydroxyethyl ester phosphate ester. Specifically, 1 mL of the compound was introduced into a glass vial, followed by the addition of 5 mL of deionized water. Upon initial observation, a distinct stratification was evident, with the mixture becoming turbid upon agitation. Subsequent to allowing the mixture to stand for 20 minutes, re-stratification occurred, with the 2-methyl-2-acrylate-2-hydroxyethyl ester phosphate ester residing in the lower layer and the upper layer comprising clarified deionized water. These observations indicate that 2-methyl-2-acrylate-2-hydroxyethyl ester phosphate ester is insoluble in water and exhibits good stability in aqueous solution.

Related modifications have been made in the revised manuscript and supplementary information.

(Main article, Page 7)

Meanwhile, to ascertain the water solubility of the material, we conducted a solubility experiment (Supplementary Fig. 3). The results demonstrated that MAHEPE was insoluble in water, the compound showed good stability when dispersed in aqueous solution.

(Supplementary Information, Page 6)

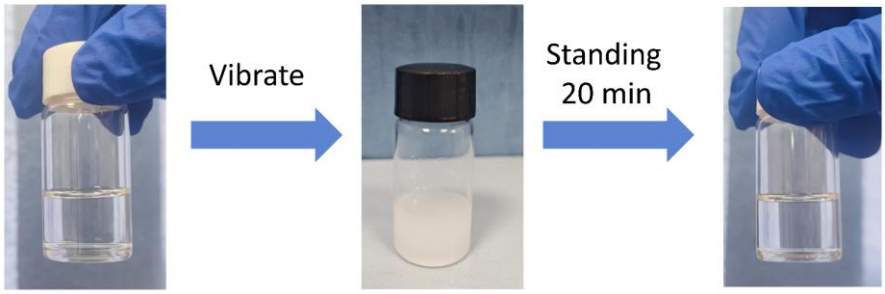

Supplementary Fig. 3 | Water solubility test of MAHEPE.

4. Many descriptions in the manuscript are superficial and lack depth. For instance, the electrochemical analyses.

Our Response: Thanks for the question from the reviewer. We have conducted a more thorough discussion on the electrochemical analysis where some expressions were previously imprecise.

Related modifications have been made in the revised manuscript.

(Main article, Page 15)

..., indicating that the HER is inhibited[26]. Simultaneously, in situ pH monitoring was utilized to assess the impact of SEI on the suppression of HER. A Zn||Zn symmetric cell assembled in a glass electrolyte cell was cycled under conditions of 20 mA cm^{-2} and 5 mAh cm^{-2}, while the pH values of the electrolyte were continuously recorded. As illustrated in Figs. 4c-d, after 40 cycles, the pH of the electrolyte in the symmetric cell

with pure Zn increased significantly from 3.1 to 3.9, indicating that the vigorous HER occurring on the Zn anode surface consumed a substantial amount of H^+, leading to a surplus of OH^-. In contrast, SEI Zn substantially delayed the pH increase, ultimately stabilizing it at approximately 3.4.

(Main article, Page 17)

To substantiate this, the activation energy (E_a) was derived using the Arrhenius equation to evaluate the influence of the artificial interface on the de-solvation process of hydrated Zn^{2+} [27]. As illustrated in Fig. 4i and Supplementary Fig. 36, the E_a for SEI Zn is markedly reduced to 27.02 kJ mol^{-1}, compared to 36.60 kJ mol^{-1} for the pure Zn anode. This significant reduction corroborates the accelerated Zn^{2+} de-solvation kinetics, which is primarily attributed to the exclusion of solvent water by the organic constituents within the SEI. To gain further insights into the reaction kinetics taking place on the surface of Zn anodes, ...

5. The thickness of the Zn in Figure 1d clearly does not match the stated 200 μm in the Methods section.

Our Response: Thanks for the question from the reviewer. We apologize for the lack of clarity. In the preparation process, a scraper with a nominal thickness of 200 micrometers (μm) is utilized. This scraper is employed in a step that involves the application of a substantial quantity of solvent. Subsequent to the scraping procedure, a drying step is implemented, resulting in the volatilization of the solvent. Consequently, the resultant thickness, post-drying and solvent evaporation, is significantly less than the initial 200 μm thickness of the scraper.

6. In the in-situ DEMS test, the authors claim a condition of 1 mA cm^{-2} and 1 mAh cm^{-2}, which is completely incorrect. The figures 4a-b clearly indicate that the current density is 1.5 mA cm^{-2}.

Our Response: Thanks for the question from the reviewer. In response to the reviewer's comments regarding the differences in the conditions of the field DEMS (differential electrochemical mass spectrometry) test, we acknowledge that the stated 1 mA cm^{-2} and 1 mAh cm^{-2} conditions are indeed incorrect. Looking closely at Figure 4a-b, it is clear that the current density used in the test is 1.5 mA cm^{-2}. We deeply regret this oversight and thank the reviewers for their attention to detail. To correct this error, we updated the text describing the in-situ DEMS test conditions to accurately reflect the current density of 1.5 mA cm^{-2} and checked any relevant calculations or interpretations that may be affected by this incorrect current density value to ensure the accuracy and completeness of our article.

Related modification has been made in the revised manuscript.

(Main article, Page 15)

In situ DEMS was used to monitor hydrogen release during battery cycling (Figs. 4a-b). For pure Zn, a strong H_2 response can be detected when cycling at a current density of 1.5 mA cm^{-2}, while no obvious H_2 signal can be seen during the entire cycle of the SEI Zn electrode, indicating that the HER is inhibited[26].

7. The DRT analysis is not rigorous. The authors claim there are peaks at ~0.01s and ~1s, but there are actually no peaks at those points.

Our Response: Thanks for the question from the reviewer. Due to our negligence in processing the data, we incorrectly analyzed the time of the DRT data. We have corrected the corresponding DRT data in the revision.

Related modifications have been made in the revised manuscript and supplementary information.

(Main article, Pages 17-18)

To gain further insights into the reaction kinetics taking place on the surface of Zn anodes, a comprehensive analysis of the in-situ electrochemical impedance

spectroscopy (in-situ EIS) and the corresponding relaxation time distribution (DRT) during Zn deposition/stripping processes was conducted (refer to Supplementary Fig. 37 and Figs. 4j-k). The observation of multiple peaks at generally similar positions in both Pure Zn and SEI Zn-assembled symmetric cells indicates a comparable electrochemical Zn deposition process occurring on the surfaces of these two types of Zn anodes. The peaks at a time constant of ≈0.05 s (τ_1), 2.2 s (τ_2), and 80 s (τ_3) stand for the adsorption and de-solvation (R_{ad}) of Zn^{2+} ions, the charge transfer of Zn^{2+} (R_{ct}) and Zn^{2+} interfacial diffusion (R_{dif}), respectively. Despite of the similar relaxation times of diverse process at the initial stage, significant difference in τ values appeared between SEI and pure Zn in the later Zn plating/stripping process. After cycling 5th, the τ values of R_{ad}, R_{ct} and R_{dif} in SEI grown smaller, while those of pure Zn fluctuate. This can be explained by the presence of the SEI layer which facilitates the de-solvation of Zn^{2+} ions, consequently reducing the relative contribution of R_{ad} to the overall impedance. Additionally, the significantly shortened relaxation time associated with R_{ct} highlights its inherently faster kinetics, which is consistent with the findings from the in-situ EIS analysis.

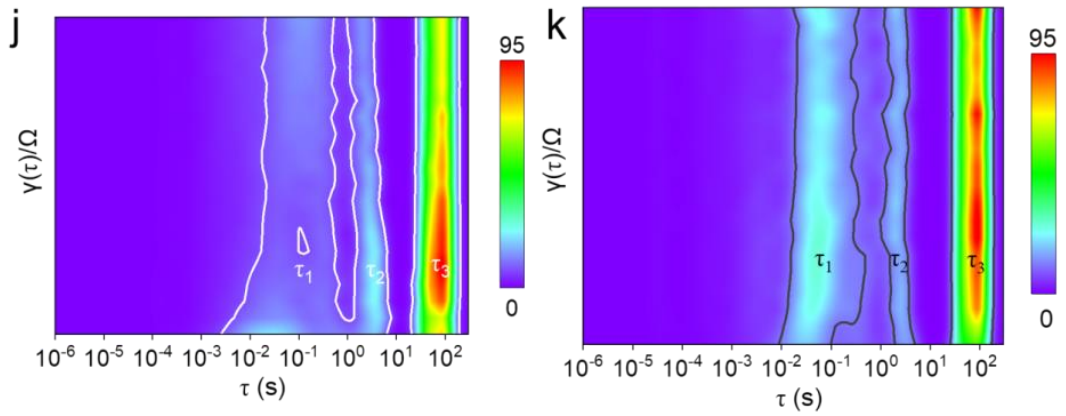

Fig. 4 | DRT analysis of the symmetric (**j**) SEI Zn and (**k**) pure Zn by operando EIS evolution.

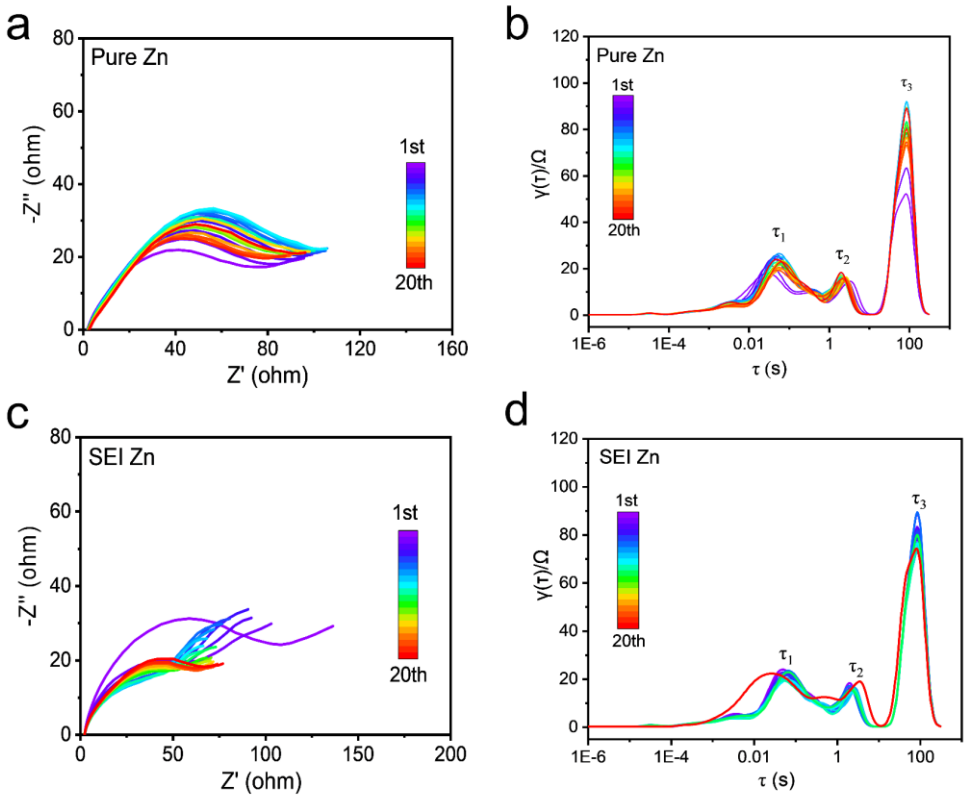

Supplementary Fig. 37 | The Nyquist plots and DRT curves of the impedance spectra monitored for Pure Zn and SEI Zn electrodes.

8. The overpotentials appear inconsistent. In Fig. 4c-d, how can the overpotential reach 1 V? In Fig. 5b, the nucleation overpotential is not representative when compared to the figures in the SI. In Fig. 6b, why is the overpotential for Pure Zn lower than that of SEI Zn?

Our Response: Thanks for the question from the reviewer. We sincerely apologize for the oversight in Figure 1, where the test conditions were incorrectly labeled due to a writing mistake. The actual test conditions are 20 mA cm^{-2} and 5 mAh cm^{-2}. Meanwhile, in situ pH monitoring was conducted by assembling a two-electrode glass cell for testing. The distance between the two anodes significantly exceeds the distance between electrodes in a typical button cell, resulting in a larger overpotential. And **We have interchanged Fig. 5b and Supplementary Fig. 38b.** In Fig. 6b, although the

$Zn_3(PO_4)_2$ component in the SEI facilitates ion transport, at high current densities, the hindering effect of the organic components on Zn^{2+} transport becomes more pronounced to some extent. In addition, the lower overpotential observed for pure Zn may be attributed to factors such as the battery assembly process and the ambient temperature during the testing period, which can introduce errors. This does not affect the fact that all other data in this manuscript are consistent with the research patterns.

Related modifications have been made in the revised manuscript and supplementary information.

(Main article, Page 19)

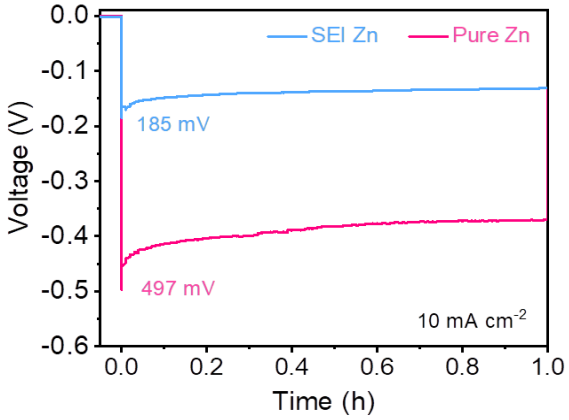

Fig. 5 | b Nucleation overpotential of Pure Zn and SEI Zn electrodes at 10 mA cm^{-2}.

(Supplementary Information, Page 42)

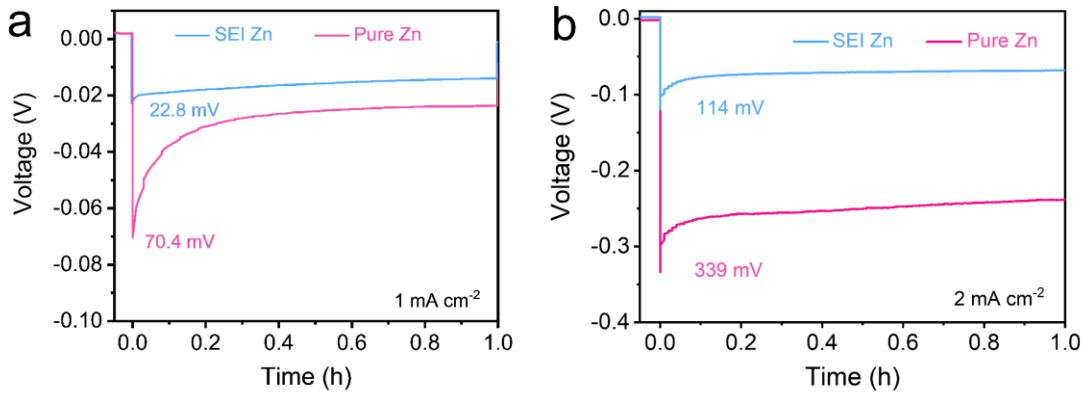

Supplementary Fig. 38 | Nucleation overpotential of Pure Zn and SEI Zn electrodes under the current densities of (a) 1 mA cm^{-2} and (b) 2 mA cm^{-2}.

9. Since the SEI transformation occurs, the conclusions about hydrophobicity derived from the contact angle results are invalid.

Our Response: Thanks for the question from the reviewer. Initially, we acknowledge that our paper did not fully consider the potential impact of solid electrolyte interphase (SEI) transition on antenna measurements and the subsequent conclusions regarding hydrophobicity. The SEI, serving as a crucial interface layer on the surface of battery materials, undergoes transformations that may significantly influence the surface properties of these materials, notably including their hydrophobicity. In light of this, we conducted contact angle measurements on SEI Zn after cycling procedures. The obtained contact angle of SEI Zn post-cycling was determined to be 91.1°, indicating that the material retains its hydrophobic nature.

Related modifications have been made in the revised manuscript and supplementary information.

(Main article, Page 14)

It is worth noting that the electrode material retained its hydrophobic properties after the cyclic test (Supplementary Fig. 24). To a certain extent, the retention of this hydrophobic property provides potential insight into how SEI electrode materials inhibit HER and enhance corrosion resistance.

(Supplementary Information, Page 28)

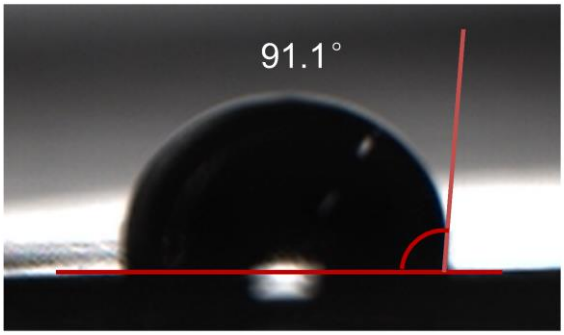

Supplementary Fig. 24 | Contact angle test on the surface of the cycled SEI Zn by using 3 M $ZnSO_4$ aqueous electrolyte.

Reviewer #2 (Remarks to the Author):

This paper addresses the development of an electrochemically driven artificial solid electrolyte interface (SEI) to enhance the performance of zinc anodes in aqueous zinc-ion batteries. The authors applied a phosphate ester coating called MAHEPE on the zinc surface to create a protective layer, which transforms into a hybrid phase rich in $Zn_3(PO_4)_2$ nanocrystals through periodic cycling. This transformation facilitates a uniform zinc ion flux, suppresses dendrite growth, and mitigates side reactions. The approach maintains stable zinc anode performance under various conditions, including high temperatures, bending, and pressure, and shows potential applicability for Zn-I_2 and Zn-O_2 batteries.

Our Response: We appreciate the reviewer for the comment and very constructive question and suggestion.

1. The author stated that Fig. 1b is FESEM image, but it appears to be a digital image based on the figure and citation. Could you please check and revise this accordingly?

Our Response: Thanks for the question from the reviewer. To ensure the precision and uniformity of the manuscript, we have implemented necessary revisions and adjustments.

Related modification has been made in the revised manuscript.

(Main article, Pages 6-7)

Fig. 1a shows the preparation process of SEI Zn, the best conditions of the preparation process were shown in Supplementary Figs. 1-2. where an organic layer is coated on the surface through a simple doctor blade method. The prepared SEI Zn sample was subjected to bending in order to evaluate the adhesion strength of the coating deposited on the Zn foil surface. Fig. 1b presents an optical micrograph depicting the outcome of this test. The field emission scanning electron microscopy (FESEM) image revealed no alteration in the SEI Zn surface coating within the bent region, indicating that the surface coating exhibited excellent adhesion. (Figs. 1c-d).

2. The author refers to Fig. 1c as the contact angle measurement, but it should be Fig. 1g.

Our Response: Thanks for the question from the reviewer. To ensure the precision and uniformity of the manuscript, we have implemented necessary revisions and adjustments.

Related modification has been made in the revised manuscript.

(Main article, Page 7)

Following this, the hydrophobicity of SEI Zn was further investigated, Fig. 1g shows the contact angle test performed in 3 M $ZnSO_4$ electrolyte. The contact angle of SEI Zn was measured at 90.4°, significantly higher than the 81.7° observed for pure Zn, indicating that SEI Zn exhibits superior hydrophobicity. The contact angle of the electrolyte on the SEI Zn surface is larger than that on the bare Zn surface, demonstrating the improved hydrophobicity of the SEI Zn surface[25].

3. It would be helpful to add a dotted line at the boundary between Zn metal and SEI layer to improve clarity.

Our Response: Thank you for your suggestion. To enhance clarity in the manuscript, we have incorporated a dotted line at the interface between the Zn metal and the SEI layer. This modification should aid in better distinguishing the two regions within the figure. Please review the updated version of the manuscript to confirm that this change meets your expectations.

Related modification has been made in the revised manuscript.

(Main article, Page 6)

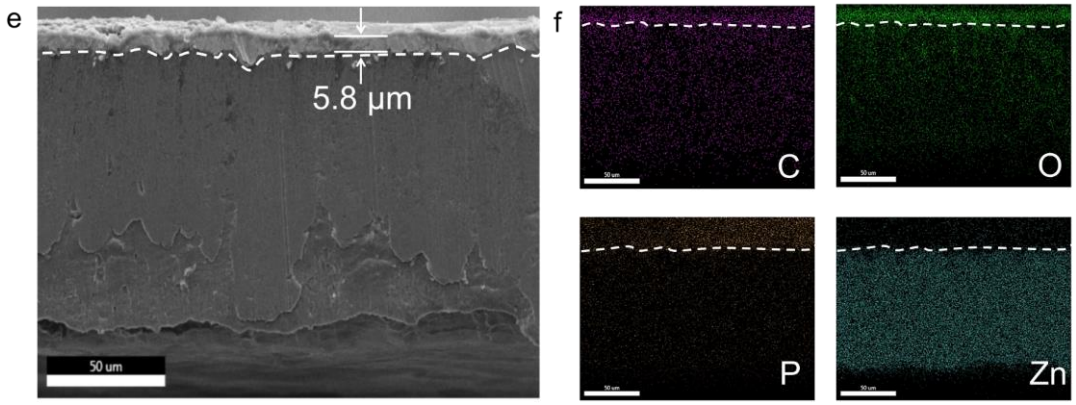

Fig. 1 | (**e**) Side-view FESEM image of SEI Zn and (**f**) corresponding EDS mapping.

4. In Fig. 2b and 2c, after the 1st and 3 rd cycles, there appears to be some dots visible on the surface. Could you explain what they are and how they are formed?

Our Response: Thanks for the question from the reviewer. To investigate the composition and formation mechanism of these dots, we conducted comparative experiments. To determine whether the formation of these visible dots is related to phosphate groups in the SEI, we used 2-methyl-2-hydroxyethyl acrylate, which has a molecular structure highly similar to that of 2-methyl-2-acrylate-2-hydroxyethyl ester phosphate ester but without phosphate groups, as a coating material to prepare Zn anodes. As shown in Supplementary Fig. 5, after immersion in 3 M $ZnSO_4$, no visible dot structures were observed on the surface of the SEI Zn and 2-methyl-2-hydroxyethyl acrylate coated Zn, indicating that the formation of these dots is unlikely to be a non-electrochemical process. However, after Zn deposition/stripping on the 2-methyl-2-hydroxyethyl acrylate coated Zn, uniformly distributed dots gradually appeared on the surface (Supplementary Fig. 6). Due to the complexity of potential organic-inorganic reactions and the extremely small size of these dots, we can only infer that this dot-like structure is likely derived from electrochemical decomposition of organic components.

Related modifications have been made in the revised manuscript and supplementary information.

(Main article, Page 9)

..., the surface morphology of the SEI Zn anode observed via FESEM after the 1st and

3rd cycles still exhibits a uniform coating, but with densely distributed dots formed from the electrochemical decomposition of organic components on its surface (Supplementary Figs. 5-6). However, it remains ...

(Supplementary Information, Pages 8-9)

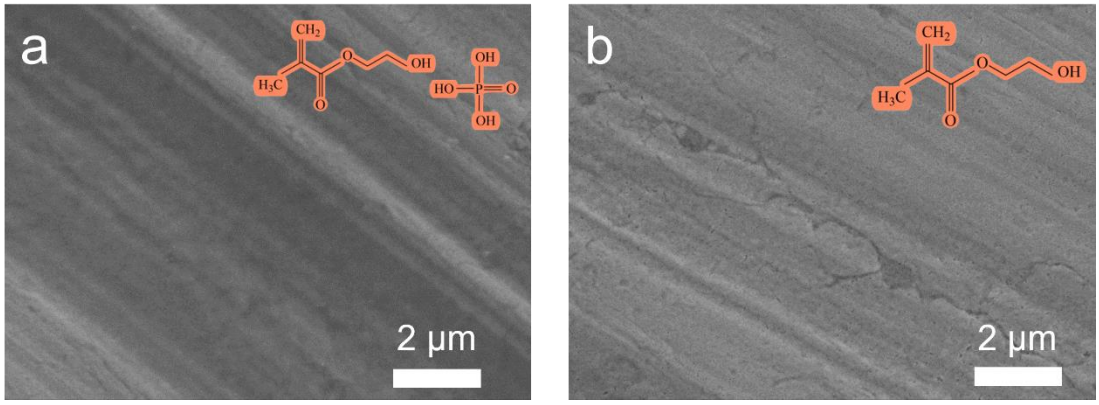

Supplementary Fig. 5 | FESEM images of (a) SEI Zn and (b) 2-methyl-2-hydroxyethyl acrylate coated Zn foil soaked in 3 M $ZnSO_4$ electrolyte for 12 h.

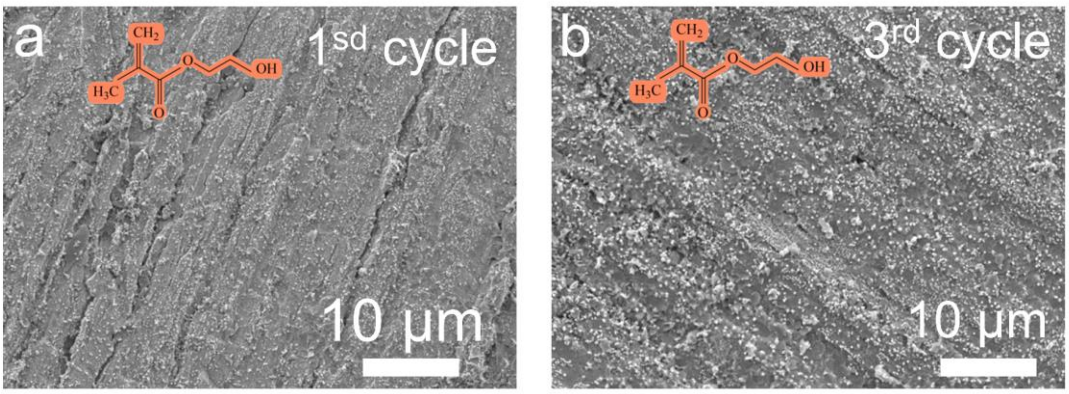

Supplementary Fig. 6 | FESEM images of the 2-methyl-2-hydroxyethyl acrylate coated Zn foil (a) after 1 cycle and (b) after 3 cycles.

To investigate the composition and formation mechanism of these dots, we conducted comparative experiments. To determine whether the formation of these visible dots is related to phosphate groups in the SEI, we used 2-methyl-2-hydroxyethyl acrylate, which has a molecular structure highly similar to that of 2-methyl-2-acrylate-2-hydroxyethyl ester phosphate ester but without phosphate groups, as a coating

material to prepare Zn anodes. As shown in Supplementary Fig. 5, after immersion in 3 M $ZnSO_4$ for 12 h, no visible dot structures were observed on the surface of the SEI Zn and 2-methyl-2-hydroxyethyl acrylate coated Zn, indicating that the formation of these dots is unlikely to be a non-electrochemical process. However, after Zn deposition/stripping on the 2-methyl-2-hydroxyethyl acrylate coated Zn, uniformly distributed dots gradually appeared on the surface (Supplementary Fig. 6). It can be defined that this dot-like structure is likely derived from electrochemical decomposition of organic components.

5. The author mentions that TOF-SIMS analysis shows three components are uniformly distributed. However, in Fig. 2(g), only PO_4^{3-} appears as scans go deeper, and in Fig. 2(i) and Fig. 2(k), certain regions are shown in black, suggesting the distribution may not be uniform. Could you clarify this?

Our Response: Thanks for the question from the reviewer. We apologize for the lack of clarity. First, the "TOF-SIMS analysis showing uniform distribution of the three components" mentioned in our paper is based on the overall statistical data and the average distribution trend. This conclusion is based on the comprehensive consideration of multiple sample points and analysis depth, aiming at a general description of the overall composition of the material. However, in Figures 2(g), 2(i), and 2(k) that you point to, we do observe a more detailed, localized distribution feature. These diagrams show the distribution of PO_4^{3-} ions as the scanning depth increases, as well as the appearance of black areas in some specific areas. These black areas usually indicate that the signal strength in the area is below the detection threshold, which may be due to extremely low ion concentrations, surface contamination, or limitations of the detection technology. We understand that this localized non-uniform distribution may seem contradictory to the conclusion of the overall uniform distribution, but in fact, it reflects the spatial complexity of the material composition. In materials science, even materials that look uniform on the macro scale may have differences in composition or structure on the micro scale. Therefore, the local non-uniformity we observed does not

exclude the possibility of global uniformity, but rather a finer description of the material's properties.

To achieve a more comprehensive understanding of this phenomenon, we have undertaken a meticulous refinement of the TOF-SIMS analysis conditions in the present study. We conducted an in-depth analysis of the three-dimensional distribution of Zn-PO_x and Zn-PO bonds in positive ion mode, which revealed a notably uniform distribution. Subsequent to cycling, the electrode energy spectrum demonstrated that the distribution of the P element on the surface remained relatively uniform. This observation, coupled with a range of experimental characterizations, strongly suggests that PO_4^{3-} ions are evenly distributed across the electrode surface.

Related modifications have been made in the revised manuscript and supplementary information.

(Main article, Page 10)

The evolutionary process of interphase can be further confirmed by time-of-flight secondary ion mass spectrometry (TOF-SIMS). Fig. 2g depicts the 3D elemental distributions of PO_4^{3-}, C, and O. It is evident that the PO_4^{3-} signal is relatively uniformly distributed across the entire plane, indicating the spontaneous construction of the artificial SEI into inorganic $Zn_3(PO_4)_2$. TOF-SIMS analysis was performed in positive ion mode to carefully analyze the three-dimensional distribution of Zn, Zn-O, Zn-PO_x and Zn-PO bonds before and after 3 cycles process, as shown in Supplementary Figs. 10-11.

(Supplementary Information, Page 14)

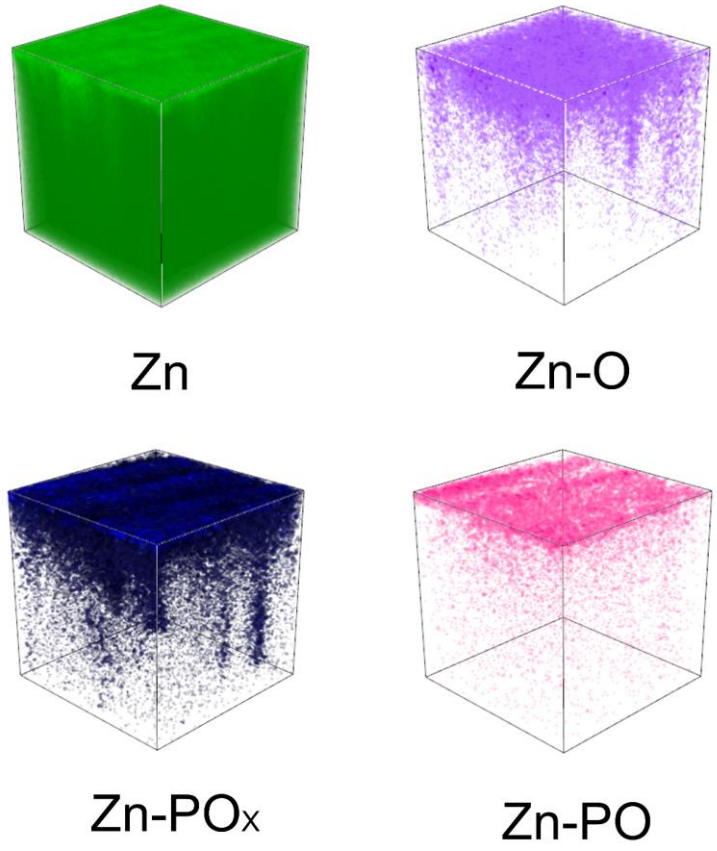

Supplementary Fig. 11 | TOF-SIMS 3D reconstruction of SEI Zn surface after 3 cycles.

(Supplementary Information, Page 20)

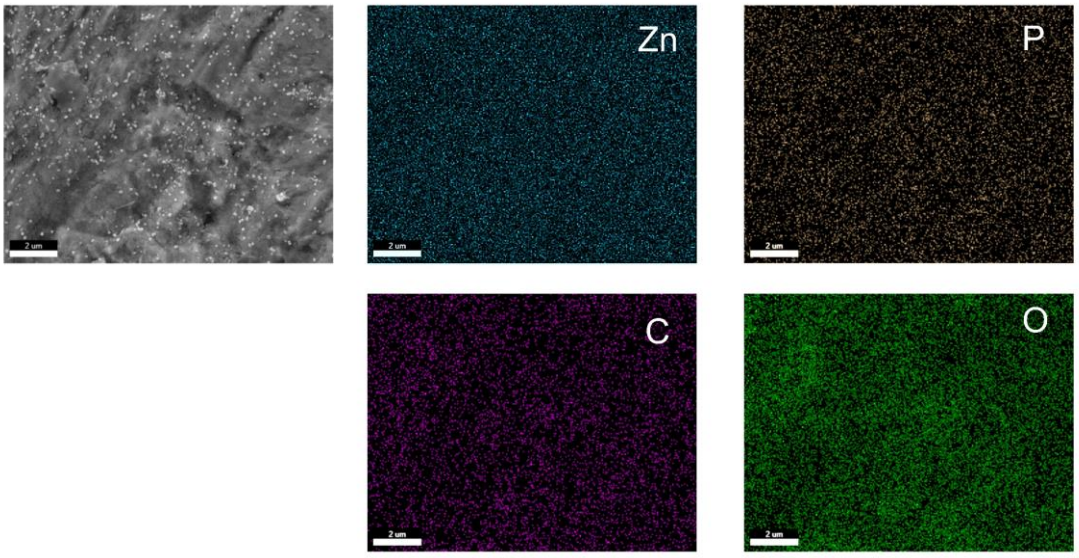

Supplementary Fig. 16 | EDS mapping image of SEI Zn after 5 cycles.

(Supplementary Information, Page 23)

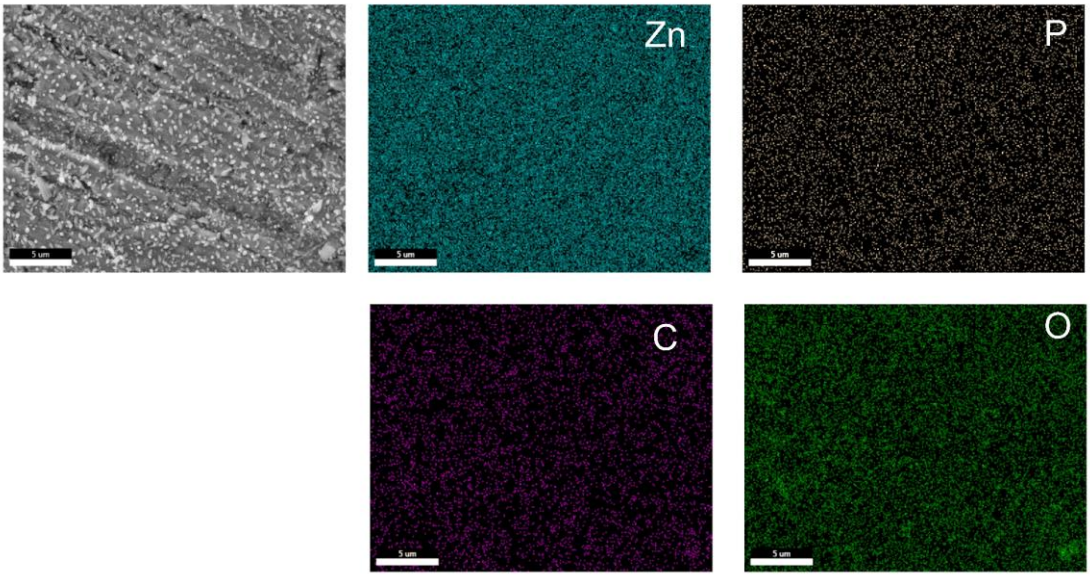

Supplementary Fig. 19 | EDS mapping image of SEI Zn after 10 cycles.

6. One question arises regarding the SEI formation: after inorganic phase is established, the organic coating layer reportedly continues decomposing, which reduces adhesion. Given this low adhesion, is there a risk of the coated layer peeling off from the Zn metal? A tangible experimental evidence that resolves this issue is required.

Our Response: Thanks for the question from the reviewer. To provide tangible experimental evidence for assessing the potential detachment of the artificial SEI due to inadequate adhesion, we conducted a detailed analysis of the electrode's surface composition after undergoing both 5 cycles and an extended number of cycles. Our findings reveal that the decomposition process is not progressive and unending; rather, it evolves into a transition where the flexible organic coating gradually transforms into an organic-inorganic hybrid interface. Ultimately, this transformation tends towards the formation of a stable, hybrid organic-inorganic interface. These observations offer crucial insights into the durability and stability of the artificial SEI, thereby enhancing our understanding of its role in electrode performance.

Related modifications have been made in the revised manuscript and supplementary

information.

(Main article, Pages 12-13)

In order to further verify whether the decomposition behavior of organic coatings during electrochemical cycling is non-terminating, detailed surface composition analysis of SEI Zn after different cycles was performed. In the Supplementary Fig. 15 of SEI Zn after 5 cycles, the presence of the phase interface can be clearly observed. This observation not only confirms the decomposition of the organic coating during the cycle, but also reveals significant changes in coating thickness. Specifically, the coating thickness after 5 cycles was significantly reduced compared to that before the cycle. This change in thickness is directly attributable to the decomposition of the organic coating. Further, by EDS analysis (Supplementary Fig. 16), C, O and P elements were evenly distributed in the decomposed coating. At the same time, the characteristic peaks of organic coatings were also detected in the XPS P 2p and O 1s spectra (Supplementary Fig. 17). The presence of these characteristic peaks indicates that even after 5 cycles, the flexible organic coating does not completely disappear, but gradually transforms into an organic-inorganic hybrid interface. When the number of cycles is further increased, it can be observed from the Supplementary Fig. 18 that the organic coating is still clearly visible, but there is a certain gap between it and the electrode, indicating that its adhesion is relatively weakened. This phenomenon is consistent with the process by which a highly viscous organic coating decomposes to form a strong inorganic phase. In addition, the distribution of C, O and P elements in the EDS spectrum remained relatively uniform, while the characteristic peaks in the XPS spectrum and FTIR spectrum were also obvious (Supplementary Figs. 19-21). Based on the above experimental results, it can be concluded that the decomposition of organic coatings in the electrochemical cycle is not infinite, but to a certain extent, and eventually tends to form an organic-inorganic hybrid interface.

(Supplementary Information, Pages 19-25)

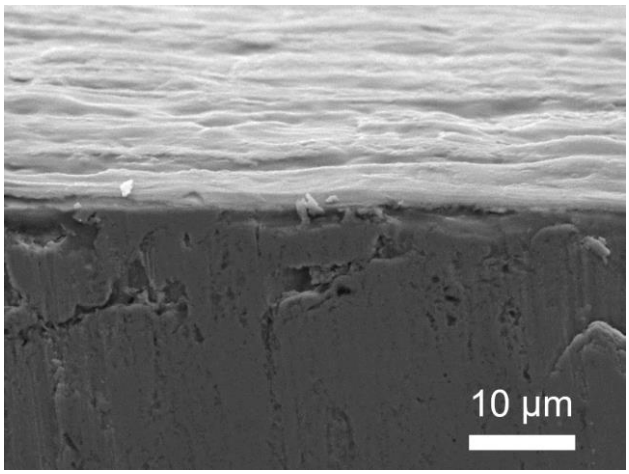

Supplementary Fig. 15 | Side-view FESEM image of SEI Zn after 5 cycles.

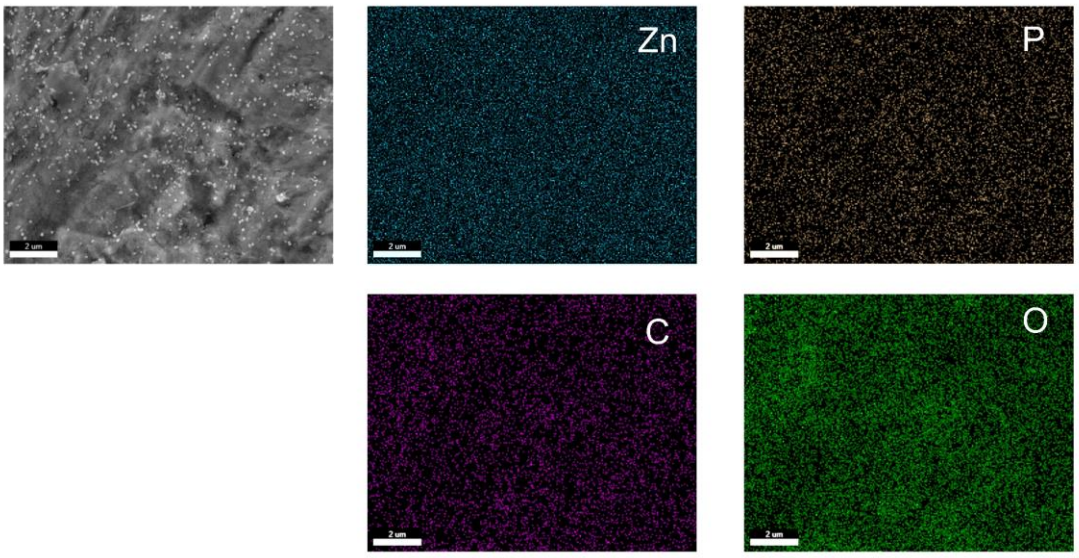

Supplementary Fig. 16 | EDS mapping image of SEI Zn after 5 cycles.

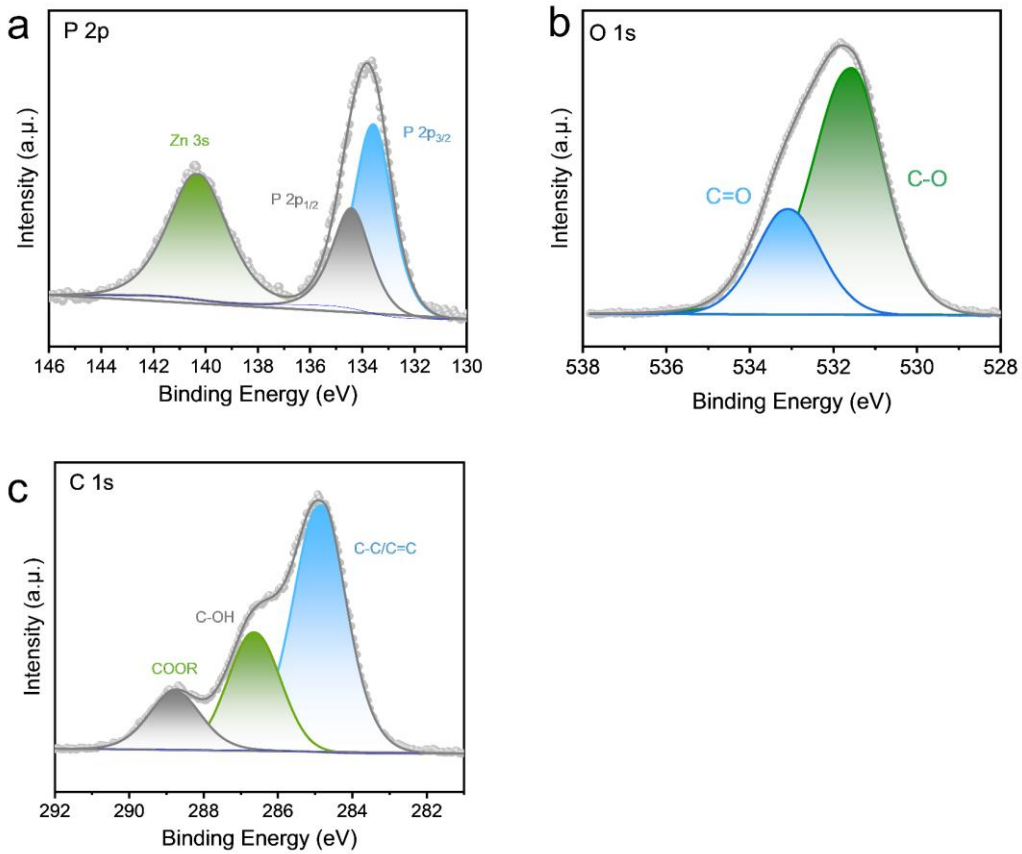

Supplementary Fig. 17 | (a) P 2p (b) O 1s and (c) C 1s XPS spectra of SEI Zn after 5 cycles.

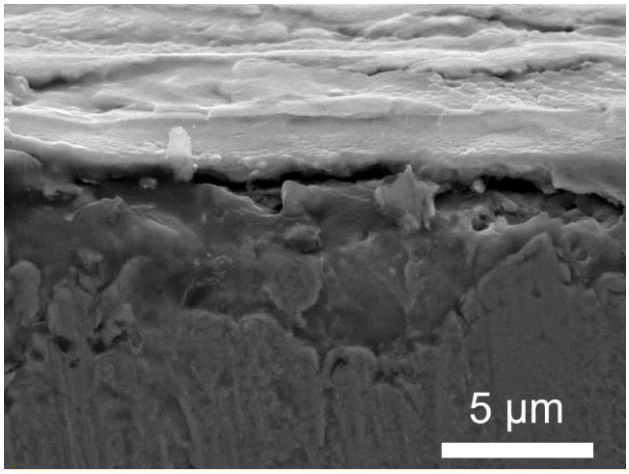

Supplementary Fig. 18 | Side FESEM image of SEI Zn after 10 cycles.

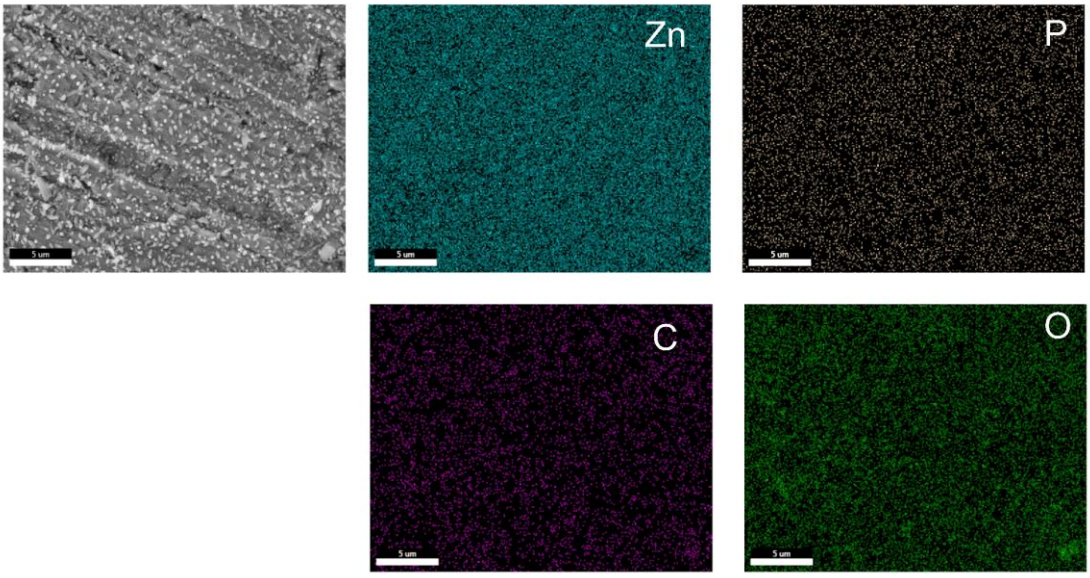

Supplementary Fig. 19 | EDS mapping image of SEI Zn after 10 cycles.

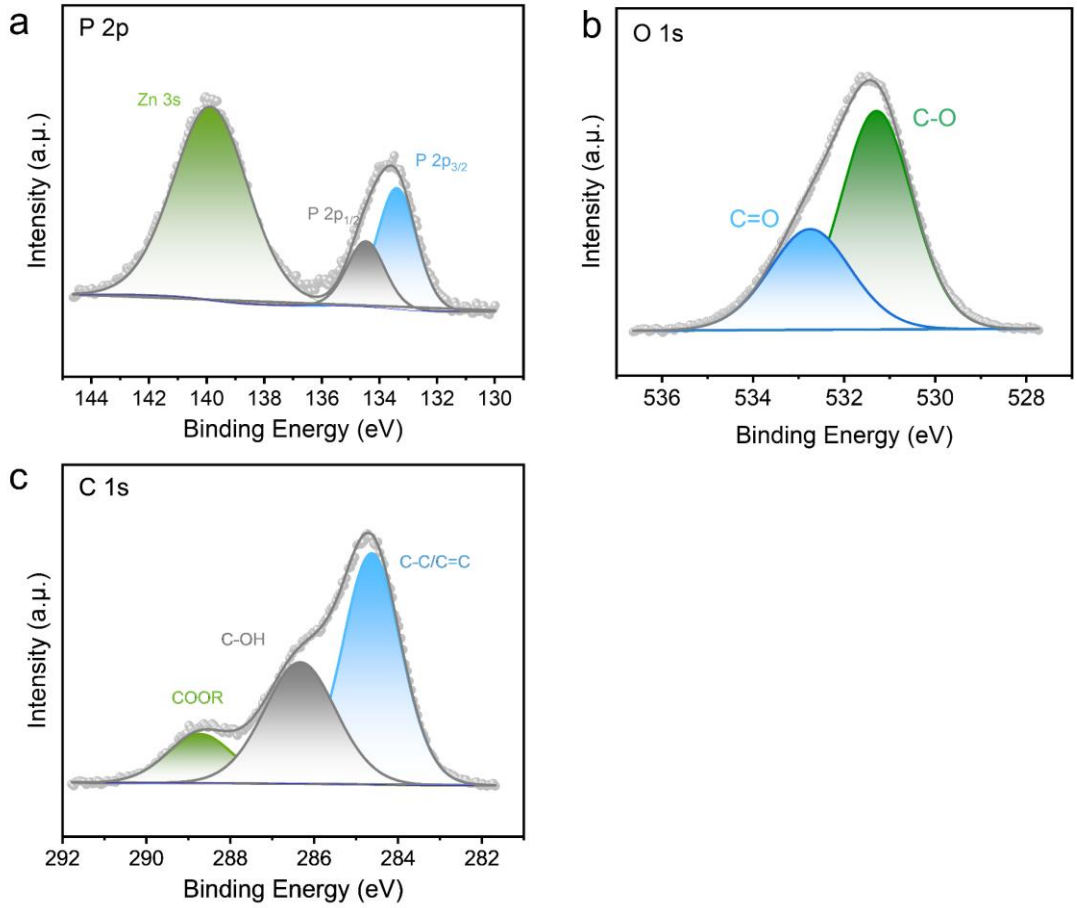

Supplementary Fig. 20 | (a) P 2p (b) O 1s and (c) C 1s XPS spectra of SEI Zn after 10 cycles.

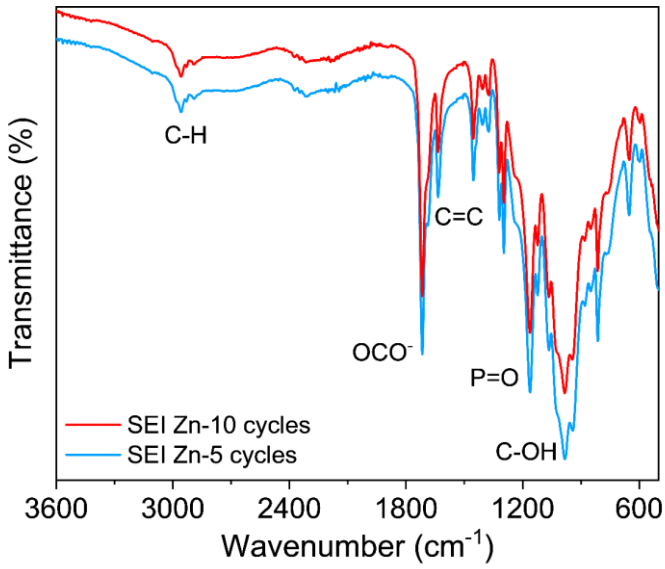

Supplementary Fig. 21 | FTIR Spectra of SEI Zn electrode after 5 and 10 cycles.

7. In Supplementary Fig. 12, how did the author calculate corrosion current density? Typically, fitting is required to obtain this value (i.e., Tafel plot); could you clarify the methodology?

Our Response: Thanks for the question from the reviewer. We apologize for the lack of clarity. The corrosion potential and corrosion current density is calculated by the following method, Using the Tafel extrapolation method, the anode and cathode sections of the polarization curve were linearly fitted. With software such as Origin, the logarithm of the current density (log I) was plotted on the Y-axis and the potential (E) on the X-axis. By solving for the intersection point of the fitting lines, the corrosion potential (E_{corr}) was obtained. Subsequently, the corrosion potential was substituted into the fitting function to derive the corrosion current density (I_{corr}). Please note that the Tafel test and related calculation methods we have been supplemented in the supplementary information.

Related modification has been made in the supplementary information.

(Supplementary Information, Page 36)

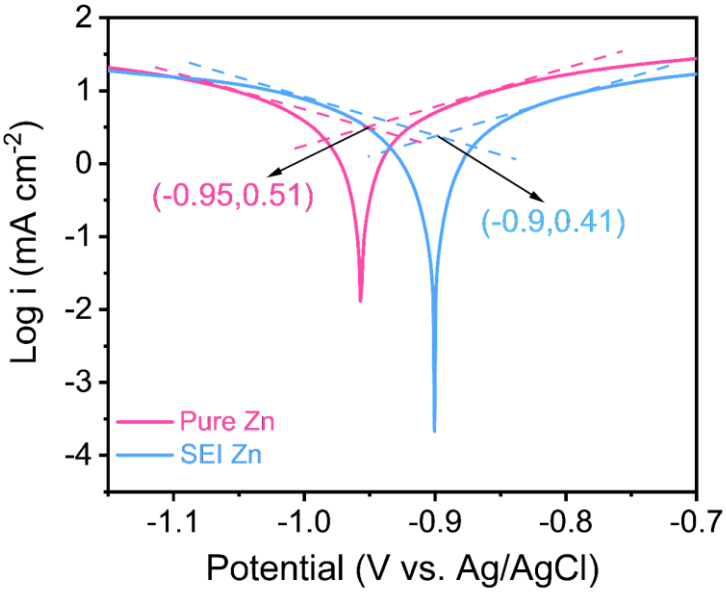

Supplementary Fig. 32 | Tafel curves of pure Zn and SEI Zn electrodes.

The Tafel test uses 3 M $ZnSO_4$ as the electrolyte, pure Zn or SEI Zn electrode as the working electrode, Pt electrode as the opposite electrode, and Ag/AgCl as the reference electrode. The test voltage range is -0.3 to 0.3 V (vs. OCP), and the sweep speed is 1 mV s^{-1}. The corrosion potential and corrosion current density is calculated by the following method, using the Tafel extrapolation method, the anode and cathode sections of the polarization curve were linearly fitted. With software such as Origin, the logarithm of the current density (log I) was plotted on the Y-axis and the potential (E) on the X-axis. By solving for the intersection point of the fitting lines, the corrosion potential (E_{corr}) was obtained. Subsequently, the corrosion potential was substituted into the fitting function to derive the corrosion current density (I_{corr}).

8. The author suggests that the high adsorption energy of SO_4^{2-} in $Zn_3(PO_4)_2$ indicates accelerated Zn^{2+} transport, but this appears to be a superficial and overinterpretation. Could the author provide additional evidence or clarify this correlation?

Our Response: Thanks for the question from the reviewer. We apologize for the lack of clarity. This view is based on the high adsorption energy of SO_4^{2-} on the surface of

$Zn_3(PO_4)_2$ observed in our experiments, the significant increase of Zn^{2+} transfer number at the artificially mixed interface, and the effect of anion adsorption on cation transport reported in the literature. In addition, we cite several related papers that report positive effects of anion adsorption on cation transport in similar systems. These studies provide additional theoretical support for our view. For example, inspired by the chemistry of host-guest interactions, the researchers introduced anion trapping agents (such as β-cyclodextrin β-CD) into the electrolyte of Zn-ion batteries. The cavity inside the β-CD has the right size and electrostatic potential distribution to encapsulate the anions in the electrolyte (such as ClO_4^-), forming an anion trap. This anion trap weakened the barrier of cations (such as Zn^{2+}) migration and increased the number of cations migration (10.1002/anie.202210979). With sodium gluconate (SG) additives, the polar functional group ($-COO^-$) preferentially anchors the Zn anode, thereby altering the migration path of Zn^{2+} and inhibiting side reactions. At the same time, the isolated cations (such as Na^+) in SG provide an electrostatic shielding effect for the uniform deposition of Zn^{2+} on a specific crystal plane, further promoting the migration of cations and the stability of the battery (10.1002/adfm.202402484). By preparing PAN nanofiber film by electrospinning technology and combining it with PEO/$Zn(OTf)_2$ electrolytic liquid phase, PAN skeleton locking anions can form a unique and rapid cation transport mechanism. To achieve a high Zn^{2+} migration number (0.71) (10.1002/adfm.202307736). In summary, anion adsorption in Zn metal batteries promotes cation migration and improves battery performance by forming anion trap, preferential adsorption and crystal surface control. This strategy provides a new idea and method for the development of Zn metal batteries.

9. In Fig. 5b and S16, the authors determined the nucleation overpotential as the difference between the lowest and the stable points on the curve. However, this calculation appears to reflect the difference in driving force between nucleation and crystal growth, rather than the nucleation overpotential. Please check this.

Our Response: Thanks for the question from the reviewer. We apologize for the confusion between nucleation overpotential and the driving force for nucleation and crystal growth. We have made the corresponding revisions in the manuscript.

Related modifications have been made in the revised manuscript and supplementary information.

(Main article, Pages 19-20)

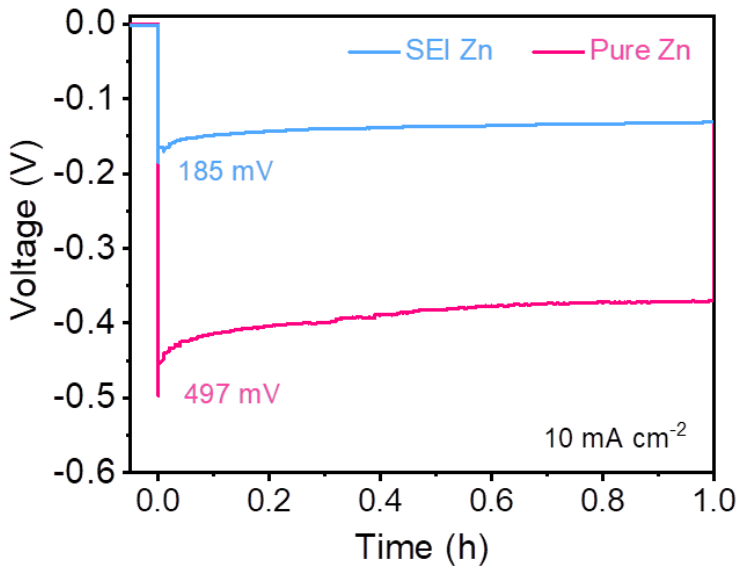

Fig. 5 | b Nucleation overpotential of Pure Zn and SEI Zn electrodes at 10 mA cm^{-2}.

As expected, the pure Zn anode showed high NOP of 70.4, 339.0 and 497.0 mV at current densities of 1, 2 and 10 mA cm^{-2}, respectively. In comparison, SEI Zn exhibits a lower NOP, with values of 22.8, 114.0, and 185.0 mV at current densities of 1, 2, and 10 mA cm^{-2}, respectively.

(Supplementary Information, Page 42)

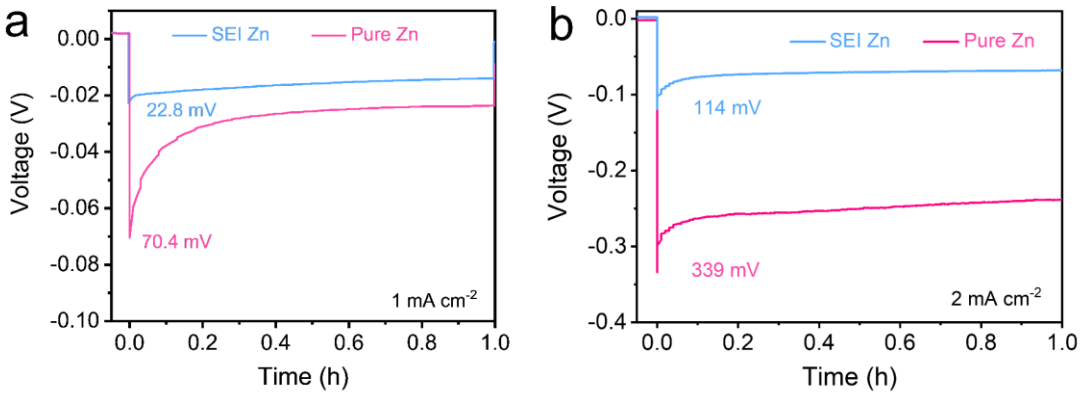

Supplementary Fig. 38 | Nucleation overpotential of Pure Zn and SEI Zn electrodes under the current densities of (a) 1 mA cm^{-2} and (b) 2 mA cm^{-2}.

10. In Fig. 5d, as deposition continues, the layer's thickness increases. Does this imply that zinc is deposited on top of the existing layer? Also, please add scale bars to improve clarity.

Our Response: Thanks for the question from the reviewer. We analyzed the side view of SEI Zn after cycling, and the experimental results showed that Zn^{2+} migrated to the electrode surface under the action of electric field and were reduced to Zn metal. These newly generated Zn metals tended to grow uniformly in the lower layer of artificial SEI, and the artificial SEI morphology remained better with the increase of the overall thickness. At the same time, in order to facilitate readers to accurately understand the size proportion in the image, we have clearly marked the corresponding scale on the picture.

Related modifications have been made in the revised manuscript and supplementary information.

(Main article, Page 20)

In contrast, on the pure Zn surface, the initial deposition of Zn^{2+} was uneven and gradually evolved into dendrites at the original nucleation sites. In order to further clarify the deposition behavior of Zn^{2+} on the SEI Zn electrode, the side morphology of SEI Zn was analyzed after the deposition time was 20 minutes (Supplementary Fig. 39). From the EDS image, it is found that the feature elements C, O and P, which represent the artificial SEI, are obviously present in the top layer. This observation suggests that Zn^{2+} is deposited mainly in the lower regions of the artificial SEI, a phenomenon attributed to the non-conductive nature of the artificial SEI layer. FESEM images show that the SEI layer remains intact after deposition. The retention of this form effectively protects the Zn anode from harmful interactions and promotes uniform deposition of Zn^{2+}. This lays the foundation for the construction of a stable electrode/electrolyte interface, which is critical for improving the performance and durability of Zn-based electrochemical devices.

(Supplementary Information, Page 43)

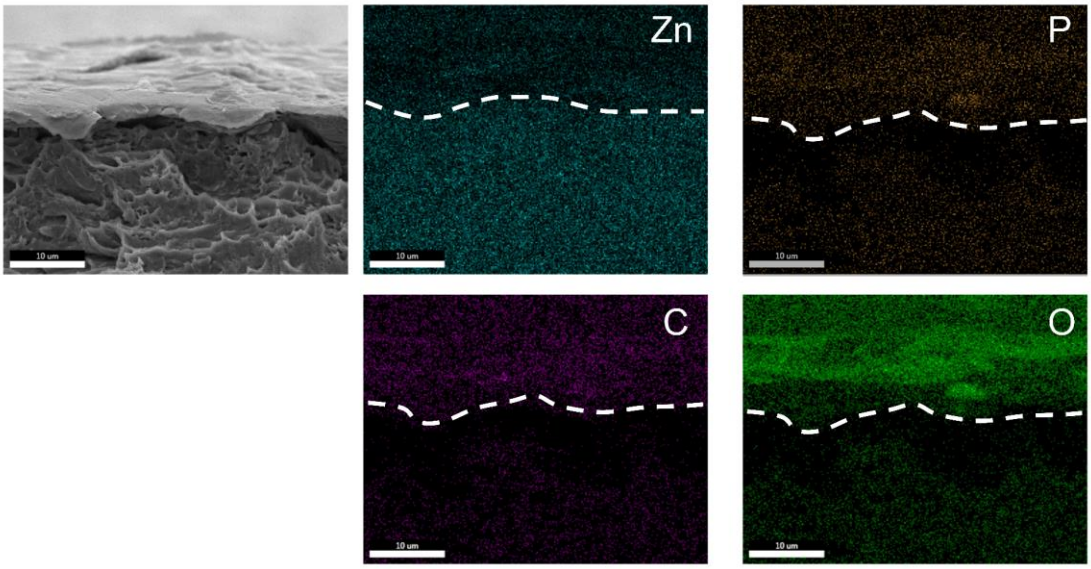

Supplementary Fig. 39 | FESEM and corresponding EDS spectra of the side view of SEI Zn electrode deposited at a current density of 20 mA cm^{-2} for 20 minutes.

11. In Fig. S19, it would be helpful to label the Miller indices for all the peaks and to add 'Intensity (a.u.)' on the y-axis for clarity.

Our Response: Thank you very much for your careful review of our paper and your valuable comments. In response to your suggestions on the modification of Fig. S19, we have made corresponding improvements. Clearly mark the Y-axis as "Intensity (a.u.)"

Related modification has been made in the supplementary information.

(Supplementary Information, Page 46)

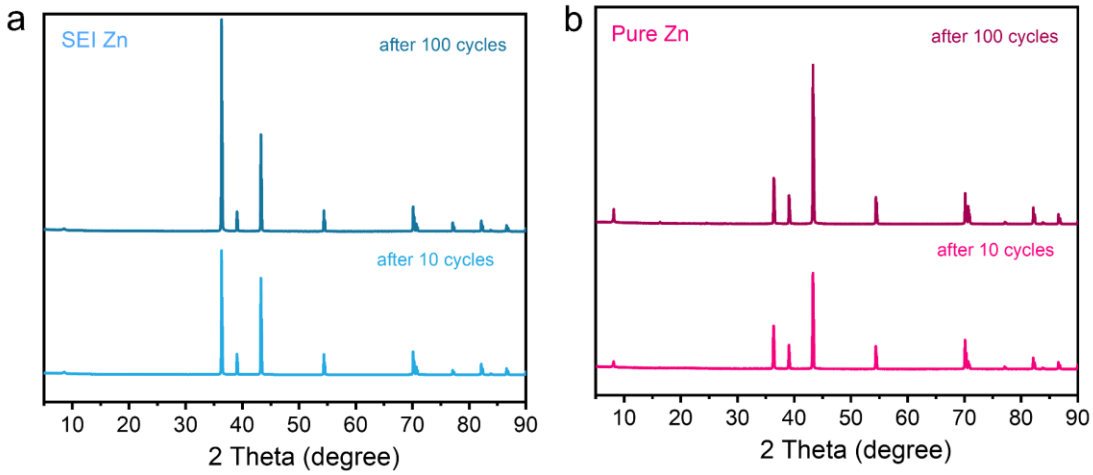

Supplementary Fig. 42 | The XRD patterns of (a) SEI Zn and (b) Pure Zn electrodes after different cycle number.

12. The concept of the paper might be challenging to grasp without scheme 1. Would it be better to place Scheme 1 earlier in the manuscript for improved comprehension?

Our Response: We appreciate the reviewer's insightful suggestion. In contrast to Schemes in other works that emphasize design principles and scientific concepts, the Scheme presented in this study predominantly functions as a synthesis of the preceding research findings. As such, positioning it earlier in the manuscript may not be entirely appropriate. In order to enhance the readers' comprehension and to refine the logical structure of the article, we have made strategic revisions and elaborations in the

introduction section.

Related modification has been made in the revised manuscript.

(Main article, Pages 5-6)

This unique SEI enables a tandem regulation of interfacial side reactions, Zn^{2+} de-solvation, interfacial transport kinetics, and preferential Zn(002) deposition, thereby significantly enhancing the stability of the Zn anode. As demonstrated, the cycle lifespan ...

13. For all cycling performance data, could you provide a zoomed-in view of the long term cycling performance (Time (h) vs Voltage (V))? This would help clarify the reaction behavior during cycling, particularly indicating whether the pattern resembles a square wave (suggesting non-uniform or unstable plating/stripping) or a typical curve shape (indicating uniform and stable ion flux and plating/stripping)?

Our Response: Thanks for the question from the reviewer. In revisiting our experimental data, we paid particular attention to the relationship between time and voltage to gain insight into the reaction behavior during the cycle. Based on your suggestions, we extracted data for key cycle intervals and created a zoomed-in view to more clearly show voltage trends over time. A broader view of the long-term cycle performance data reveals that the voltage changes over time in a more stable curve shape rather than an obvious square wave shape. This indicates that the ion flux and plating/stripping behavior are relatively uniform and stable throughout the cycle. Specifically, the voltage curve maintains a relatively consistent trend in both the rising and falling stages of each cycle, and there are no obvious fluctuations or sudden changes, which supports our discussion of cycle stability in the paper.

Related modifications have been made in the revised manuscript and supplementary information.

(Main article, Page 24)

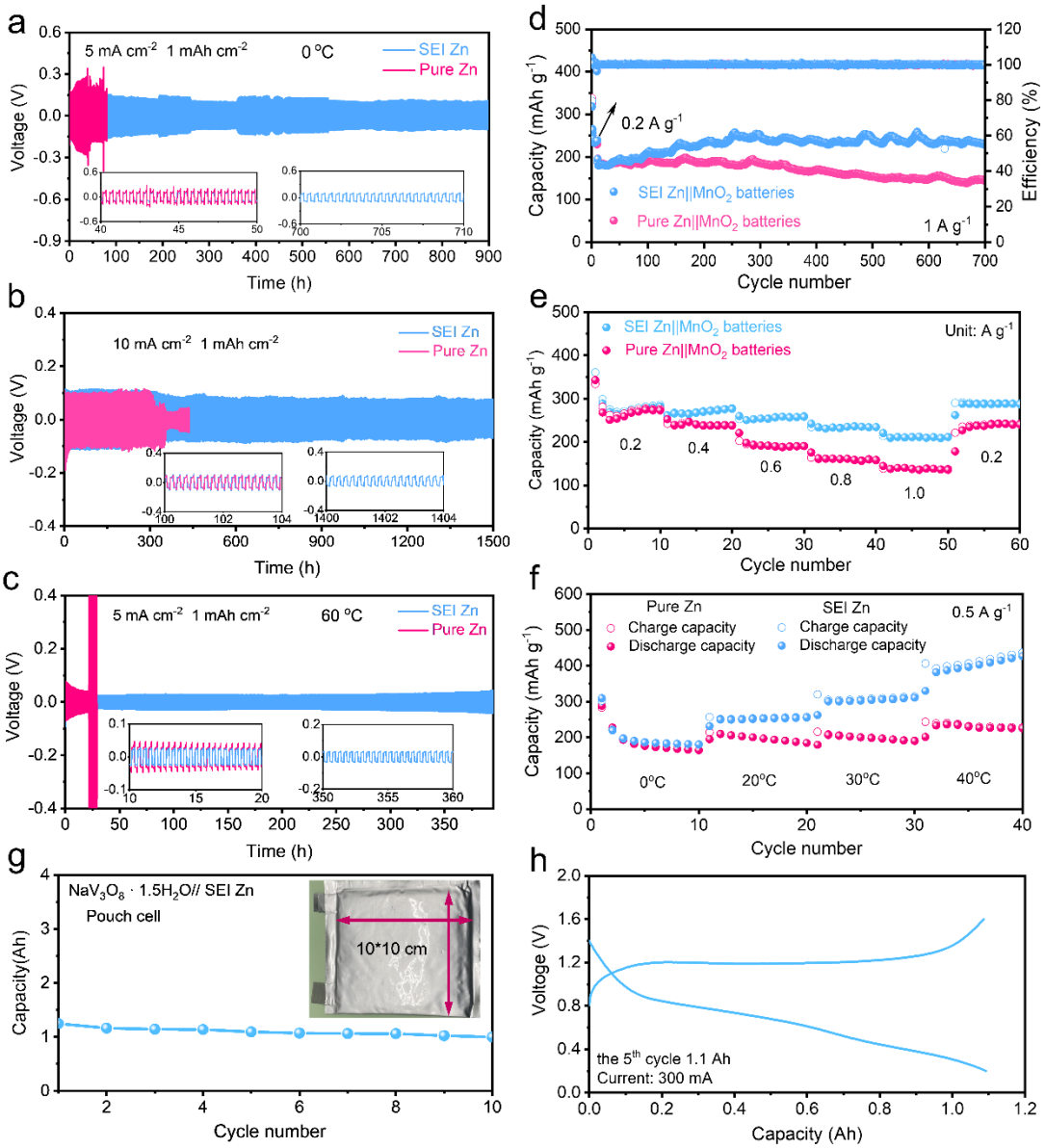

Fig. 6 | Wide temperature range application and large capacity pouch cell performance of SEI Zn. Long-term cycle performance of pure Zn and SEI Zn anodes at the conditions of **(a)** 5 mA cm^{-2}, 1 mAh cm^{-2} and 0°C; **b** 10 mA cm^{-2}, 1 mAh cm^{-2} and 25°C; and (**c**) 5 mA cm^{-2}, 1 mAh cm^{-2} and 60°C. **d** Cycle performance of the Zn||MnO_2 batteries at 1 A g^{-1}. Rate performance of (**e**) various current densities, and (**f**) various temperature environments. **g** Cycle performance test of SEI Zn||$NaV_3O_8 \cdot 1.5H_2O$ pouch battery and its (**h**) corresponding GCD curve.

(Supplementary Information, Page 47)

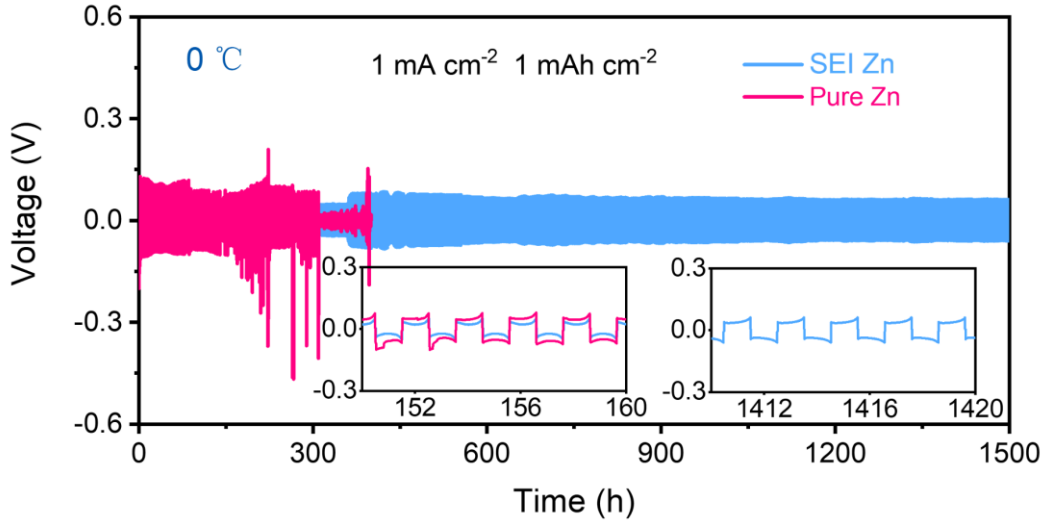

Supplementary Fig. 43 | Long-term cycle performance of pure Zn and SEI Zn electrodes at the condition of 1 mA cm^{-2} and 1 mAh cm^{-2} at 0°C.

(Supplementary Information, Page 49)

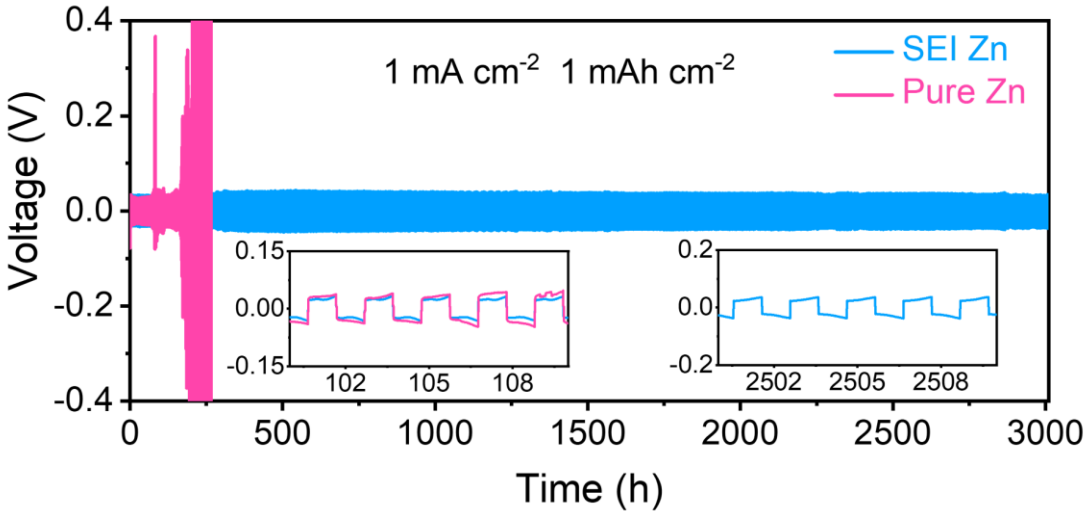

Supplementary Fig. 45 | Long-term cycle performance of pure Zn and SEI Zn electrodes at the condition of 1 mA cm^{-2} and 1 mAh cm^{-2} at 25°C.

(Supplementary Information, Page 50)

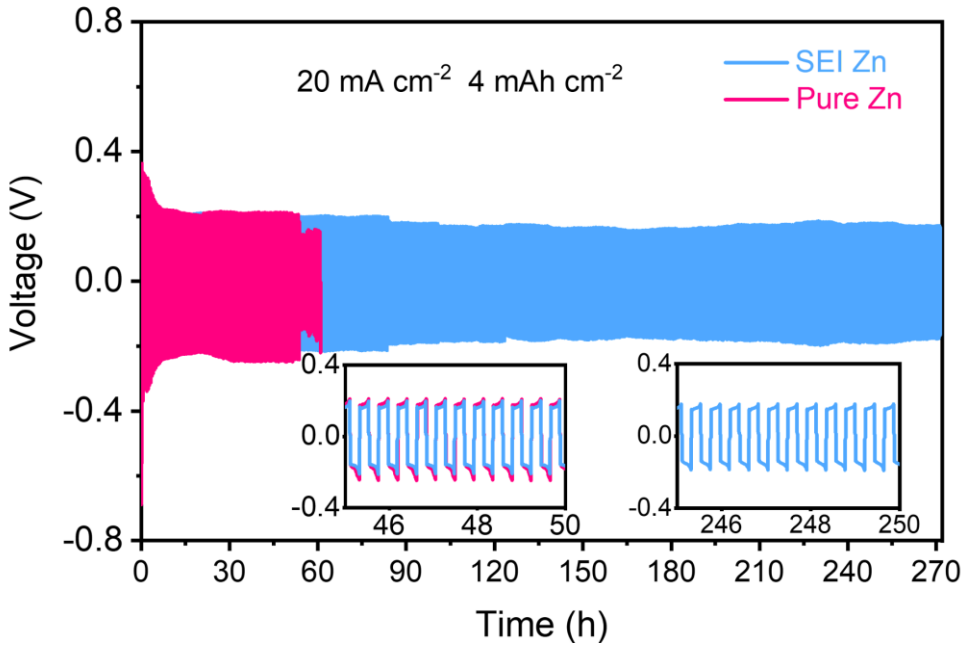

Supplementary Fig. 46 | Long-term cycle performance of pure Zn and SEI Zn electrodes at the condition of 20 mA cm^{-2} and 4 mAh cm^{-2} at 25℃.

14. Could the author include CV data for the full cell to determine whether any side reactions occur during cycling?

Our Response: Thanks for the question from the reviewer. We have included the cyclic voltammetry (CV) data of the whole battery in our analysis to explore the occurrence of any side reactions during the cycle. The experimental results show that, the CV curves of the SEI Zn||MnO_2 system exhibit the same redox reaction behavior as those of batteries using pure Zn electrodes, as shown in supplementary Fig. 51. This observation shows that the cathode reaction mechanism remains unchanged and no side reactions occur during the cycle.

Related modifications have been made in the revised manuscript and supplementary information.

(Main article, Page 26)

The cyclic voltammetry (CV) curves of the SEI Zn||MnO_2 system exhibit the same redox reaction behavior as those of batteries using pure Zn electrodes, as shown in supplementary Fig. 51. This observation shows that the cathode reaction mechanism remains unchanged and no side reactions occur during the cycle.

(Supplementary Information, Page 55)

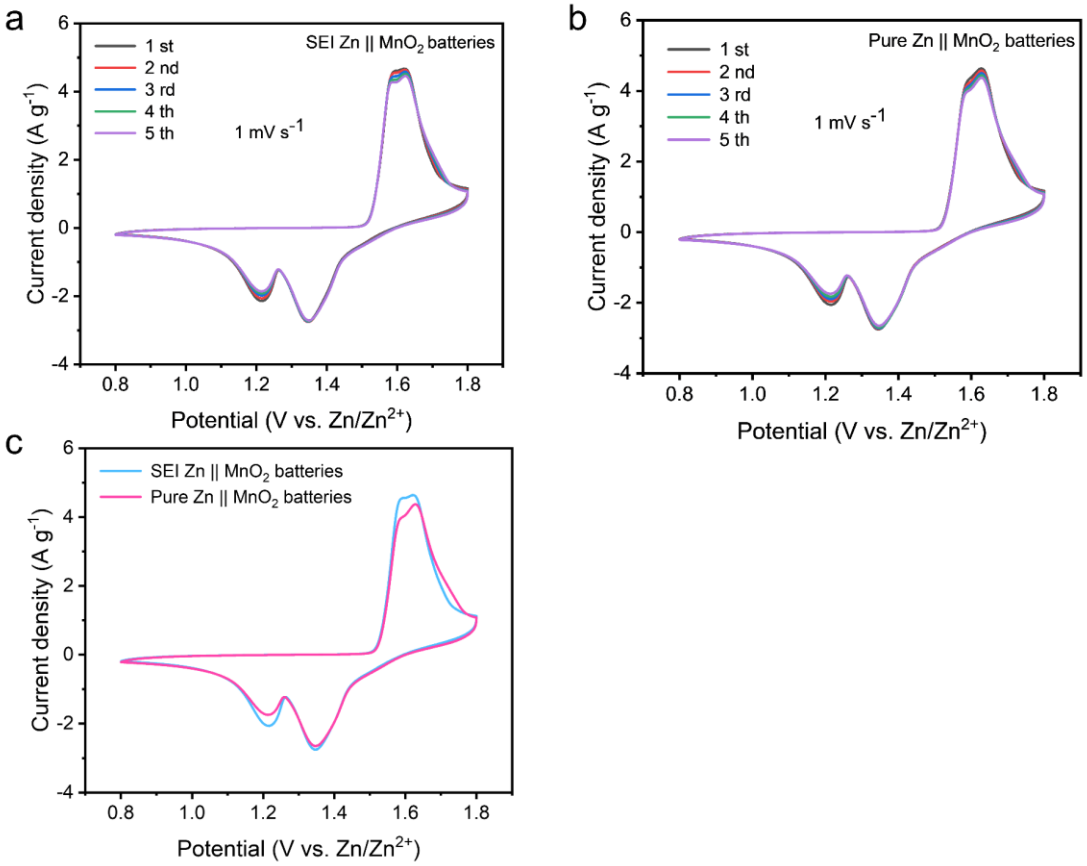

Supplementary Fig. 51 | The CV curves of Zn||MnO_2 batteries with (a) SEI Zn (b) Pure Zn in the initial 5 cycles at a scanning rate of 1 mV s^{-1}. (c) Their comparison of CV curves in the second cycle.

15. To clearly assess the performance of SEI Zn at full cell made with MnO_2, it is essential to isolate the SEI Zn electrode as the sole independent variable. However, the author has added $MnSO_4$ as an electrolyte additive, which could influence the results.

Could you rerun the cell without $MnSO_4$ additive to better isolate the SEI Zn electrode's performance?

Our Response: Thanks for the question from the reviewer. In accordance with your suggestion, we conducted supplementary experiments to operate the entire battery system without the inclusion of $MnSO_4$ as an additive. This approach enabled us to more accurately isolate the performance characteristics of the SEI Zn electrode and to assess its specific influence on the overall battery performance. The experimental outcomes demonstrate that the cycle stability of the battery featuring the SEI Zn||MnO_2 is enhanced in the absence of $MnSO_4$. This observation validates the positive impact of the artificial SEI Zn layer on the comprehensive performance of the Zn||MnO_2 battery system. These findings further underscore the significance of the SEI Zn electrode in optimizing battery performance and highlight the importance of conducting rigorous experimental validation to isolate and understand the contributions of individual components within complex battery systems.

Related modifications have been made in the revised manuscript and supplementary information.

(Main article, Page 26-27)

Simultaneously, to eliminate the potential interference of $MnSO_4$ in the electrolyte on the performance of the SEI Zn, we assembled a Zn||MnO_2 battery utilizing SEI Zn and pure Zn as the anodes, MnO_2 as the cathode, and 3 M $ZnSO_4$ as the sole electrolyte. At a current density of 1 A g^{-1} (following an initial activation phase of 10 cycles at 0.2 A g^{-1}), the stability of the full battery equipped with the SEI Zn anode was observed to be enhanced, as evidenced in Supplementary Fig. 52. After undergoing 1200 cycles, the SEI Zn||MnO_2 full battery exhibited a discharge specific capacity of 142.87 mAh g^{-1}, surpassing the performance of the pure Zn||MnO_2 full battery, which delivered 108.30 mAh g^{-1} after 500 cycles. These findings further corroborate the beneficial effects of the artificial SEI Zn layer on the overall performance of the Zn||MnO_2 battery system.

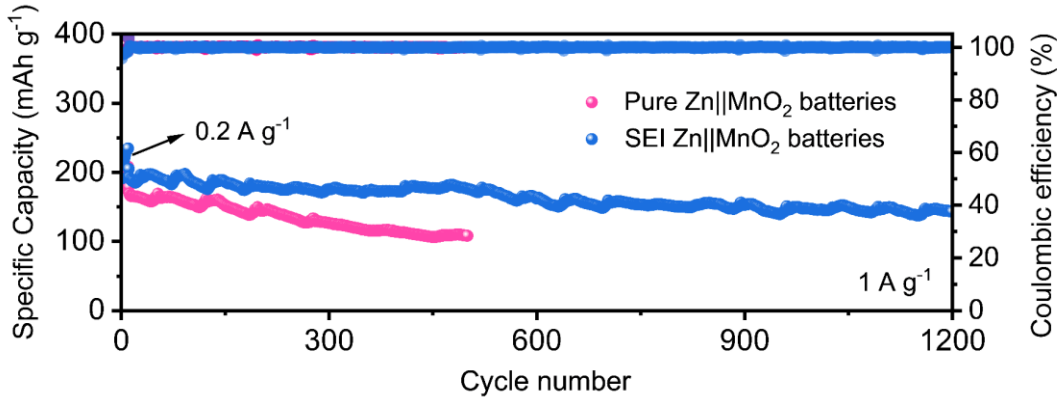

Supplementary Fig. 52 | Cycle performance test of the Zn||MnO_2 batteries in 3 M $ZnSO_4$ electrolyte and at the current density of 1 A g^{-1}.

Reviewer #3 (Remarks to the Author):

Manuscript ID: NCOMMS-24-62966

An Electrochemically Driven Hybrid Interphase-Supported Multi-scene Compatible Zinc Metal Anodes

Comments to the Authors

In this manuscript, the authors developed organic-inorganic ($Zn_3(PO_4)_2$)-based solid electrolyte interphase (SEI) during electrochemical cycling. The SEI fabrication method is very impressive because it is thought to be an application of the concept that electrolyte additives participate in the formation of stable SEI during electrochemical reactions to artificial SEI. It seems that this transition in occurrence allowed for the formation of a more robust and stable SEI. Also, the authors especially closely evaluated the performance of the developed SEI Zn from various aspects (the Scheme 1 in the Supporting Information) for practical aqueous Zn metal batteries and demonstrated excellent performances. However, studies on forming in-situ $Zn_3(PO_4)_2$-based SEI have already been reported in various previous researches. Therefore, the authors should present a more definite novelty and merits for the electrochemically driven hybrid interphase. In addition, some of the analyses need to be supplemented in the discussion and logicality. After the major comments mentioned below are well addressed, this manuscript should be considered for publication in Nature Communication.

Our Response: We appreciate the reviewer for the encouraging comment and very constructive question and suggestion.

1. There have been many previous reports on $Zn_3(PO_4)_2$-based SEI (10.1002/smll.202310497, 10.1002/anie.202215600, 10.1002/aenm.202301193, 10.1002/adma.202007416, and 10.1039/D1EE00308A, etc.). This study should be supplemented with a clearer explanation of the differences from previously reported $Zn_3(PO_4)_2$-based SEI.

Our Response: Thanks for the question from the reviewer. Indeed, the use of $Zn_3(PO_4)_2$

for the modification of Zn anodes has been extensively reported in the literature. We have thoroughly reviewed the relevant references provided by the reviewers, as well as other studies focused on the design of $Zn_3(PO_4)_2$-based SEIs. However, we have identified certain limitations in these approaches when compared to the current work. For instance, in previous research, investigators have employed NaH_2PO_4 solution to etch the Zn anode surface (10.1002/smll.202310497), or fabricated $Zn_3(PO_4)_2$ or phosphate-based protective layers using techniques such as blade coating (10.1002/adfm.202004885) and hydrothermal methods (10.1002/adfm.202208230). These methods are primarily ex situ approaches. In contrast, in situ SEI layers can dynamically adjust their structure and composition during the battery's charge-discharge cycles, effectively accommodating changes on the electrode surface, thus offering superior compatibility. Furthermore, many studies have explored electrolyte modification strategies to form $Zn_3(PO_4)_2$-based SEIs. However, these approaches often involve the incorporation of substantial amounts of phosphorus-containing organic solvents (10.1038/s41467-023-41276-9, 10.1002/anie.202215600, 10.1002/aenm.202301193), which impede the reaction kinetics of the battery and run counter to the design principles of aqueous Zn-ion batteries. Although some works have suggested the use of small quantities of inorganic additives to promote the in situ formation of $Zn_3(PO_4)_2$ SEIs (10.1002/adma.202007416, 10.1039/D1EE00308A), the purely inorganic $Zn_3(PO_4)_2$ SEIs often lack sufficient flexibility and strong adhesion to the anode, making the SEI susceptible to cracking or detachment, thereby compromising the battery's performance. In this work, we have developed an organic-inorganic hybrid $Zn_3(PO_4)_2$-based SEI using an electrochemical in situ method, which exhibits superior interfacial adhesion and rapid reaction kinetics, offering significant advantages over previously reported approaches.

Related modifications have been made in the revised manuscript.

(Main article, Page 4)

In detail, single organic component will be in-situ transformed into highly dispersed $Zn_3(PO_4)_2$ nanocrystalline-enriched hybrid phases after initial electrochemical cycles.

This electrochemically mediated in situ synthesis approach facilitates the development of a highly compatible and flexible $Zn_3(PO_4)_2$-based hybrid SEI on the Zn anode surface, obviating the need for extensive incorporation of organic solvents. Ex-situ atomic force microscopy (AFM) research also indicates the significantly enhanced modulus but reduced adhesion of the interphase, owing to the decomposition of high-adhesion organic component and formation of high-modulus inorganic nanocrystalline.

2. A clear discussion is needed regarding the mechanism by which the 2-methyl-2-acrylate-2-hydroxyethyl ester phosphate ester (MAHEPE) layer transformed to $Zn_3(PO_4)_2$ during electrochemical cycling.

Our Response: Thanks for the question from the reviewer. As depicted in Supplementary Fig. 7, $Zn_3(PO_4)_2$ is not observed to form during the electrode's resting phase; however, during the Zn deposition/stripping cycles, characteristic XRD peaks corresponding to ($\bar{3}$ 02), ($\bar{1}$ 06), and (106) plane of $Zn_3(PO_4)_2$ phase emerge on the SEI Zn surface, progressively intensifying with continued cycling. This observation suggests that the formation of $Zn_3(PO_4)_2$ is electrochemically driven. Specifically, during Zn deposition/stripping on the electrode surface, Zn^{2+} traverse the SEI, with a portion of them reacting with phosphate groups within the SEI to yield $Zn_3(PO_4)_2$. Furthermore, the TOF-SIMS analysis of the SEI Zn surface provides compelling evidence for the electrochemically-driven evolution of $Zn_3(PO_4)_2$. As depicted in Supplementary Figs. 10-11, in the pristine state, a prominent Zn-O signal is observed on the SEI Zn surface, which can be attributed to the intimate adhesion of the coating to the Zn anode via oxygen-containing functional groups. Additionally, the presence of minor amounts of $Zn\text{-}PO_x$ and Zn-PO species suggests that the phosphate groups, which are zincophilic in nature, interact with the Zn at the interface between the coating and the anode. Upon cycling, there is no significant variation in the Zn-O component, indicating the persistent adhesion of the coating to the anode. In contrast, the $Zn\text{-}PO_x$ and Zn-PO signals notably intensify, underscoring that during the charge-discharge

process, the migration of Zn^{2+} within the SEI results in the formation of an increased amount of $Zn_3(PO_4)_2$.

Related modifications have been made in the revised manuscript and supplementary information.

(Main article, Pages 9-10)

To further explore the phase evolution of the solid electrolyte interface (SEI) on the Zn surface after cycling, the XRD, XPS and FTIR characterization were performed (Supplementary Figs. 7-9). The findings reveal that the immersion of SEI Zn in a 3 M $ZnSO_4$ did not induce the formation of any novel phases on its surface. Conversely, characteristic diffraction peaks of the $Zn_3(PO_4)_2$ phase were detected at 31.96°, 33.11°, and 34.68° on the surface of SEI Zn after cycling. These peaks correspond to the ($\overline{3}$ 02), ($\overline{1}$ 06), and (106) crystal planes (PDF#97-006-8362). This phenomenon suggests that, under the electrochemical driving force, Zn^{2+} migrate through the SEI and engage in a reaction with PO_4^{3-}, thereby catalyzing the formation of insoluble $Zn_3(PO_4)_2$. Note that, the peaks were skewed to the left due to the smaller grain size and larger lattice constant. In the XPS spectrum, for the P 2p region, peaks at 133.58 eV and 134.43 eV associated with P-O bonds were clearly visible. In the infrared spectrum, the wavenumbers at 1161.15 cm^{-1} confirm the existence of P=O bond, which were representative peaks of $Zn_3(PO_4)_2$. Based on the above experimental results indicate that the surface of the SEI Zn anode spontaneously evolves into an organic-inorganic hybrid layer after cycling.

The evolutionary process of interphase can be further confirmed by time-of-flight secondary ion mass spectrometry (TOF-SIMS). Fig. 2g depict the 3D elemental distributions of PO_4^{3-}, C, and O. It is evident that the PO_4^{3-} signal is relatively uniformly distributed across the entire plane, indicating the spontaneous construction of the artificial SEI into inorganic $Zn_3(PO_4)_2$. TOF-SIMS analysis was performed in positive ion mode to carefully analyze the three-dimensional distribution of Zn, Zn-O, Zn-PO_x and Zn-PO bonds before and after 3 cycles process, as shown in Supplementary Figs.

10-11. The comparative analysis shows that the signal strength of Zn-O bonds is basically unchanged before and after the cycle. The results show that Zn preferentially binds oxygen atoms on organic components at SEI Zn. Notably, at the initial state, the Zn-PO_x and Zn-PO components mainly originate from the intimate contact between the Zn anode and the PO_4^{3-} groups in the SEI. After cycling, the signal strength of both Zn-PO_x and Zn-PO bonds increased after cycling. This enhancement is attributed to electrochemically derived $Zn_3(PO_4)_2$ during cycling, resulting in the conversion of the organic coating to the organic/inorganic hybrid phase.

(Supplementary Information, Pages 10-14)

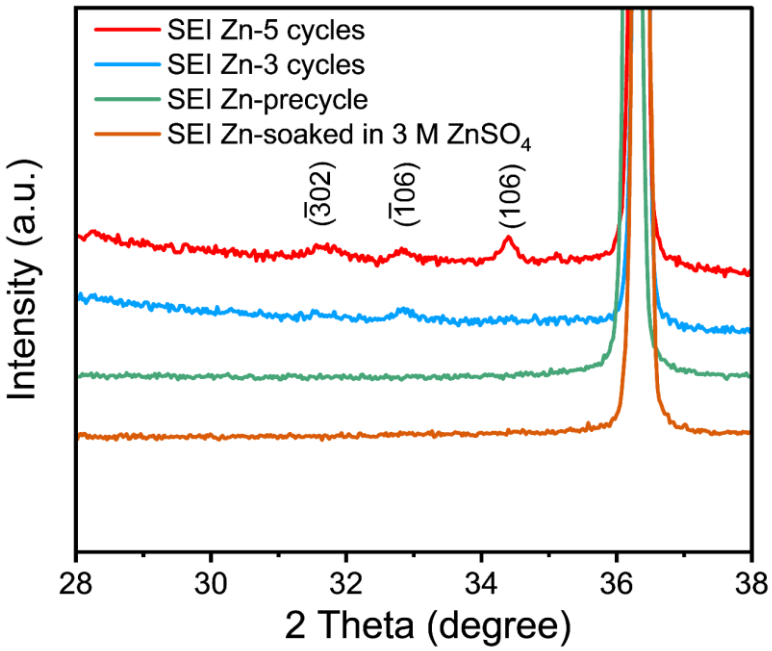

Supplementary Fig. 7 | XRD patterns of the cycled SEI Zn, precycle SEI Zn and soaked SEI Zn surface.

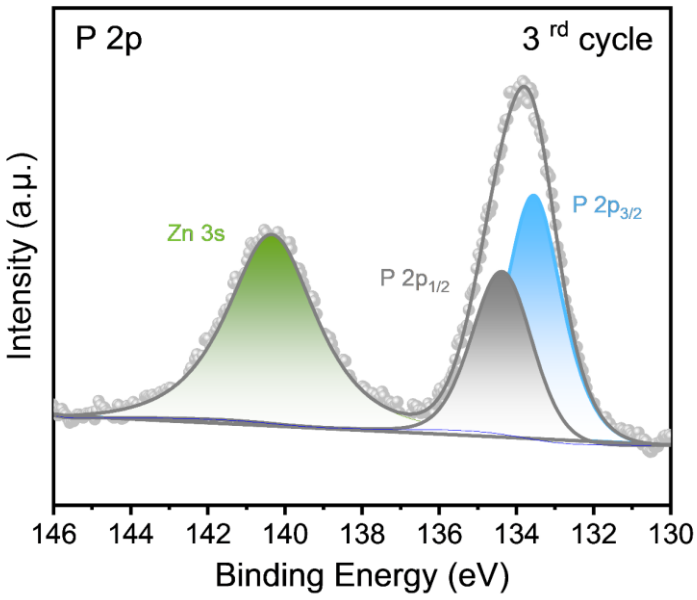

Supplementary Fig. 8 | P 2p XPS spectra of SEI Zn surface after 3 cycles.

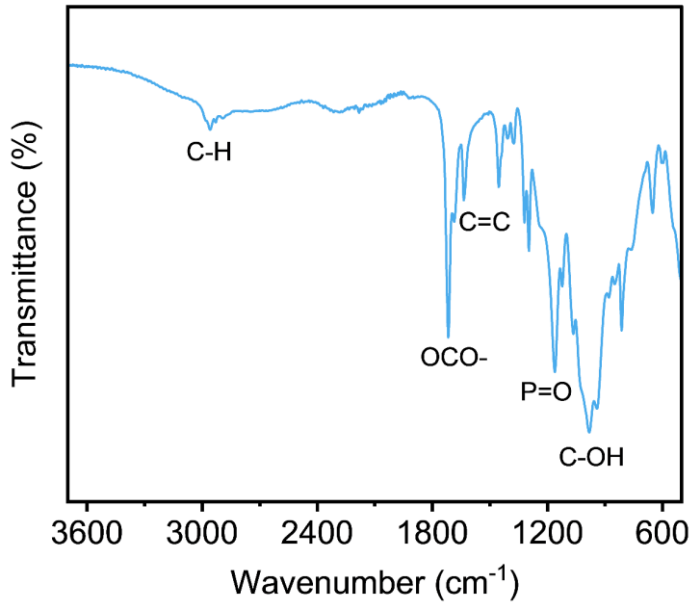

Supplementary Fig. 9 | FTIR spectra of SEI Zn surface after 3 cycles.

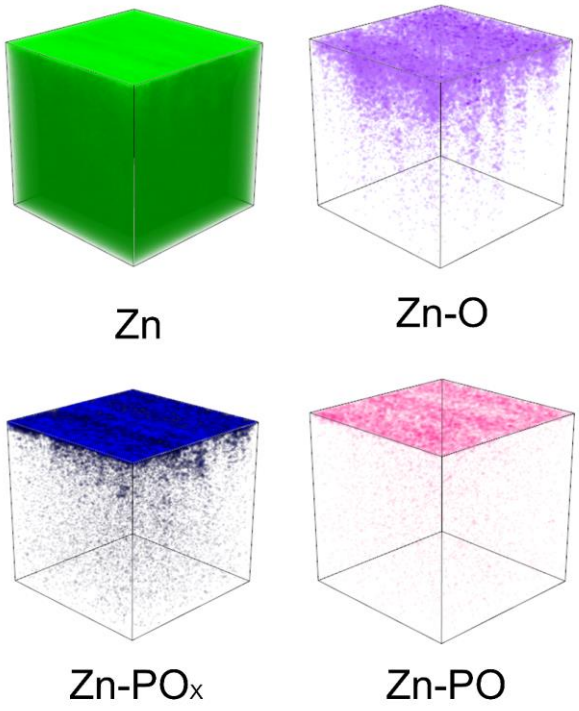

Supplementary Fig. 10 | TOF-SIMS 3D reconstruction of SEI Zn surface before cycling.

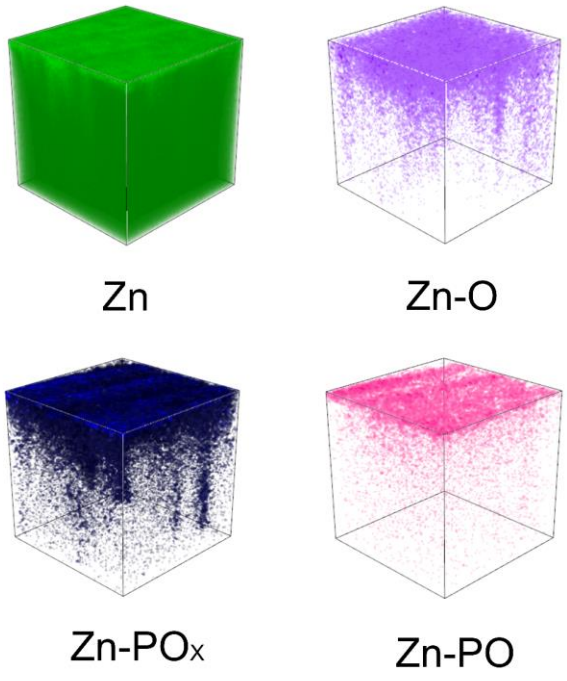

Supplementary Fig. 11 | TOF-SIMS 3D reconstruction of SEI Zn surface after 3 cycles.

3. How were the concentration and coating thickness of the solution containing MAHEPE optimized?

Our Response: Thanks for the question from the reviewer. We have taken a systematic approach in optimizing the concentration and coating thickness of solutions containing MAHEPE. First, through a series of pre-experiments, we determined an initial range of MAHEPE solution concentrations designed to cover key concentration regions that are likely to exhibit the best performance. Then, using the control variable method, we set several concentration gradients in this concentration range and analyze the specific scraping conditions of the prepared coatings at each concentration. After determining the optimal concentration, further focus is placed on the optimization of the coating thickness. We prepared a series of samples with different coating thicknesses. The electrochemical properties of Zn||Zn-symmetric cells with coating at each concentration were tested to evaluate the effect of coating thickness on the properties of the cells. Finally, by comprehensively comparing various parameters at different concentrations and coating thickens, we determined the optimal concentration (0.02 g mL^{-1}) and coating thickness (200 μm) of the MAHEPE solution, which play a key role in ensuring coating uniformity, improving the stability of the electrode and electrolyte interface, and optimizing the overall performance of the battery. This optimization process not only improves our experimental efficiency, but also lays a solid foundation for subsequent battery performance improvements.

Related modifications have been made in the revised manuscript and supplementary information.

(Main article, Page 6)

Fig. 1a shows the preparation process of SEI Zn, the optimized conditions of the preparation process were shown in Supplementary Figs. 1-2 where an organic layer is coated on the surface through a simple doctor blade method.

(Supplementary Information, Pages 3-5)

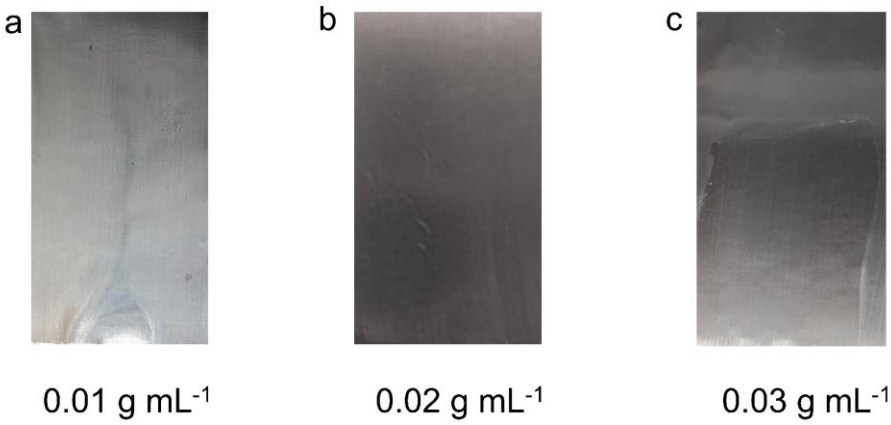

Supplementary Fig. 1 | Optical images of SEI Zn prepared by scraping coating with solutions of different MAHEPE concentrations. (a) 0.01 g mL^{-1}, (b) 0.02 g mL^{-1}, (c) 0.03 g mL^{-1}.

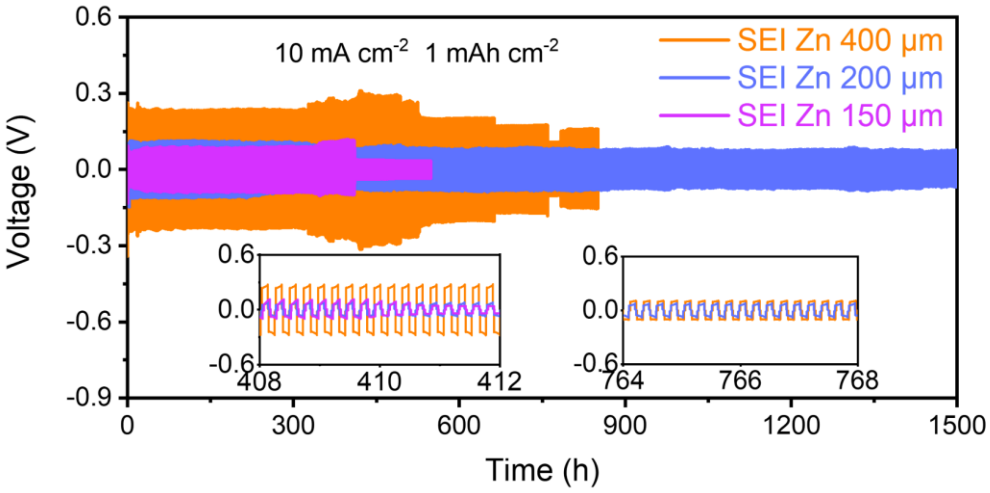

Supplementary Fig. 2 | Long cycle performance of Zn||Zn symmetric batteries assembled with SEI Zn prepared by scraping coating with different thicknesses.

In initial investigation of the process conditions, the influence of the concentration of MAHEPE dispersed in ethanol was investigated. Specifically, solutions with concentrations of 0.01 g mL^{-1}, 0.02 g mL^{-1}, and 0.03 g mL^{-1} were prepared, while all other conditions were held constant. These solutions were subsequently applied to Zn foil via a scraping technique (Supplementary Fig. 1). Experimental outcomes revealed that solutions with concentrations of 0.01 g mL^{-1} and 0.03 g mL^{-1} resulted in non-

uniform coatings. This phenomenon may be attributed to the insufficient viscosity of the thinner solution, preventing adequate adhesion of organic matter to the Zn metal surface, and the excessive concentration of the thicker solution, leading to uneven scraping. Consequently, a solution concentration of 0.02 g mL^{-1} was selected for further study.

Subsequently, we explored the optimal thickness of the scraped coating. Using the 0.02 g mL^{-1} solution, SEI Zn electrodes with thicknesses of 150 μm, 200 μm, and 400 μm were fabricated and assembled into Zn||Zn symmetric batteries. These batteries underwent long-cycle testing at a current density of 10 mA cm^{-2} with a capacity of 1 mAh cm^{-2} at 25°C (Supplementary Fig. 2). The results indicated that the electrode with a 400 μm thickness exhibited a larger polarization voltage, whereas the electrode with a 150 μm thickness short-circuited within 420 h. Notably, the 200 μm SEI Zn||Zn symmetric battery demonstrated stable cycling for 1500 h, demonstrating excellent reversibility of Zn deposition/stripping. Therefore, 200 μm was selected as the best scraping thickness in this research.

4. Generally, the binding energy for C-C of C 1s is known to be 284.8 eV. In Fig. 1i-j and Supplementary Fig. 1, is there a reason why the binding energy of C-C of C 1s is 284.58? If not, refitting after calibration based on C-C binding energy is required.

Our Response: Thanks for the question from the reviewer. The accurate measurement of binding energy is essential for understanding the chemical composition and bonding state of the material. Therefore, we re-examined the experimental data and analysis methods and decided to recalibrate and fit the experimental data based on the standard binding energy of the C-C bond (284.8 eV). With this step, we expect to be able to more accurately reflect the true chemical state of the sample and improve the reliability and accuracy of the data.

Related modifications have been made in the revised manuscript and supplementary information.

(Main article, Pages 6-7)

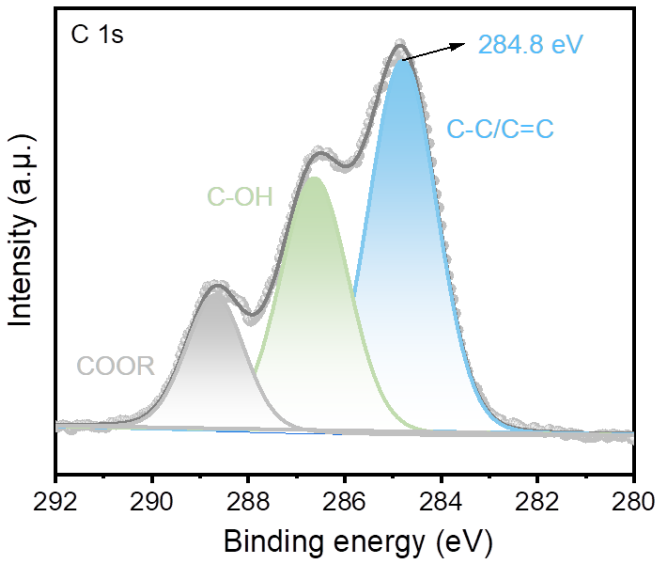

Fig. 1 | **(j)** C 1s XPS spectra of SEI Zn.

X-ray Photoelectron Spectroscopy (XPS) further analyzed the chemical composition and surface element state of the modified layer (Figs. 1i-j and Supplementary Fig. 4). Firstly, for P 2p, the peaks at 133.73 and 134.48 eV may be related to P-O bonds. Then, for C 1s, the peaks at 284.8, 286.65 and 288.5 eV correspond to C-C/C=C, C-OH and COOR respectively.

5. To further demonstrate the transformation of MAHEPE to $Zn_3(PO_4)_2$ during electrochemical cycling, it would be helpful to also present the XPS data after cycling.

Our Response: Thanks for the question from the reviewer. We supplemented the post-cycle XPS data and analyzed the key energy levels of the electrode material such as C 1s, O 1s, P 2p and Zn 2p after cycling to evaluate the chemical composition and bonding state of the material surface.

Related modifications have been made in the revised manuscript and supplementary information.

(Main article, Page 9)

In the XPS spectrum, for the P 2p region, peaks at 133.58 eV and 134.43 eV associated

with P-O bonds were clearly visible. In the infrared spectrum, the wavenumbers at 1161.15 cm^{-1} confirm the existence of P=O bond, which were representative peaks of $Zn_3(PO_4)_2$. Based on the above experimental results indicate that the surface of the SEI Zn anode spontaneously evolves into an organic-inorganic hybrid layer after cycling.

(Main article, Page 10)

Meanwhile, the signals of C and O elements also exhibit relatively uniform distribution across the entire plane, combined with the XPS data results (Supplementary Fig. 12), O 1s analysis showed that at 531.33 eV and 532.78 eV, corresponding to the C-O and C=O bonds, respectively. Peaks at 284.8, 286.53, and 288.83 eV in the C 1s correspond to C-C/C=C, C-OH, and COOR, respectively, which can be attributed to organic components within the SEI.

(Supplementary Information, Page 11)

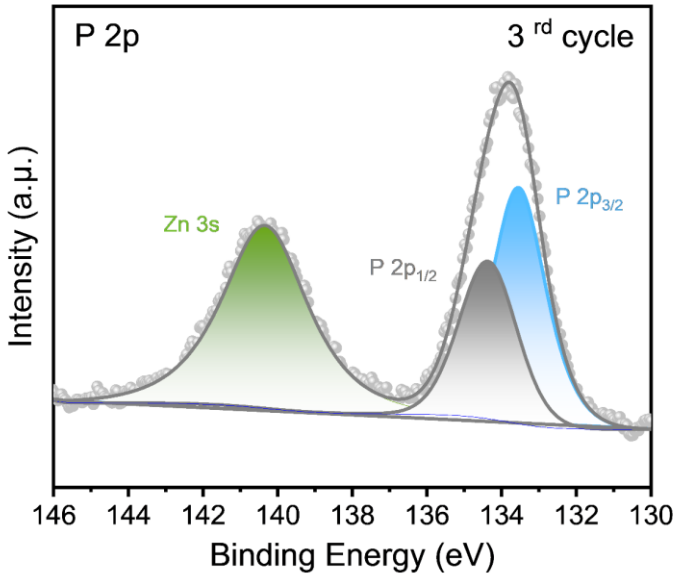

Supplementary Fig. 8 | P 2p XPS spectra of SEI Zn surface after 3 cycles.

(Supplementary Information, Page 15)

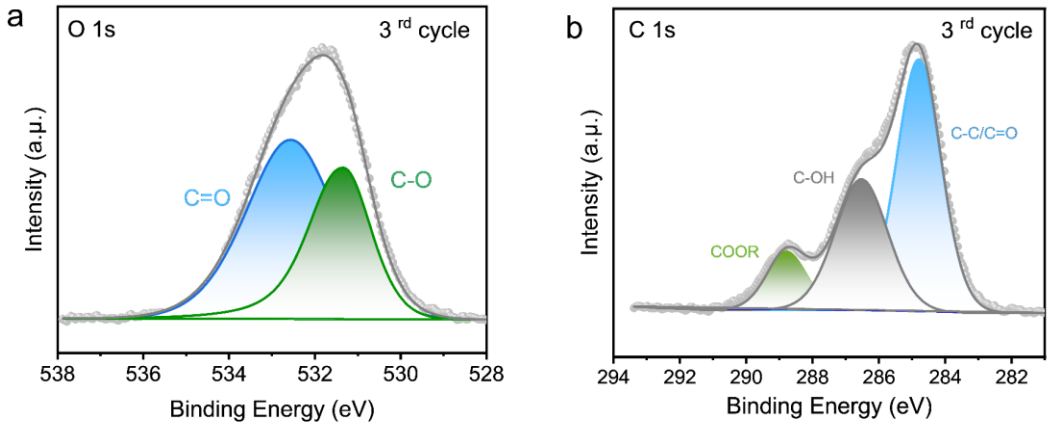

Supplementary Fig. 12 | (a) O 1s and (b) C 1s XPS spectra of SEI Zn after 3 cycles.

6. In TOF-SIMS depth profiles (Fig. 2g-k), C-, PO_4^{3-}, and O- species appear to be observed in the MAHEPE layer before electrochemical cycling as well. Therefore, TOF-SIMS data on species related to Zn ions are required to observe the evolution of $Zn_3(PO_4)_2$ in MAHEPE.

Our Response: Thanks for the question from the reviewer. At your suggestion, we redesigned the TOF-SIMS experiment with a special focus on species associated with Zn^{2+} By adjusting the experimental parameters and data analysis methods, we successfully obtained the depth profile data on the distribution of Zn^{2+} in the MAHEPE layer. These data not only reveal the initial distribution of Zn^{2+} before the electrochemical cycle, but also clearly show the evolution of $Zn_3(PO_4)_2$ during the electrochemical cycle. In the Supplementary TOF-SIMS data (Supplementary Figs. 10-11), we can observe the presence of Zn ion signals in the MAHEPE layer, and these signals change after electrochemical cycling. Especially after electrochemical cycling, we observed the interaction between Zn^{2+} and PO_x species, which is closely related to the formation and evolution of $Zn_3(PO_4)_2$. These observations are consistent with the electrochemical properties and behavior of $Zn_3(PO_4)_2$ as discussed in our paper. We have integrated these new TOF-SIMS data and analytical results into the corresponding sections of the paper, and have modified and supplemented the relevant discussion as

appropriate. We believe that these supplementary data will further enhance the reliability of the conclusions of the paper.

Related modifications have been made in the revised manuscript and supplementary information.

(Main article, Page 10)

The evolutionary process of interphase can be further confirmed by time-of-flight secondary ion mass spectrometry (TOF-SIMS). Fig. 2g depict the 3D elemental distributions of PO_4^{3-}, C, and O. It is evident that the PO_4^{3-} signal is relatively uniformly distributed across the entire plane, indicating the spontaneous construction of the artificial SEI into inorganic $Zn_3(PO_4)_2$. TOF-SIMS analysis was performed in positive ion mode to carefully analyze the three-dimensional distribution of Zn, Zn-O, Zn-PO_x and Zn-PO bonds before and after 3 cycles process, as shown in Supplementary Figs. 10-11. The comparative analysis shows that the signal strength of Zn-O bonds is basically unchanged before and after the cycle. The results show that Zn preferentially binds oxygen atoms on organic components at SEI Zn. Notably, at the initial state, the Zn-PO_x and Zn-PO components mainly originate from the intimate contact between the Zn anode and the PO_4^{3-} groups in the SEI. After cycling, the signal strength of both Zn-PO_x and Zn-PO bonds increased after cycling. This enhancement is attributed to electrochemically derived $Zn_3(PO_4)_2$ during cycling, resulting in the conversion of the organic coating to the organic/inorganic hybrid phase.

(Supplementary Information, Pages 13-14)

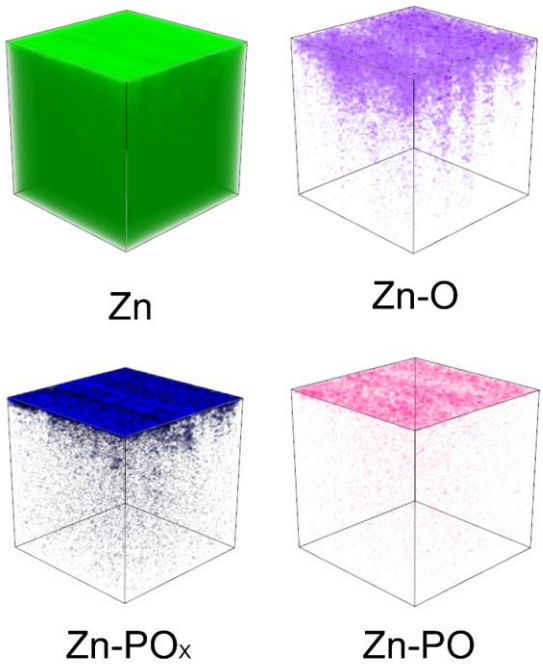

Supplementary Fig. 10 | TOF-SIMS 3D reconstruction of SEI Zn surface before cycling.

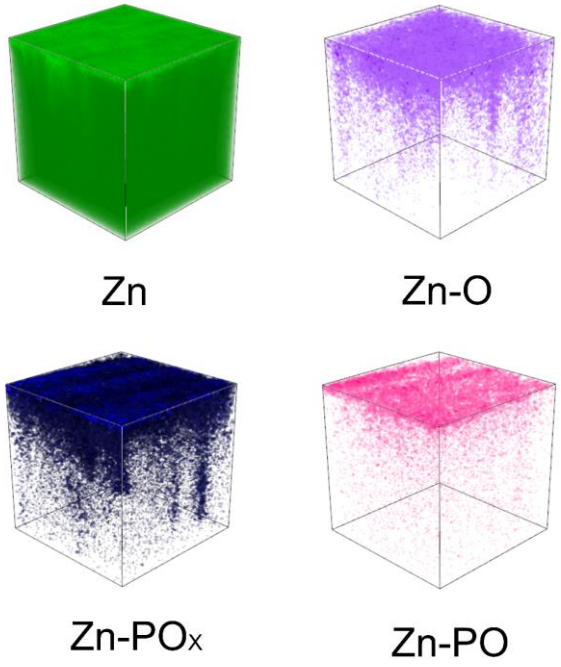

Supplementary Fig. 11 | TOF-SIMS 3D reconstruction of SEI Zn surface after 3 cycles.

7. Why is the AYM of Zn dendrites larger than that of pure Zn anodes?

Our Response: Thanks for the question from the reviewer. For metallic materials, the Young's modulus is not a constant but varies depending on the distribution of crystal axes. Unlike crystal planes, crystal axes serve as reference directions for describing the geometric orientation of the crystal structure and are directional in nature. There is no specific relationship between crystal axes and crystal planes. However, in certain studies, the Zn [001] crystal axis is often used to represent the Zn (002) crystal plane due to its perpendicularity to the horizontal Zn (002) crystal plane (10.1002/anie.202215552, 10.1002/adma.202100445). We calculated the Young's moduli of the Zn [100], Zn [010], and Zn [001] crystal axes (Supplementary Fig. 14), and the results show that the Young's modulus of the Zn [001] crystal axis, representing the horizontal direction, is the lowest at 137.417 GPa, while the Young's moduli of the Zn [100] and Zn [010] crystal axes, representing the vertical directions, are 207 GPa. This indicates that the Zn crystal plane in the horizontal state has a lower Young's modulus. In dendrites growing vertically, the crystal planes oriented in the vertical direction dominate, and the Young's moduli measured along these axes are higher, resulting in a higher AYM for the dendrites compared to pure Zn.

Related modifications have been made in the revised manuscript and supplementary information.

(Main article, Page 12)

Meanwhile, the increase in the AYM of the pure Zn anode is primarily attributed to the gradual formation of Zn dendrites with high Young's modulus (Supplementary Fig. 14). The corresponding...

(Supplementary Information, Pages 17-18)

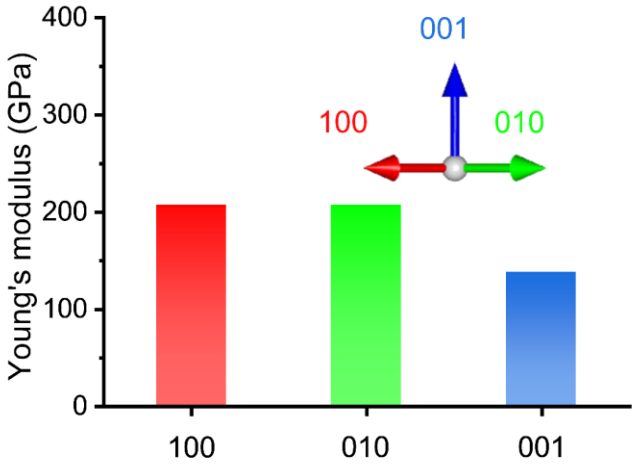

Supplementary Fig. 14 | The Young's modulus of Zn along different crystal axes, and a schematic diagram of the crystal axis directions.

The higher average AYM of Zn dendrites can be attributed to the dominant orientation of crystal planes in the vertical growth direction. Here, the theoretical research of Young's modulus was carried out by the following Methodology.

All the calculations are implemented by the VASP code. The GGA-PBE functional is selected for the exchange and correlation potential. Weak van der Waals interaction is considered by the DFT-D3 functional. The cut off energy for the plane-wave is 400 eV. The Gamma point in the Brillouin-zone is chosen for integration. Total energies of the systems converge to 10^{-5} eV in the iteration solution of Kohn-Sham equation. The force on each atom reduce to 0.05 eV/Å after geometry optimization. Then, the elastic constants are determined using second-order derivatives of equilibrium energy with respect to strains via the following equation:

$$C_{\alpha\beta} = \frac{1}{V}\frac{\partial^2 E}{\partial\gamma\alpha\partial\gamma\beta}$$

where γ's are applied strains in Voigt's notion around the equilibrium position. The average Young's modules and the directional dependence are derived from the elastic constants.

Specifically, the Young's modulus varies with the crystallographic axes, with the Zn [100] and Zn [010] axes (representing vertical directions) exhibiting a higher

modulus of 207 GPa, compared to the Zn [001] axis (representing the horizontal direction) with a lower modulus of 137.417 GPa. In vertically growing dendrites, the crystal planes oriented along the high-modulus axes (Zn [100] and Zn [010]) are predominant. As a result, the measured Young's moduli along these axes are higher, leading to an elevated AYM for the dendrites compared to pure Zn.

8. As shown in Fig. 3f, as $Zn_3(PO_4)_2$ is formed in MAHEPE layer, the adhesion of the SEI layer decrease rapidly. Due to the weak adhesion of about 50 nN, it is necessary to evaluate whether there is any peeling or detachment of the SEI layer after cycling.

Our Response: Thanks for the question from the reviewer. To provide tangible experimental evidence for assessing the potential detachment of the artificial SEI due to inadequate adhesion, we conducted a detailed analysis of the electrode's surface composition after undergoing both 5 cycles and an extended number of cycles. Our findings reveal that the decomposition process is not progressive and unending; rather, it evolves into a transition where the flexible organic coating gradually transforms into an organic-inorganic hybrid interface. Ultimately, this transformation tends towards the formation of a stable, hybrid organic-inorganic interface. These observations offer crucial insights into the durability and stability of the artificial SEI, thereby enhancing our understanding of its role in electrode performance.

Related modifications have been made in the revised manuscript and supplementary information.

(Main article, Pages 12-13)

In order to further verify whether the decomposition behavior of organic coatings during electrochemical cycling is non-terminating, detailed surface composition analysis of SEI Zn after different cycles was performed. In the Supplementary Fig. 15 of SEI Zn after 5 cycles, the presence of the phase interface can be clearly observed. This observation not only confirms the decomposition of the organic coating during the

cycle, but also reveals significant changes in coating thickness. Specifically, the coating thickness after 5 cycles was significantly reduced compared to that before the cycle. This change in thickness is directly attributable to the decomposition of the organic coating. Further, by EDS analysis (Supplementary Fig. 16), C, O and P elements were evenly distributed in the decomposed coating. At the same time, the characteristic peaks of organic coatings were also detected in the XPS P 2p and O 1s spectra (Supplementary Fig. 17). The presence of these characteristic peaks indicates that even after 5 cycles, the flexible organic coating does not completely disappear, but gradually transforms into an organic-inorganic hybrid interface. When the number of cycles is further increased, it can be observed from the Supplementary Fig. 18 that the organic coating is still clearly visible, but there is a certain gap between it and the electrode, indicating that its adhesion is relatively weakened. This phenomenon is consistent with the process by which a highly viscous organic coating decomposes to form a strong inorganic phase. In addition, the distribution of C, O and P elements in the EDS spectrum remained relatively uniform, while the characteristic peaks in the XPS spectrum and FTIR spectrum were also obvious (Supplementary Figs. 19-21). Based on the above experimental results, it can be concluded that the decomposition of organic coatings in the electrochemical cycle is not infinite, but to a certain extent, and eventually tends to form an organic-inorganic hybrid interface.

(Supplementary Information, Pages 19-25)

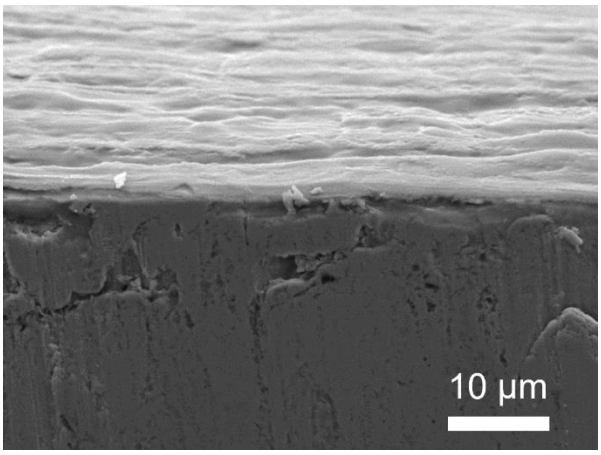

Supplementary Fig. 15 | Side-view FESEM image of SEI Zn after 5 cycles.

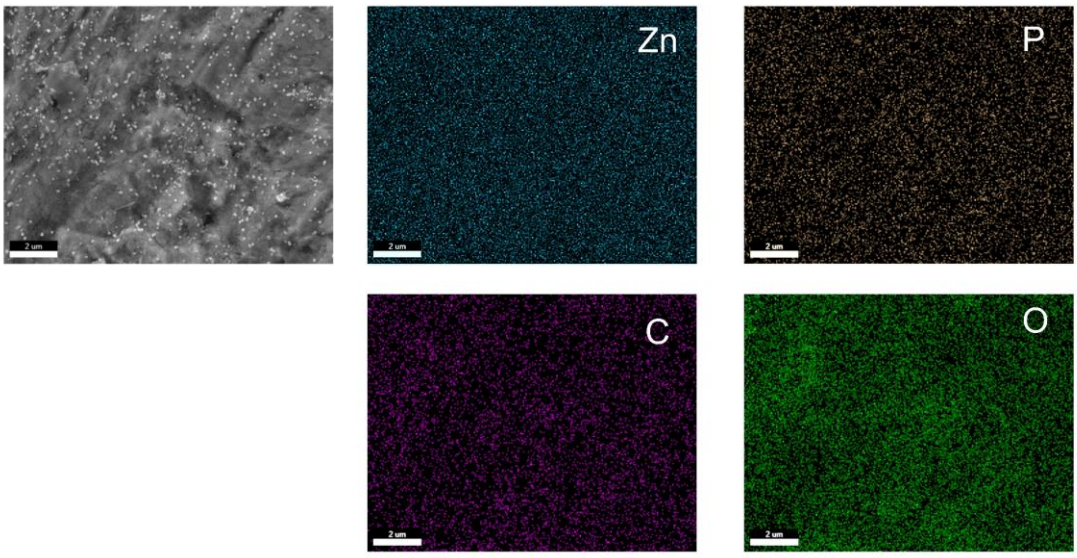

Supplementary Fig. 16 | EDS mapping image of SEI Zn after 5 cycles.

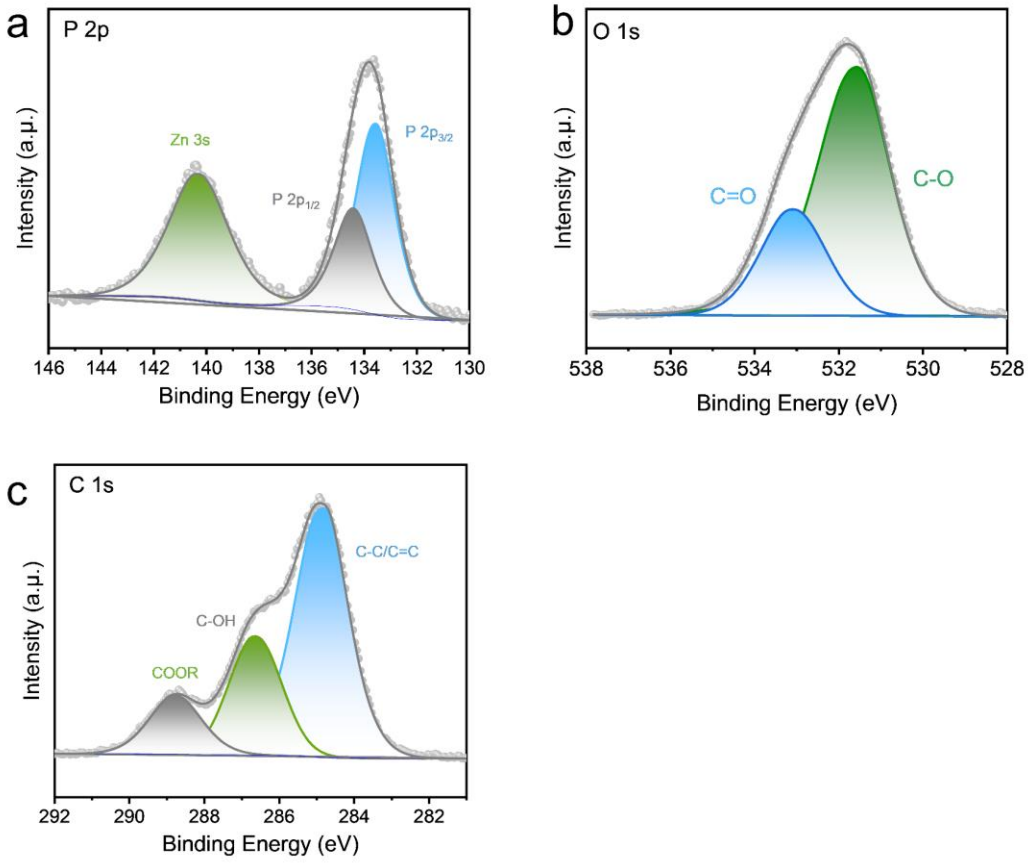

Supplementary Fig. 17 | (a) P 2p, (b) O 1s and (c) C 1s XPS spectra of SEI Zn after 5 cycles.

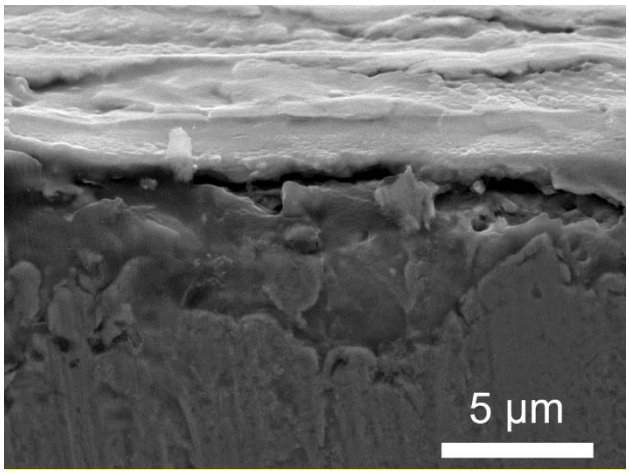

Supplementary Fig. 18 | Side FESEM image of SEI Zn after 10 cycles.

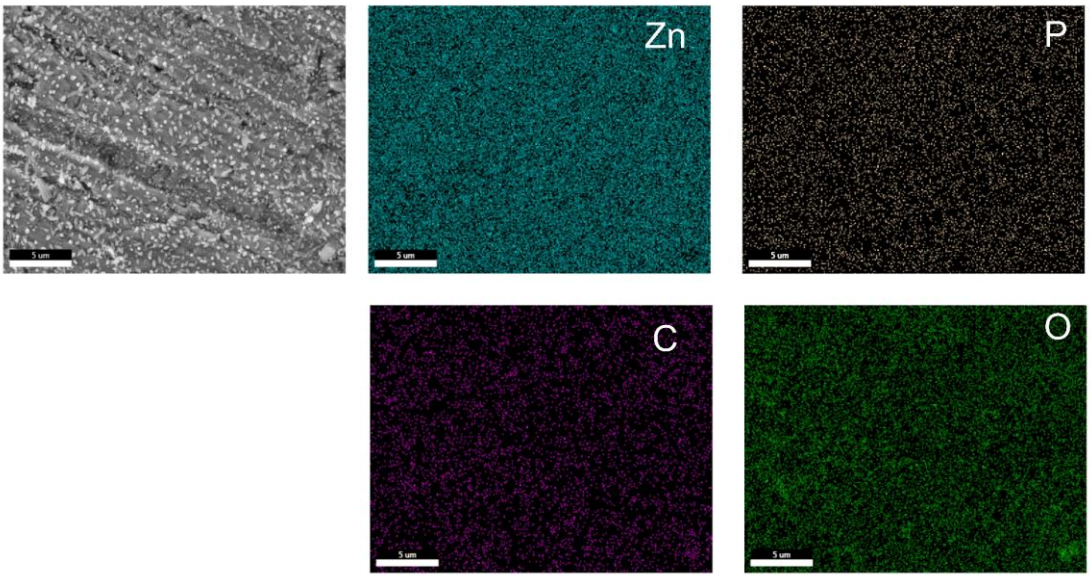

Supplementary Fig. 19 | EDS mapping image of SEI Zn after 10 cycles.

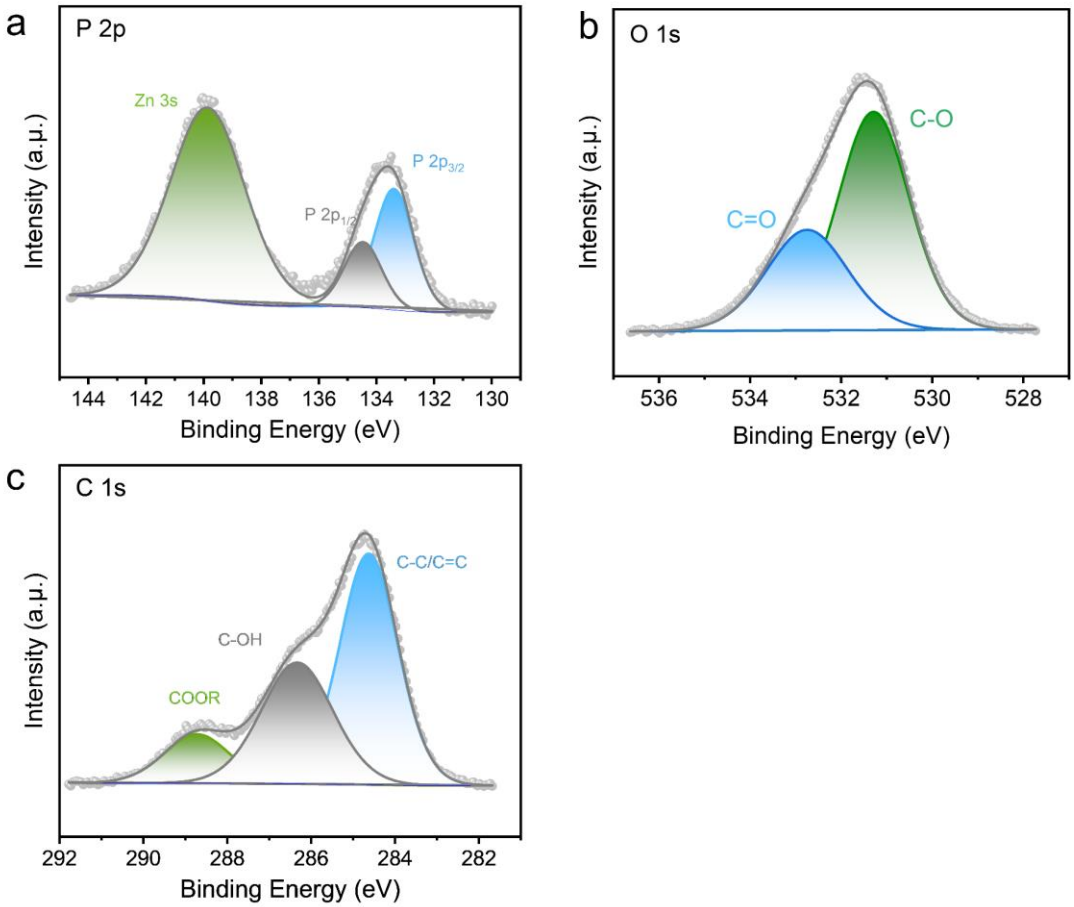

Supplementary Fig. 20 | (a) P 2p (b) O 1s and (c) C 1s XPS spectra of SEI Zn after 10 cycles.

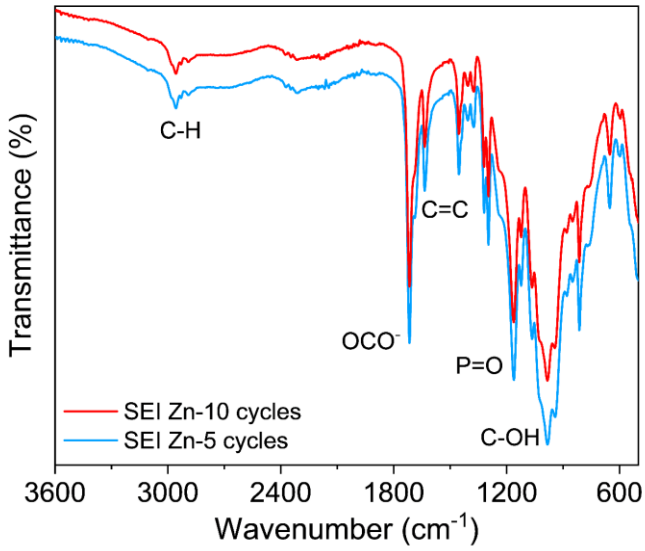

Supplementary Fig. 21 | FTIR Spectra of SEI Zn electrode after 5 and 10 cycles.

9. A clear basis is needed for the cause of SEI Zn inducing growth of Zn deposits along the Zn(002) plane. The authors attributed this phenomenon to zincophilic phosphate groups, but the presented DFT results show that the affinity between $Zn_3(PO_4)_2$ and Zn atoms is not high at all. In addition, the Zn(002) surface deposition phenomenon is not a phenomenon that appears only when Zn affinity is high. Therefore, a clear explanation of this will be able to improve readers' understanding.

Our Response: We would like to express our gratitude to the reviewer for pointing out the inaccuracies. After a thorough review and comparison, we have revised our interpretation of the Zn(002) deposition mechanism. Previous studies have demonstrated that $Zn_3(PO_4)_2$ compounds exhibit fast ion conductivity for Zn^{2+} (10.1021/acsnano.3c05640; 10.1021/acsnano.3c05640), with their intrinsic ionic channels facilitating the rapid transport of Zn^{2+}. As indicated by the DFT results in Fig. 4e, the binding interaction between $Zn_3(PO_4)_2$ and Zn^{2+} is relatively weak, suggesting a low energy barrier for Zn^{2+} migration. The uniformly distributed $Zn_3(PO_4)_2$ within the SEI enhances the efficient transport of Zn^{2+} and promotes the homogenization of the ionic flux. Furthermore, $Zn_3(PO_4)_2$ shows a stronger adsorption affinity for SO_4^{2-}, which effectively anchors the anions and selectively permits the rapid passage of Zn^{2+} (10.1021/acs.nanolett.3c00258). This mechanism aids in mitigating interfacial concentration polarization, ensuring a uniform deposition rate, coupled with the role of organic components in suppressing the 2D diffusion of Zn^{2+} during the nucleation stage, facilitates the orderly deposition of Zn(002).

Related modifications have been made in the revised manuscript.

(Main article, Pages 20-21)

During Zn deposition, the relatively weak binding interaction between $Zn_3(PO_4)_2$ in the SEI Zn electrode and Zn^{2+} results in a low migration energy barrier for Zn^{2+} within the ionic channels of $Zn_3(PO_4)_2$. Meanwhile, SO_4^{2-} are effectively anchored by $Zn_3(PO_4)_2$, enabling selective transport of Zn^{2+} and thereby reducing concentration polarization. The synergistic effect of these mechanisms, combined with the high 2D diffusion

energy barriers of organic components, homogenizes the Zn^{2+} flux and optimizes Zn nucleation. As a result, the Zn (002) plane of the SEI Zn electrode becomes the preferred orientation for Zn deposition. Consequently, the relative intensity of...

10. Please correct the typos in the text.

e.g.) page 2, line 6, $Zn_3(PO_4)_2$nanocrytals / $Zn_3(PO_4)_2$ nanocrystals

page 12, line 5, 1 $mAcm^{-2}$ / 1 mA cm^{-2}

page 12, line 20, 3M $ZnSO_4$ / 3 M $ZnSO_4$

Our Response: Thanks for the question from the reviewer. We have corrected the typos in the text and have carefully reviewed the remaining content to ensure its accuracy.

Related modifications have been made in the revised manuscript.

(Main article, Page 2)

Upon cycling, the protective layer in situ transforms into a hybrid phase enriched with well dispersed $Zn_3(PO_4)_2$ nanocrystals. This transformation ensures a uniform Zn^{2+} flux, effectively suppresses dendrite growth, and mitigates side reactions.

(Main article, Page 15)

For pure Zn, a strong H_2 response can be detected when cycling at a current density of 1.5 mA cm^{-2}, while no obvious H_2 signal can be seen during the entire cycle of the SEI Zn electrode, indicating that the HER is inhibited[26].

The digital photos of the SEI Zn electrode and pure Zn electrode, soaked in 3 M $ZnSO_4$ for three days at room temperature ...

Point-by-point response to the reviewers' comments

Dear Reviewers:

We sincerely appreciate your precious time and very valuable comments on improving the quality of this manuscript. In this revision, we have studied the comments carefully and have made full correction which we hope to meet with approval. Provided below is our detailed response to every question.

Reviewer #1 (Remarks to the Author):

This paper is well revised resolving all concerns that I raised. However, the key concept about the in-situ formation of hybrid interphase and interfacial chemistry should be more clarified in the session of introduction considering the recently published important papers (Nat. Commun., 2023, 14, 5443; EES, 2024, 17, 7870; ACS Energy Lett., 2024, 9, 209). The originality of this work needs to be further emphasized in the introduction part.

Our Response: We appreciate the expert advice provided by the reviewer. In this revision, we have conducted an in-depth study and comparison of the aforementioned insightful papers and integrated these findings with our work for further discussion. This allows us to refine and deepen the core concepts of our research, with the aim of presenting its originality more clearly and intuitively to the readers. Besides, those important papers (Nat. Commun., 2023, 14, 5443; EES, 2024, 17, 7870; ACS Energy Lett., 2024, 9, 209) also have been cited in the introduction part of this manuscript, owing to their good guidance for our work.

Related modifications have been made in the revised manuscript.

(Main article, Page 4)

In detail, ~~single-organic-component will be in-situ transformed into highly-dispersed $Zn_3(PO_4)_2$ nanocrystalline-enriched hybrid phases after initial electrochemical cycles.~~ during the initial electrochemical cycling, the electric field drives Zn^{2+} to migrate

through the PO_4^{3-}-rich organic coating, where they coordinate with PO_4^{3-} to nucleate highly dispersed $Zn_3(PO_4)_2$ nanocrystals. This dynamic process facilitates the in-situ evolution of an organic-inorganic hybrid interfacial phase. Although organic electrolyte additives such as trimethyl phosphate (TMP)[25], succinimide (H-SU)[26], and poloxamers[27], have been recently proved as effective mediators to regulate the anode-electrolyte interface chemistry. In contrast to electrolyte additive-enabled interface engineering, the SEI derived from the in-situ electrochemical transformation of the pre-coating layer offers superior manipulability, enabling precise regulation of both its structure and thickness while concurrently exhibiting exceptional stability and mechanical flexibility. Moreover, its enhanced environmental adaptability ensures broad electrolyte compatibility, substantially extending the applicability of this strategy across a wide range of battery systems. ~~This electrochemically mediated in situ synthesis approach facilitates the development of a highly compatible and flexible $Zn_3(PO_4)_2$ based hybrid SEI on the Zn anode surface, obviating the need for extensive incorporation of organic solvents.~~ Ex-situ atomic force microscopy (AFM) research…

(Main article, Page 39)

25. Wang, W. et al. Regulating interfacial reaction through electrolyte chemistry enables gradient interphase for low-temperature zinc metal batteries. *Nat. Commun.* **14**, 5443 (2023).
26. Huang, S.Y. et al. Molecularly engineered multifunctional imide derivatives for practical Zn metal full cells. *Energy Environ. Sci.* **17**, 7870-7881 (2024).
27. Yang, K. et al. Poloxamer Pre-solvation Sheath Ion Encapsulation Strategy for Zinc Anode–Electrolyte Interfaces. *ACS Energy Lett.* **9**, 209-217 (2024).

Reviewer #2 (Remarks to the Author):

I can see the substantial improvements made in response to the reviewers' comments. However, some essential revisions are still required for clarity and completeness:

Our Response: We appreciate the expert advice provided by the reviewer.

1. Electrochemical decomposition (Point 4): Authors stated that the observed dots result from the electrochemical decomposition of organic components. However, further validation is required to confirm that these dots do not induce any side reactions that could impact long-term battery stability. Please provide experimental evidence supporting this claim.

Our Response: We appreciate the expert advice provided by the reviewer. In this revision, we have added additional results to show the non-electrochemical activity of the observed dots. From the evolution analysis of morphology, bonding structure and valence state of elements, Figs. 2a-c, and Supplementary Figs. 16, 20, and 23 indicate that such observed dots are mainly resulted from the electrochemical decomposition of organic components initial few cycles, then well maintain the dot-like morphology even after 100 cycles. Besides, FTIR spectra (Supplementary Fig. 22) and XPS spectra (Supplementary Figs. 12, 17, and 21) also prove that both bonding structure and valence state of elements of the organic components in SEI remained stable after cycling. Therefore, it can be concluded that the decomposition of organic coatings in the electrochemical cycle is limited and non-electrochemical activity, and eventually tends to form a stable organic-inorganic hybrid interface.

Then, in order to evaluate whether it has an impact on the long-term battery stability, we will conduct a comprehensive analysis from the perspectives of the Zn metal anode and electrode-electrolyte interface, as well as the MnO_2 cathode. ***For the Zn metal anode and electrode-electrolyte interface***, the contact angle test shows that SEI Zn electrode can retain its hydrophobic properties after the cyclic test (Supplementary Fig. 26). Then, LSV curve test (Supplementary Fig. 28), in-situ DEMS (Figs. 4a-b) and in-situ pH (Figs. 4c-d) indicate the enhanced anti-HER performance by SEI protection. Beyond that, dynamic pH test of the cycled Zn-aqueous electrolyte system was further

conducted, aiming to compare the pH evolution of aqueous electrolyte with increased H_2SO_4 or NaOH content. This test can evaluate the effectiveness of SEI protection against Zn metal anodes from a more rigorous perspective. As depicted in **Fig. R1**, compared to the cycled Pure Zn case, the pH of cycled SEI Zn-aqueous electrolyte system shows a narrower acid-base fluctuations enabled by the regulation of $Zn_3(PO_4)_2$-based hybrid SEI, thus improving the corrosion resistance of Zn metal anode.

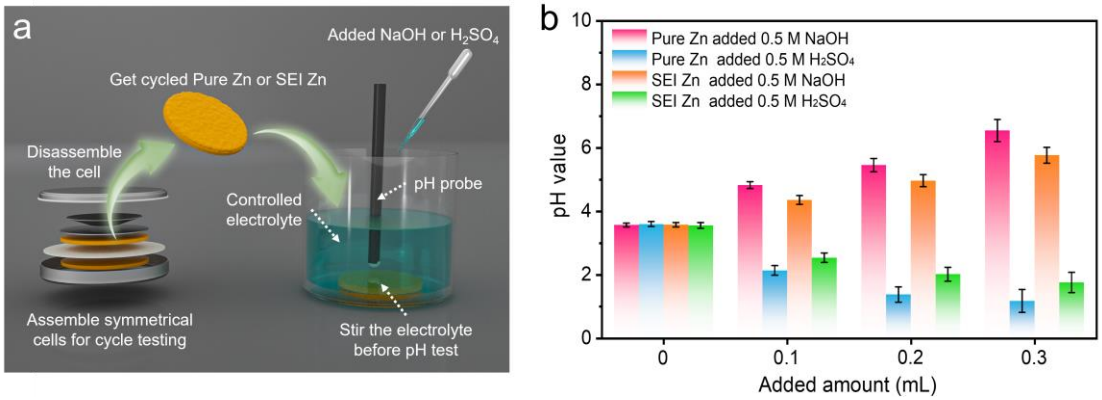

Fig. R1 | Dynamic pH test of the cycled Zn-aqueous electrolyte system, to compare the pH evolution of aqueous electrolyte with increased H_2SO_4 or NaOH content. (a) Test flow diagram and (b) the corresponding test result.

Moreover, the comprehensive results of DFT calculation (Figs. 4e-g and Supplementary Figs. 36-37), electrochemical tests (Figs. 4h-i and Supplementary Figs. 38-39) and in-situ EIS and DRT analysis (Figs. 4j-k and Supplementary Figs. 40) also confirm the enhanced Interfacial ion transport kinetics for SEI Zn electrode. Therefore, benefited from the hydrophobic and zincophilic characteristic of stable organic-inorganic hybrid interface, long-term cycle performance tests show that SEI Zn anodes exhibit significantly longer cycle lifespan than Pure Zn at different temperature and current density conditions (Figs. 6a-c, and Supplementary Figs. 46-51). ***While for MnO_2 cathode***, both CV curve (Supplementary Fig. 54) and ex-situ XRD (Supplementary Fig. 55) characterizations indicate that the storage mechanism of MnO_2 cathode is similar in Pure Zn and SEI Zn system, this suggests that the SEI do not induce side reactions to influence the crystal structure of MnO_2. Moreover, long-term cycle performance tests of aqueous Zn||MnO_2 batteries conducted at different temperature

and current density conditions (Figs.6d-f, and Supplementary Figs. 52, 53, 56) prove the obviously enhanced cyclic stability in the SEI Zn system.

In summary, we directly and indirectly analyze the influence of organic phase dots-enriched SEI on the cycle stability of zinc batteries from different perspectives. The results demonstrate that the observed dots result from the electrochemical decomposition of organic components should be stable with non-electrochemical activity after initial few cycles. Benefited from the hydrophobic, zincophilic and stable organic-inorganic hybrid interface, the long-term cycle performance of Zn symmetrical cell and Zn||MnO_2 batteries can be significantly improved under the conditions of different temperature, pH environment, and charge/discharge rate, so as to support the multi-scenario applications of zinc metal batteries.

Related modifications have been made in the revised manuscript and supporting information.

(Main article, Page 13)

In addition, the distribution of C, O and P elements in the EDS spectrum remained relatively uniform, while the characteristic peaks in the XPS spectrum and FTIR spectrum were also obvious (Supplementary Figs. 20-22). More importantly, the morphological evolution (Supplementary Fig. 23) confirm that the observed dots resulted from the electrochemical decomposition of organic components did not significantly change even after 100 cycles, indicating the stable structure and non-electrochemical activity. Based on the above experimental results, it can be concluded that the decomposition of organic coatings in the electrochemical cycle is limited and non-electrochemical activity ~~not infinite~~, ~~but to a certain extent,~~ and eventually tends to form ~~an~~ a stable organic-inorganic hybrid interface.

(Supporting Information, Page 27)

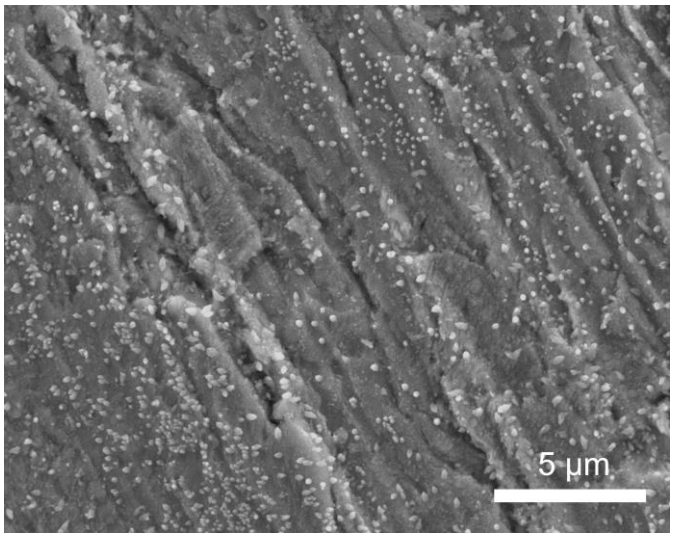

Supplementary Fig. 23 | FESEM images of SEI Zn electrode after 100 cycles.

(Main article, Page 16)

Besides, such inhibitory effect can be maintained after cycling, demonstrating a good anti-HER performance of the modified electrode (Supplementary Fig. 28). ~~It also shows that the modified electrode has good anti-HER performance.~~

(Supporting Information, Page 32)

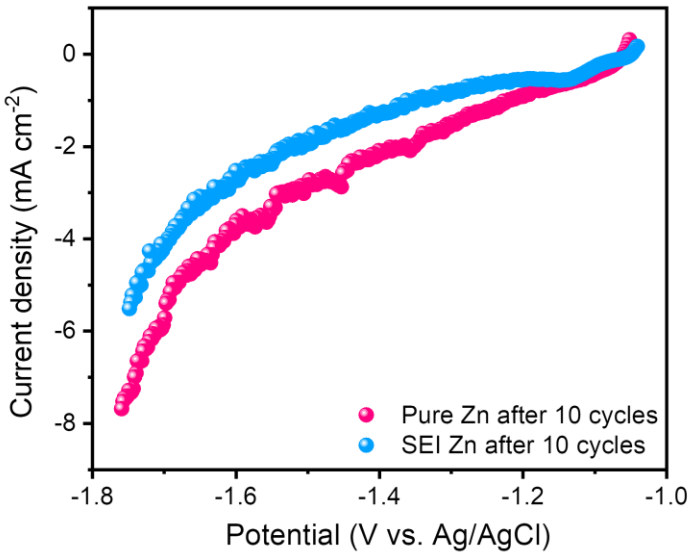

Supplementary Fig. 28 | LSV curves of the Pure Zn and SEI Zn electrodes after 10 cycles tested in 1 M Na_2SO_4 electrolyte.

(Main article, Page 27)

The cyclic voltammetry (CV) curves of the SEI Zn||MnO_2 system exhibit the same redox reaction behavior as those of batteries using pure Zn electrodes, as shown in supplementary Fig. 54. In addition, ex-situ XRD analysis also proves that the crystal structure of MnO_2 cathode is similar in both Pure Zn and SEI Zn systems after cycling (Supplementary Fig. 55). ~~This observation shows~~ Therefore, CV and XRD results show that the cathode reaction mechanism is similar in Pure Zn and SEI Zn system, ~~remains unchanged and no side reactions occur during the cycle,~~ suggesting the SEI do not induce side reactions yet improve the long-term battery stability by stabilizing the Zn-electrolyte interface.

(Supporting Information, Page 59)

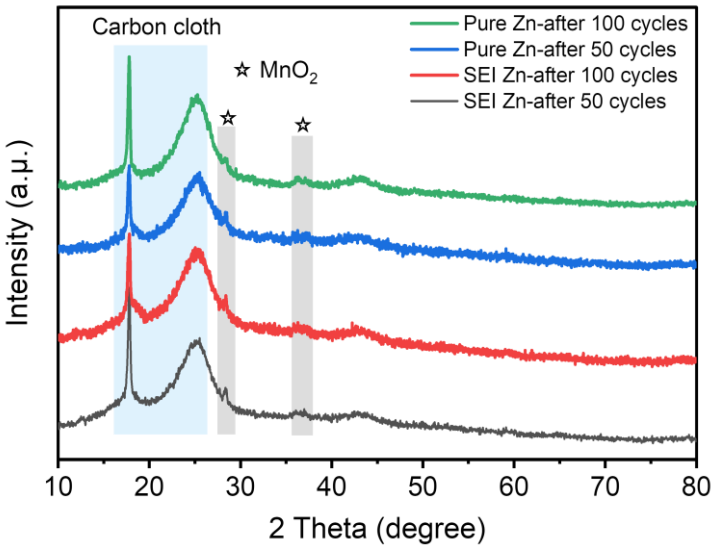

Supplementary Fig. 55 | XRD pattern of MnO_2 cathode after different cycles in the Pure Zn or SEI Zn anode system.

2. Peeling off during cycling (Point 6): In the side-view image of the zinc metal, some void spaces are observed. However, this image alone does not sufficiently address the concern regarding potential peeling off the SEI layer during cycling. A more detailed analysis would be required to enhance the argument.

Our Response: We appreciate the expert advice provided by the reviewer. In the cross-sectional FESEM images of the SEI Zn anode, the formation of voids may result from the differential contraction between the coating and the Zn anode at extremely low temperatures during liquid nitrogen treatment. To avoid this possible influence, we omitted the liquid nitrogen treatment during the sample preparation process. As shown in Supplementary Fig. 18, after 20 cycles, the SEI remains tightly bonded to the Zn anode even under a bent state. Furthermore, after 50 cycles and immersion in the electrolyte for 30 minutes, the structure of SEI Zn remains consistent with that before immersion, with no observable SEI detachment (Supplementary Fig. 19). Therefore, we infer that the good adhesion between the SEI and the Zn anode prevents delamination, which is consistent with the conclusions presented in the main text. Besides, in order to avoid misunderstanding to readers and to eliminate the concern of reviewer, we have updated the morphological characterizations into Supplementary Figs. 18-19.

Related modifications have been made in the revised manuscript and supporting information.

(Main article, Page 13)

When the number of cycles is further increased to 20 and 50 cycles, it can be observed from the Supplementary Figs. 18-19 that the organic coating is still clearly visible and tightly bonded to the Zn anode, even at the bending state or after electrolyte soaking treatment.~~, but there is a certain gap between it and the electrode, indicating~~ This indicates that although the adhesion of SEI is ~~relatively~~ weakened after organic coating decomposition, it can still maintain a good binding to the Zn anode without obvious delamination. ~~This phenomenon is consistent with the process by which a highly viscous organic coating decomposes to form a strong inorganic phase.~~ In addition, the distribution of C, O and P elements in the EDS…

(Supporting Information, Page 22)

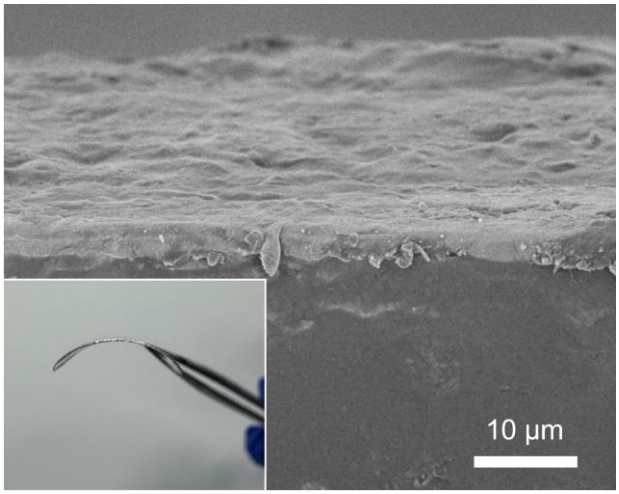

Supplementary Fig. 18 | Side view FESEM image of SEI Zn anode after 20 cycles at the bending state.

(Supporting Information, Page 23)

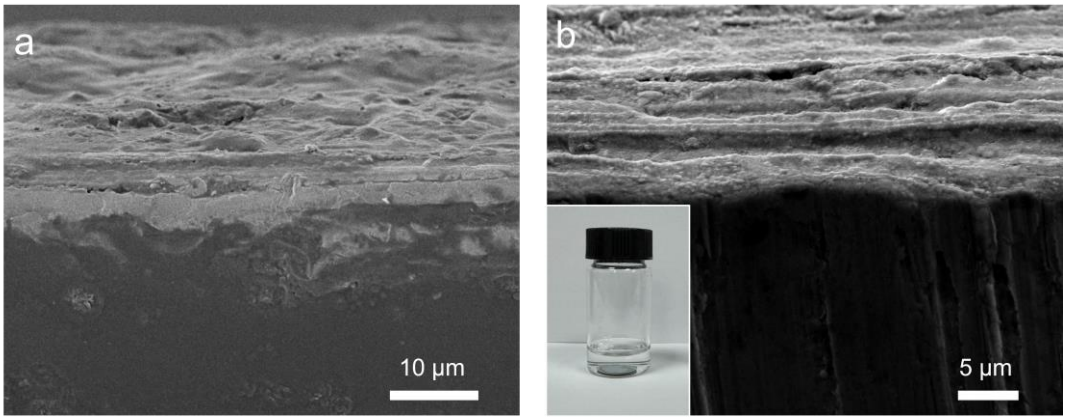

Supplementary Fig. 19 | Side view FESEM images of SEI Zn anode after 50 cycles, (a) without and (b) with electrolyte soaking treatment for 30 min.

3. In-situ morphology analysis (Fig. 5d): The provided figure appears to depict in-situ morphological observations, potentially from digital microscopy. However, it lacks scale bars and clear proof that Zn^{2+} ions are depositing beneath the SEI layer. Please add a scale bar and provide more conclusive evidence.

Our Response: We appreciate the expert advice provided by the reviewer. In this revision, we have added the scale bar in the Fig. 5d of in-situ optical observation.

Besides, in order to further prove that Zn^{2+} ions are depositing beneath the SEI layer, we further provided the FESEM images of the side view of SEI Zn electrode after depositing at 20 mA cm^{-2} for 10 minutes (Supplementary Figs. 42a, 42b). The results indicate that SEI Zn electrode has a three-layer structure after deposition, and the deposited Zn are beneath the SEI layer.

Related modifications have been made in the revised manuscript and supporting information.

(Main article, Page 19)

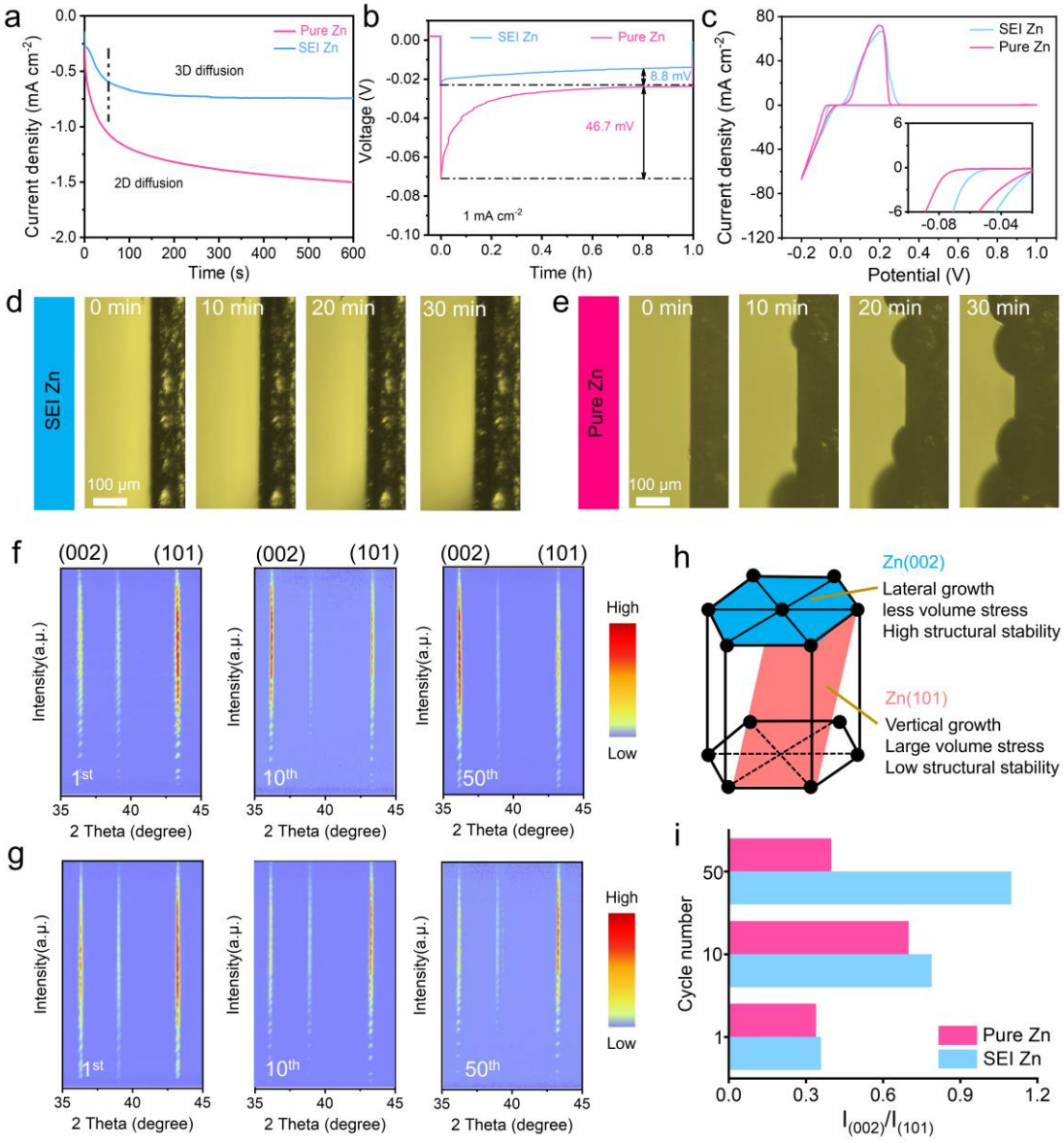

Fig. 5 | Comparison of nucleation and electroplating/stripping processes between SEI Zn

and Pure Zn. a The CA curves of pure Zn and SEI Zn electrodes. **b** Nucleation overpotential of Pure Zn and SEI Zn electrodes at 10 mA cm^{-2}. **c** CV curves of SEI Zn|| SEI Cu and Pure Zn|| Pure Cu asymmetric cell. In-situ optical observation of the (**d**) SEI Zn and (**e**) pure Zn electrode during the Zn deposition process at the current density of 20 mA cm^{-2}. Ex-situ 2D XRD analysis of the (**f**) SEI Zn and (**g**) Pure Zn electrode after different cycles. **h** The crystal structure of metallic Zn and (**i**) corresponding ratio change of $I_{(002)}/I_{(101)}$.

(Main article, Pages 20-21)

In order to further clarify the deposition behavior of Zn^{2+} on the SEI Zn electrode, the side morphology of SEI Zn was analyzed after the deposition ~~time was~~ for 10 and 20 minutes (Supplementary Fig. 42). The results of FESEM and corresponding EDS mapping indicate that SEI Zn electrode has a three-layer structure after deposition, and the deposited Zn are beneath the SEI layer. ~~From the EDS image, it is found that the feature elements C, O and P, which represent the artificial SEI, are obviously present in the top layer. This observation suggests that Zn^{2+} is deposited mainly in the lower regions of the artificial SEI, a~~ Such phenomenon attributed to the non-conductive nature of the artificial SEI layer.

(Supporting Information, Page 46)

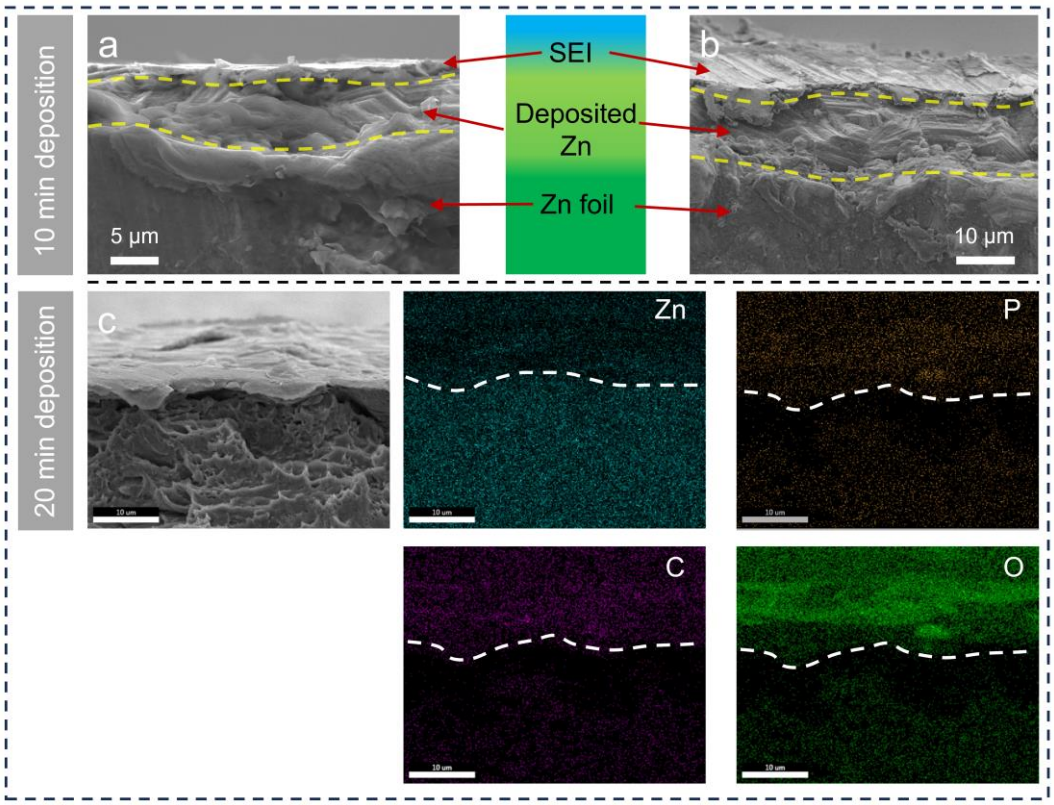

Supplementary Fig. 42 | (a, b) FESEM images of the Side view of SEI Zn electrode deposited at a current density of 20 mA cm^{-2} for 10 minutes. (c) FESEM and corresponding EDS spectra of the side view of SEI Zn electrode deposited at a current density of 20 mA cm^{-2} for 20 minutes.

4. XRD (Fig. S19): The Miller indices and y-axis labels remain unchanged. Authors did not address the previous concerns about this.

Our Response: We deeply apologize to the reviewer for our previous carelessness. In this revision, we have labeled the Miller indices for all the peaks and added "Intensity (a.u.)" on the y-axis in the XRD pattern (original Fig. S19) for clarity. Again, we appreciate the expert advice provided by the reviewer.

Related modification has been made in the revised supporting information.

(Supporting Information, Page 49)

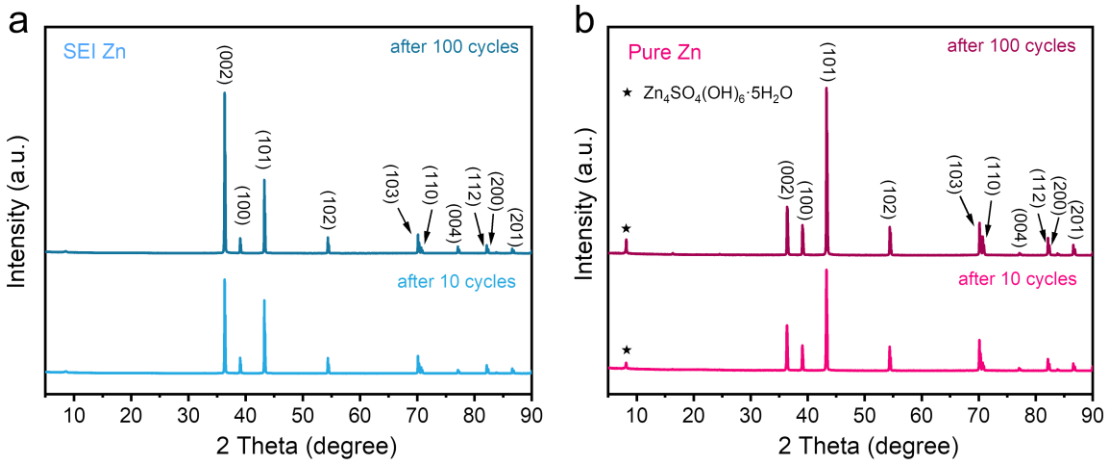

Supplementary Fig. 45 | The XRD patterns of (a) SEI Zn and (b) Pure Zn electrodes after different cycle number.

5. CV data for the MnO_2 full cells (Fig. S51): It is notable that no SEI formation peak appears in the first cycle. Furthermore, while authors mentioned that the observed dots are due to the electrochemical decomposition of organic components, this process does not seem to be manifested in the CV data either. Can authors clarify why these phenomena do not produce distinguishable peaks in the CV curves?

Our Response: We appreciate the questions from the reviewer. The cyclic voltammetry (CV) technique investigates the kinetics, mechanisms, and material properties of electrochemical reactions by measuring the current response of the electrode at different potentials, primarily reflecting the electrochemical reactions occurring at the working electrode. The counter electrode provides the necessary electrons for the reaction as the source or sink of current but does not directly participate in the measurements. The reference electrode offers a stable reference potential, ensuring the accuracy of potential control, but does not partake in the reaction.

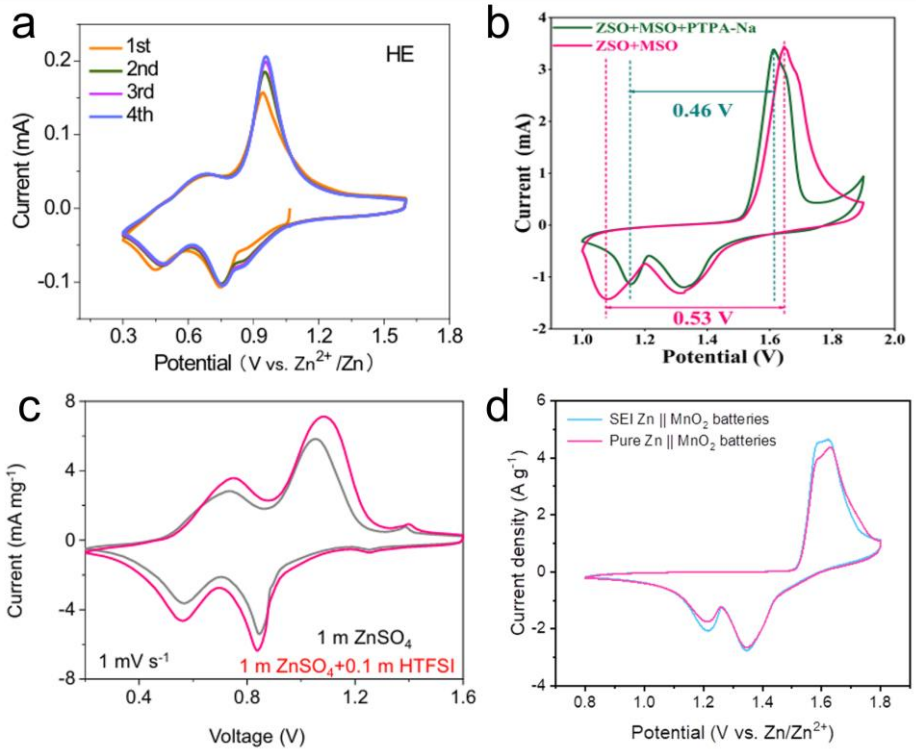

Fig. R2. | The comparison of CV curves of Zn-ion full cells in recently published papers about SEI formation. (a) *Nat. Commun.* **14**, 2720 (2023); (b) *Angew. Chem. Int. Ed.* **63**, e202409642 (2024); (c) *Nat. Commun.* **15**, 4303 (2024); (d) The CV curves of the Zn||MnO_2 full cells in this work (Supplementary Fig. 54c).

Normally, in the Zn||MnO_2 full cell, the Zn anode serves as both counter and reference electrode, while MnO_2 functions as the working electrode. In this case, the CV curves of the Zn||MnO_2 full cell reflects the redox reaction of MnO_2 but does not detect the electrochemical reaction on the Zn anode side, thus preventing the observation of the SEI formation peak. Similarly, in other recently published works about SEI formation, SEI-related peaks are also not observed in the CV curves of the full cells (**Fig. R2**). Therefore, it may be difficult to observe the formation of the anode surface SEI through the CV curve of full cells. Furthermore, a comparison with recently published papers on Zn anode SEI suggests that in CV tests of the Zn||Cu or Zn||Ti asymmetric cells, although there is solid evidence of SEI formation on the Zn anodes, only the peaks related to Zn deposition/stripping on the Cu/Ti surface are typically observed (**Fig. R3**).

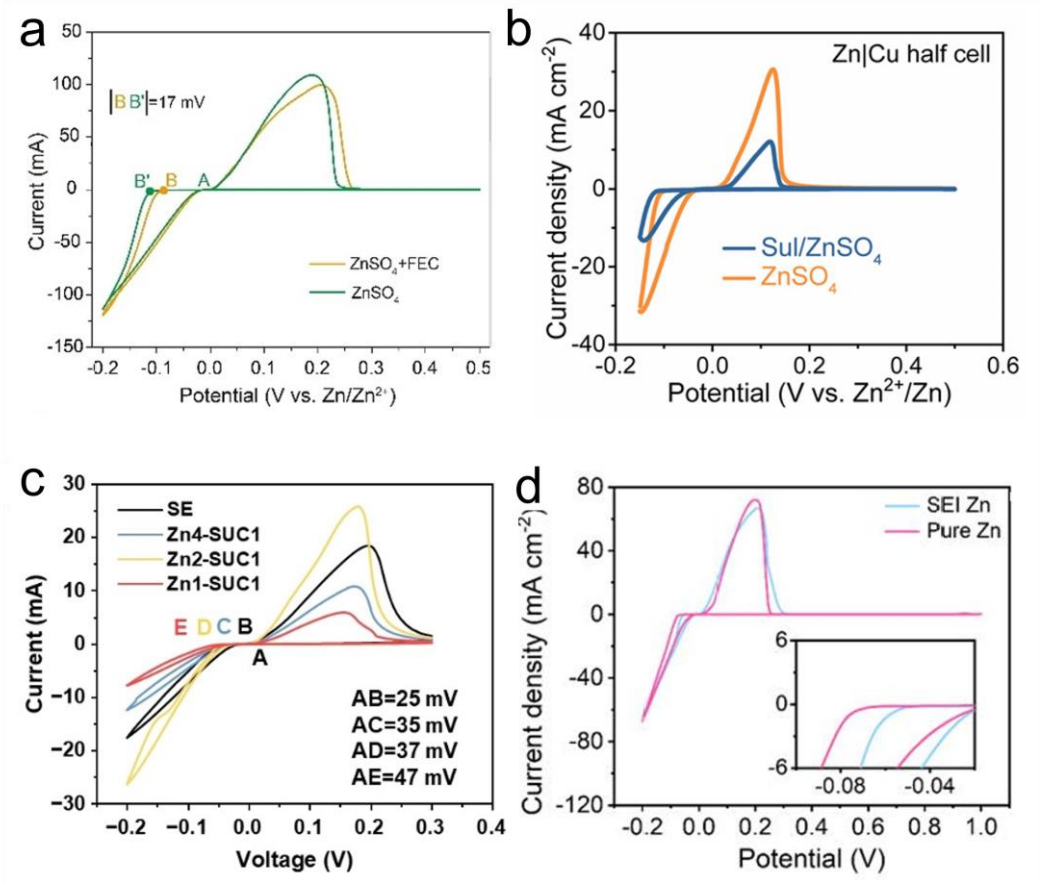

Fig. R3. | The comparison of CV curves of the Zn-based asymmetric cells in recently published papers about SEI formation. (a) *Angew. Chem. Int. Ed.* **62**, e202216934 (2023); (b) *Energy Environ. Sci.*, **16**, 1721(2023); (c) *Angew. Chem. Int. Ed.* **63**, e202401974 (2024); (d) The CV curves of the Zn||Cu asymmetric cells in this work (Fig. 5c).

Therefore, since the relevant reactions might be not violent, the detection of SEI-related peaks of CV curves in aqueous Zn metal batteries still be challengeable in the current research stage. More advanced characterization techniques are necessary in future work. In this case, we appreciate the reviewer again for the valuable comment. This will inspire us to focus on learning and applying advanced characterization techniques to further explore the functions and formation mechanisms of the Zn anode SEI in subsequent studies.

Reviewer #3 (Remarks to the Author):

The author has significantly improved the manuscript in response to the previous suggestions and addressed the concerns I raised during the initial review. The author employed an in-situ Zn3(PO4)2-based organic-inorganic hybrid interphase. This strategy makes a significant contribution to the field of Aqueous Rechargeable Zinc-Metal Batteries.

The author provides a clear exposition of the study's background, objectives, methods, and results. The structure and logic of the article have been thoughtfully organized, enabling readers to gain a clear understanding of the research's significance and contributions.

I believe the manuscript has reached the level suitable for publication.

Our Response: We appreciate the positive comment from the reviewer, and supporting the publication of our manuscript.